Anna Bjørke Kallestad

Field-Scale Modeling of Low Salinity Water Flooding - Wettability Alteration

Master's thesis in Petroleum Engineering
Supervisor: Ashkan Jahanbani Ghahfarokhi
Co-supervisor: Ole Torsæter
June 2021

Master's thesis

NTNU
Norwegian University of Science and Technology
Faculty of Engineering
Department of Geoscience and Petroleum

NTNU
Norwegian University of
Science and Technology

Anna Bjørke Kallestad

Field-Scale Modeling of Low Salinity Water Flooding - Wettability Alteration

Master's thesis in Petroleum Engineering
Supervisor: Ashkan Jahanbani Ghahfarokhi
Co-supervisor: Ole Torsæter
June 2021

Norwegian University of Science and Technology
Faculty of Engineering
Department of Geoscience and Petroleum

NTNU
Norwegian University of
Science and Technology

Abstract

Low salinity water flooding (LSWF) is an EOR-method where the ion composition and salinity of the injected brine are modified. The technique has a low chemical cost and is considered environmentally friendly compared to other EOR-methods. Extensive laboratory studies and some pilot-field trials have also shown favorable increase in oil recovery. Among the proposed mechanisms behind LSWF, the wettability alteration towards a more water wet state is the widely agreed mechanism. Dang et al. (2013) proposed a mechanistic numerical model for LSWF that included ion exchange, geochemistry, and wettability alteration on core-scale. The new LSWF model used the equation-of-state (EOS) compositional simulator GEM^{TM} by CMG.

This thesis addresses field-scale modeling of LSWF in GEM^{TM} by using the geochemical model presented by Dang et al. (2016) as a fundament. To make the field-scale model more realistic, the geological model is based on the Gullfaks K1/K2 segment. The geological data from Gullfaks K1/K2 segment's Eclipse file is converted to GEM^{TM} by using the software DataImporter and considerable manual modifications. The crude oil composition is generated and lumped in WinProp based on information of a Statfjord formation core found in the Gullfaks-database. Since the Gullfaks K1/K2 segment is lacking water analysis of the formation water, the water analysis from Fjelde et al. (2012) is used with some modifications. The wettability alteration process is modeled based on a shift in wettability due to geochemical reactions. Two sets of relative permeability curves are defined representing high salinity curves and low salinity curves. Interpolation occurs between the two relative permeability sets, based on the ion exchange equivalent fraction of Ca^{2+} on the clay surface.

Optimization on well control was done in CMOST to establish an optimal base case for high salinity water flooding (HSWF). The final oil recovery seen for LSWF was higher compared to HSWF. The results indicated that ion exchange and adsorption took place, which was in agreement with the hypotheses presented by Dang et al. (2016). A sensitivity analysis on grid refinement stated that the original grid was fine enough for further evaluation. Further sensitivity of timing of injection revealed that LSWF in secondary mode was more effective compared to tertiary mode. In addition, lowering the salinity of the LSW brine was found to be favorable for the wettability alteration process. A sensitivity analysis on two relative permeability models with varying change in K_{ro} from HS curves to LS curves indicated that the

corresponding interpolant values and S_{or} is what mainly determines the incremental oil recovery. This thesis provides an insight on how wettability alteration modeling of field-scale LSWF is configured in GEM.

Sammendrag

Injeksjon av vann med lavt saltinnhold (LSWF) er en økt oljeutvinningsmetode (EOR) der ionsammensetning og saltinnhold er modifisert. Utvinningsteknikken har en lav kostnad og regnes som miljøvennlig sammenlignet med andre utvinningsmetoder. Omfattende laboratoriestudier og enkelte pilot-feltforsøk har også vist inkrementell oljeutvinning ved bruk av denne metoden. Blant de foreslåtte mekanismene bak LSWF, er endring i fuktbarheten mot en mer vann våt tilstand den mest omtalte mekanismen. Dang et al. (2013) foreslo en mekanistisk numerisk modell for LSWF på kjerneskala, som inkluderte ionutveksling, geokjemiske reaksjoner og fuktighetsendring. Den nye LSWF-modellen brukte reservoarsimulatoren GEM^{TM} av teknologiselskapet Computer Modeling Group Ltd.

Denne avhandlingen tar for seg feltskalamodellering av LSWF, der modellen presentert av Dang et al. (2016) er brukt som grunnlag. For å gjøre feltskalamodellen mer realistisk, er den geologiske modellen basert på Gullfaks K1/K2-segmentet. De geologiske dataene fra Gullfaks K1/K2 segmentets Eclipse- datafil er konvertert til GEM^{TM} ved hjelp av programvaren DataImporter og betydelige manuelle modifikasjoner. Oljesammensetningen er generert i WinProp basert på informasjon fra en Statfjord-kjerne. Siden Gullfaks K1/K2-segmentet mangler en analyse av formasjonsvannet, er vannanalysen fra Fjelde et al. (2012) brukt med noen justeringer. Fuktighetsendringen er modellert basert på ionutveksling og geokjemiske reaksjoner. To sett med relative permeabilitetskurver er definert som representerer kurver med høyt saltinnhold og kurver med lavt saltinnhold. Interpolering mellom de to relative permeabilitetssettene ble gjort basert på hvor mye Ca^{2+} som er absorbert på leireoverflaten.

Optimalisering på brønnkontroll ble gjort i CMOST for å etablere en optimal base for vannflom med høy saltholdighet (HSWF). Den endelige oljeutvinningen sett for LSWF var høyere sammenlignet med HSWF. Resultatene indikerte at ionutveksling og adsorpsjon fant sted, som var i samsvar med hypotesene presentert av Dang et al. (2016). En sensitivitetsanalyse av rutenettet brukt i reservoarmodellen viste at det opprinnelige rutenettet hadde fin nok oppløsning for videre evaluering. Videre sensitivitetsanalyse for tidspunkt for vanninjeksjon viste at LSWF i sekundær modus var mer effektiv sammenlignet med tertiær modus. I tillegg ble det funnet at å senke saltinnhold ytterligere var gunstig for endring i fuktighet. En sensitivitetsanalyse på to relative permeabilitetsmodeller med varierende endring i K_{ro} fra HS-

kurver til LS-kurver indikerte at de tilsvarende interpolantverdiene og S_{or} er det som hovedsakelig bestemmer den inkrementelle oljeutvinningen. Denne avhandlingen gir et innblikk i hvordan modellering av feltskala LSWF kan konfigureres i GEM.

Acknowledgments

First and foremost, I would like to express my appreciation to my supervisor Ashkan Jahanbani Ghahfarokhi, for the guidance and support throughout the semester. Thank you.

Furthermore, I would like to thank the member of our research group for exciting and useful discussions at our regular meetings. Although most of the meetings has been online due to the covid-situation, I was motivated by the constructive feedback you all gave me.

Special mention to my fellow students at NTNU. Thank you for all the laughs, enthusiasm and discussions at lunch breaks, coffee breaks, etc. You have given me motivation and inspiration throughout the whole semester.

Finally, I would like to thank my family and friends, especially my parents back home in Bergen. I could not have done this without your support and engagement.

TABLE OF CONTENTS

List of figures

List of tables

Nomenclature

List of Abbreviations

AH	Amott-Harvey
AN	Acid Number
BHP	Bottom Hole Pressure
BP	British Petroleum Company
Ca^{2+}	Calcium Ion
CEC	Cation Exchange Capacity
CMG	Computer Modelling Group Ltd
CO_2	Carbon Dioxide
COBR	Crude Oil/Brine/Rock
DE	Differential Evolution
DLE	Double-layer Expansion
EOR	Enhanced Oil Recovery
EOS	Equation of State
FW	Formation Water
H^+	Hydrogen Ion
HSW	High Salinity Water
HSWF	High Salinity Water Flooding
LSW	Low Salinity Water
LSWF	Low Salinity Water Flooding
MBC	Modified Brooks and Corey model
Mg^{2+}	Magnesium Ion
MIE	Multicomponent Ion Exchange
Na^+	Sodium Ion
NaCl	Sodium Chloride
OH^-	Hydroxide Ion
OOIP	Original Oil in Place
PR	Peng-Robinson
PSO	Particle Swarm Optimization
PVT	Pressure-volume-temperature

SRK	Soave-Redlich-Kwong
SW	Seawater
SWCTT	Single Well Chemical Tracer Test

Subscripts

eff	Effective
g	Gas
i	Fluid phase
ineff	Ineffective
o	Oil
so	Solid-oil
sw	Solid-water
tot	Total
w	Water
wo	Water-oil

List of Variables

$\hat{A}$	Reactive Area
m_i	Molality of the species
γ_i	Activity coefficient
ϕ	Porosity
A	Cross sectional area
g	Gravitational acceleration (9.8 m/s^2)
H	Height over the column
j	Specific fluid (oil, gas or water)
K	Absolute permeability
k	Rate Constant
K_e	Effective permeability

K_{eq}	Chemical Equilibrium Constant
K_r	Relative permeability
K_{ro}	Oil relative permeability
K_{rw}	Water relative permeability
L	Length of tube
m	Molality
n	Corey exponent to water
N	Number of Moles
P_c	Capillary pressure
P_{nw}	Pressure of the non-wetting phase at interface
P_w	Pressure of the wetting phase at interface
Q	Flow rate
r	Radius of tube
R	Radii of curvature
S_i	Saturation
V_{avg}	Average velocity
V_p	Pore volume
V_t	Total volume
Δp	Pressure difference
ΔP_g	Pressure difference over the oil-water surface due to gravity
$\Delta \rho$	Differences in density between two phases
μ	Viscosity
θ	Contact angle
σ	Interfacial tension

GEM Keywords

KRINTRP	Interpolation set number
INCOMP	Composition of injected fluid
EQVFRIEX	Ion exchange equivalent fraction
CEC-IEX	Cation exchange capacity
INTCOMP_VAL	Value of interpolation parameter
VOLUME_FRACTION-MINERAL	Volume fraction mineral
TSORW	Residual oil saturation
REFINE	Local refinement of grid block
COORD	Corner point locations for x,y-direction
ZCORN	Corner point depths
POR	Porosity
PERMI/J/K	Permeability in I,J,K-direction
NETGROSS	Net to gross multipliers
NULL	Null block indicator
TRANSI/J/K	Transmissibility multipliers in I,J,K-direction
DI, DJ, DK	Grid block size in I, J, K-direction

1. Introduction

1.1 Background

The total world energy consumption is predicted to increase in the coming decades. Although renewables are expected to be the primary energy resource before the end of 2050, the petroleum industry is still needed for many years to come (U.S Energy Information Administration, 2020). Since it is becoming more challenging to discover new giant oil fields, the oil companies are now focusing on maximizing the oil recovery factors of the already discovered reservoirs (Muggeridge et al., 2013).

Waterflooding is the most widely used secondary recovery technique to improve the recovery factor. This is mainly because water has a unique ability to spread through a formation and efficiently displace oil. In general, water already produced from the reservoir or available seawater is injected into the reservoir to assist with pressure maintenance and recovery of the original oil in place (OOIP) after primary producing mechanisms (Craig, 1971; Esmaeili & Maaref, 2011; Katende & Sagala, 2019; Rausch & Beaver, 1964). For conventional reservoirs, the recovery factors after primary and secondary recovery are expected to be in the ranges of 35% to 45%, on average (Zitha et al., 2011).

The target for the operating oil companies is to improve the recovery factors after secondary recovery in an environmentally friendly and profitable way. By utilizing the engineer's expertise, incremental recovery factors in maturing fields can be obtained using thermal, chemical, alternative, gas injection, and other EOR methods (Zitha et al., 2011). Among the EOR techniques, there has been growing interest in how modification of the injected brine concentration can reduce the residual oil abundant in the reservoir. The technique is referred to as low salinity water flooding (LSWF) in this thesis, but also goes by the names smart waterflooding, LoSal and designer waterflood in literature (Al-Shalabi P.E, 2014; Derkani et al., 2018; Katende & Sagala, 2019). LSWF has led to significant improvement in oil recovery for several laboratory and field-scale studies (Abdulla et al., 2013; Al-Qattan et al., 2018; McGuire et al., 2005; Skrettingland et al., 2011; Webb et al., 2004). The benefits of LSWF are

that no expensive chemicals are added, and it is considered environmentally friendly compared to the other EOR methods.

Low salinity water flooding discussed in literature has given rise to several suggested mechanisms behind the incremental oil recovery. The most frequently discussed mechanisms are multicomponent ion exchange (MIE), double layer effect, migration of fines, pH-increase, and wettability alteration. In the last few years, there has been a mutual understanding that wettability alteration towards a more water wet state is the main mechanism behind the low salinity effect.

Numerical modeling of LSWF is complex due to the multiple reactions that occur in the crude oil-brine-rock system when low salinity water is injected. Dang et al. (2013) used the EOS compositional reservoir simulator GEM^{TM} by CMG for building a geochemical LSWF model on core scale. The wettability alteration during LSWF was modeled based on the amount of adsorbed divalent ions on the clay surface. They matched the Fjelde et al. (2012) core flooding experiment with the new LSWF model, which included mineral reactions, intra-aqueous reactions, and multiple ion exchange.

Few papers are published on field-scale numerical modeling of LSWF. Dang et al. (2016) extended their geochemical core-scale model to field-scale for the Brugge field. They implemented the geological model as a starting point before comprehensive waterflooding optimization and closed-loop management were done. This model was the inspiration for this thesis, where geological data from the Gullfaks K1/K2 segment is used as a starting point for investigating LSWF modeling on field-scale using GEM^{TM}.

1.2 Objectives

The overall objective was to build and test a numerical field-scale LSWF model based on the wettability alteration mechanism. Using an actual geological model from an Eclipse file, the first step was to get a deeper insight into how a reservoir model is built in GEM^{TM} compared to Eclipse 100. Other tasks included learning how to use a PVT-software to build a fluid model that included oil compositional data, and working with mineral and intra-aqueous reactions, and multicomponent ion exchange that occurs during LSWF. Subsequently, an extensive sensitivity analysis was performed on grid refinement, timing of injection, brine concentrations, and two relative permeability models.

1.3 Scope and Structure

This thesis is a continuation of the specialization project presented last semester (Kallestad, 2020). Hence, some of the theoretical material introduced in the specialization project is revised in this study. Nevertheless, additional literature studies were reviewed on LSWF and how the wettability alteration mechanism proposed could be modeled at field-scale.

A base case for this field-scale modeling study was created based on Eclipse conversion and synthetic data. The Eclipse conversion required insight into how a numerical model was built in Eclipse compared to GEM^{TM}, which was a time-consuming process. Optimization on well control in CMOST was done to create an optimal base case for further sensitivity. Afterwards, sensitivity analysis of LSWF modeling was done on grid refinement, timing of injection, brine concentrations and two different relative permeability models.

This thesis consists of six chapters. Chapter 2 introduces a comprehensive literature review on recovery methods, fundamental rock and fluid properties, and an introduction to LSWF. Fundamental properties such as wettability, relative permeability and capillary pressure are reviewed to understand the reactions that occur when LSW is injected. In addition, the background theory of LSWF with the associated proposed mechanisms and modeling is introduced. Chapter 3 presents the methodology which contains description of the reservoir

simulation software. The chapter also includes an extensive description of the LSWF simulation model, and LSWF screening of the Gullfaks K1/K2 segment. Chapter 4 provides the results obtained for this study together with a discussion. In Chapters 5 and 6, the conclusions and the recommendations for future work are provided.

2. Theory

This chapter covers the three stages of hydrocarbon recovery, basic principles in reservoir engineering, and an introduction to LSWF presented in literature. The fundamental petrophysical and fluid flow properties are needed to understand the complex interactions between crude oil-brine-rock (COBR) when low salinity water is injected.

2.1 Recovery Methods

The recovery methods are defined based on the production method, and the point in time they happen. Therefore, the different recovery stages are commonly subdivided into three distinct categories; primary, secondary and tertiary recovery stages (Ahmed, 2010).

2.1.1 Primary Recovery

The first recovery stage describes how natural energy present in the reservoir results in hydrocarbon displacement. The natural energy sources available are natural water drive, solution gas drive, gas cap drive, fluid and rock expansion, and gravity drainage. Artificial lift technologies (e.g. gas lifts and electrical submersible pump) are also defined as primary recovery techniques, even though they are not natural energy sources. In the first stage of recovery roughly 5-15% of the original oil in place (OOIP) is produced. Over time, the natural energy sources will start to diminish, and the oil production rate will drop. When the oil production rate is no longer feasible, external energy is needed to maintain the reservoir pressure (Mahmud et al., 2019; Willhite, 1998).

2.1.2 Secondary Recovery

Secondary recovery methods are man-made solutions created to maintain the pressure when the natural recovery mechanisms are insufficient for oil displacement. Two techniques that are frequently used are oil displacement by water or gas injection. Water flooding is the dominant secondary recovery method due to the easily accessible water and water abilities to displace

residual oil in the reservoir. In ideal situations, water will displace oil from reservoir rocks in a piston-like manner. However, water flooding efficiency is dependent on several factors such as fluid viscosities, capillary pressure, relative permeability of water and oil, reservoir rock and heterogeneity, pore size distribution, fluid saturations and well placement (Miller, 1996).

Gas can either be injected into a gas cap for pressure maintenance or applied for immiscible oil displacement. Commonly, water flooding is more efficient in recovery. Still, gas injection is often preferred in low permeable reservoirs with swelling clays, fractured and steeply dipping reservoirs. The injection of gas can also be miscible, which means that a viscosity reduction or oil welling is observed. However, miscible gas displacement is considered a tertiary recovery technique (Ahmed, 2010; Miller, 1996; Willhite, 1998).

2.1.3 Tertiary Recovery/Enhanced Oil Recovery

Tertiary recovery methods or enhanced oil recovery (EOR) are injection of fluids not commonly present in the reservoir to improve the recovery. The most prevalent methods mentioned in the literature are chemical flooding, gas injection, and thermal methods (Table 2.1). Multiple of the EOR methods that are employed today are also tested as secondary displacement methods. This also applies to water injection methods where the chemical composition is modified, such as low salinity water flooding (LSWF) (Dake, 1978; Satter & Iqbal, 2016b).

Table 2.1: Classification of an excerpt of EOR methods presented in literature (Ahmed, 2010; Nwidee et al., 2016; Satter & Iqbal, 2016b).

Thermal	Steam flooding Cyclic steam stimulation In-situ combustion Electrical heating Huff and puff
Chemical	Polymer flooding Surfactant - polymer flooding Alkaline flooding Surfactant flooding Alkaline – surfactant - polymer flooding
Gas injection	CO_2 flood (miscible and immiscible) N_2 flood (miscible)
Alternative	Foam Water alternating gas Low salinity water flooding

2.2 Wettability

Wettability is defined as "the tendency of one fluid to spread over or adhere to a solid surface in the presence of other immiscible fluids" (Craig, 1971). How much the immiscible fluids spread over or adhere is dependent on the balance of intermolecular forces and surface energy. One fluid phase usually is more strongly attracted to the rock surface and is therefore said to be the wetting phase fluid. Wettability is measured by examining the interfacial forces between oil-water-solid at force balance. This force balance is measured at the line of intersection and is expressed by the Young's equation:

$$\boldsymbol{\sigma_{so} - \sigma_{sw} = \sigma_{wo} \cos \theta} \tag{2.1}$$

The contact angle measured at the line of intersection is then:

$$cos\theta = \frac{(\sigma_{so} - \sigma_{sw})}{\sigma_{wo}} \tag{2.2}$$

Where σ_{so}, σ_{sw} and σ_{wo} are the IFT's between solid-oil, solid-water, and water-oil, and θ is the contact angle.

For angles larger than 90°, the reservoir rock is considered oil wet which means that smaller pores are imbibed with oil and larger pores are filled with water. Respectively, for angles less than 90°, the reservoir rock is considered water wet. In contrast to an oil wet state the smaller pores are filled with water. However, if the contact angle approaches 0° or 180°, the reservoir rock is strongly water wet or strongly oil wet, respectively. Intermediate wet or neutral wet is used for contact angles around 90° when two phases wet the solid equally (Figure 2.1) (Willhite, 1998).

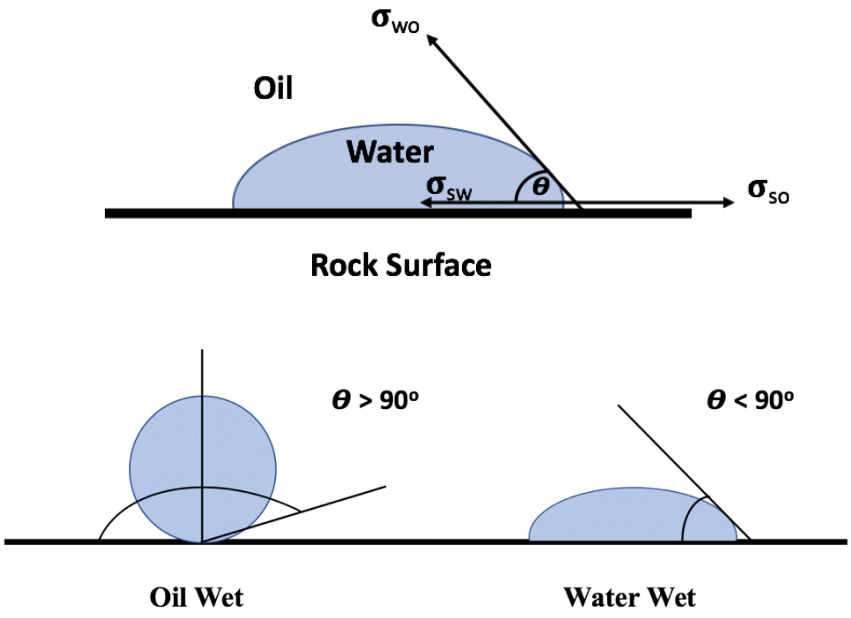

Figure 2.1: Interfacial interactions of water drop in contact with rock surface in the presence of an oil phase (Ganat, 2020).

The Amott-Harvey method can also be used to describe the wettability of oil-brine-rock system on core scale. This method qualitative method agrees with contact angle method, but it is less expensive and more convenient for experimental investigations. The Amott-Harvey method captures the amount of water imbibed into the rock during spontaneous imbibition of water, forced imbibition of water, spontaneous imbibition of oil and imbibition of oil. The ratio of the measurements during these four stages gives the value of the Amott-Harvey index, I_{AH}:

$$I_{AH} = \frac{Spontanous\ water\ imbibition}{Total\ water\ imbibition} - \frac{Spontanous\ oil\ imbition}{Total\ oil\ imbibition}$$

The index values are in the ranges from 1 to -1, were values from 0.3 to 1.0 correspond to water wet and negative values from -0.3 to -1 corresponds to oil wet. For a mixed wet system with Amott-Harvey index close to zero, this method may not be optimal because it applies to a wide range of contact angles from approximately 70^o to 110^o (Amott, 1959).

The majority of the hydrocarbon reserves are found in either sandstone or carbonate reservoir rocks. The initial wetting condition for a typical sandstone reservoir can vary in ranges from intermediate wet to strongly water wet. However, laboratory studies show that the initial wetting of a petroleum reservoir is influenced by the absence or presence of active polar components in crude oil (Craig, 1971). Sedimentary reservoirs can be considered oil-wet if polar components are physically and chemically attached to the surface, resulting in oil wet surfaces. Carbonate reservoirs are usually considered oil wet, ranging from intermediate to strongly oil wet (Donaldson & Alam, 2008).

Understanding the wetting conditions when implementing a new waterflooding method or EOR method is important because it controls the distribution of fluids and fluid flow. Wettability affects how much oil that is recovered after a waterflooding process. The residual oil saturation, S_{or}, can give a valuable indication if the waterflooding has been beneficial. Water can penetrate wat wet layers more readily, resulting in delayed water breakthrough and higher recovery compared to an oil wet reservoir. This is due to capillary and imbibition forces that determine how water flows in the pores and thereby the displacement of oil (Abdallah et al., 2007).

2.3 Effective and relative permeability

In a hydrocarbon reservoir, two or three fluids are present in the pore space. To measure the ability of one phase to flow in the presence of other fluid phases, effective permeability is defined. For multiphase flow, a generalization of Darcy's law is used:

$$q_j = k_{je} \frac{A}{\mu_j} \frac{\Delta p_j}{\Delta x} \tag{2.3}$$

Where:
j = Fluid phase
k_{je} = Effective (phase) permeability
A = Cross sectional area
Δx = Length
μ_j = Viscosity (phase)
Δp_j = Pressure difference (phase)
q_j = Flow rate (phase)

Relative permeability is a relation between absolute permeability and effective permeability. The relative permeability is a strong function of saturation of the given phase, but it is also dependent on rock properties (e.g. pore size distribution) and wettability. Note that relative permeability does not have any units and is the ratio of two permeability values (Zolotuchin, 2000):

$$k_{ri} = \frac{k_{ei}}{K}, \quad i = w, o, g \tag{2.4}$$

Where k_{ri} is the relative permeability for a given phase, k_{ei} is the effective permeability for a given phase and *K* is the absolute permeability.

Reservoir engineers try to obtain detailed knowledge about the behavior of relative permeability curves to determine reservoir performance. Scenarios such as primary recovery of oil and gas from conventional reservoirs, water flooding and chemical EOR methods are examples of

scenarios where relative permeability plays a critical role. Detailed knowledge about relative permeability is deducted from various core samples from different well locations and geologic layers to make realistic reservoir models.

For mathematical modelling of two-phase or multi-phase flow, relative permeability is normally handled as a function of saturation only. This assumption makes determination of relative permeability curves in laboratory experiments more accessible. A typical relative permeability curve when two phases are present is illustrated in Figure 2.2.

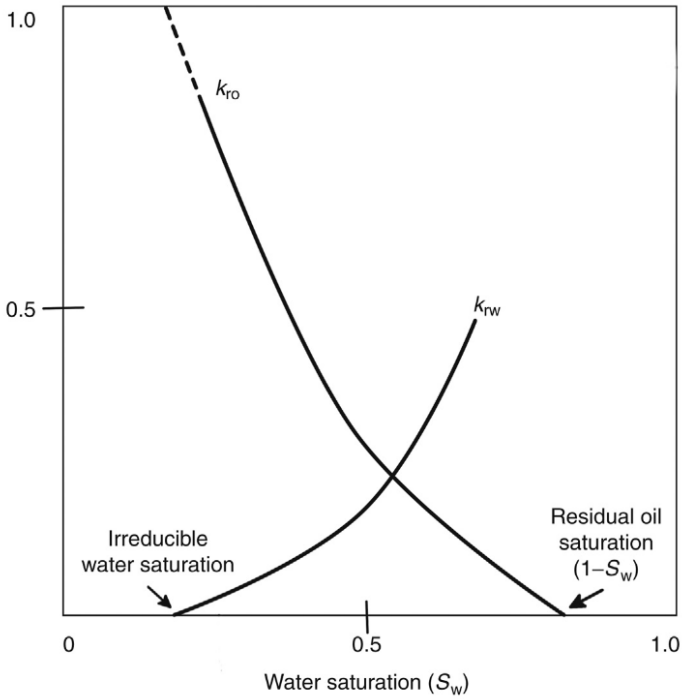

Figure 2.2: Typical two-phase relative permeability of water and oil phases (Satter & Iqbal, 2016a).

Figure 2.2 illustrates that the relationship between relative permeability and phase saturation is not linear. The water relative permeability, k_{rw}, will in general increase proportional with the water saturation. The endpoint saturation for water, $k_{rw} = 0$, is found at the irreducible water saturation, the point where water is immobile. At the other end of the scale where $k_{rw} = 1$, only water phase is flowing. The oil relative permeability behavior, k_{ro}, will decrease proportionally to water saturation. k_{ro} is found to be 0 at endpoint saturation known as residual oil saturation. When $k_{ro} = 1$, only oil phase is flowing. For values of k_{rw} and k_{ro} between 0 and 1, oil and water are flowing simultaneously (Satter & Iqbal, 2016a).

There are many papers reviewing techniques to calculate relative permeability curves from capillary pressure (Li & Horne, 2006). One of the three main approaches is Purcell (1949) which used pore distribution calculated from mercury-injection capillary pressure curves. Another approach is Burdine (1953) which developed similar equations as Purcell's method but also included the tortuosity factor. The last one is the most commonly used method today, the modified Brooks and Corey model (MBC) (Brooks & Corey, 1966). The MBC modeled can be expressed as follow:

$$k_{ro} = {k_{ro}}^{0}(S_{on})^{n_o} = {k_{ro}}^{0}\left(\frac{1 - S_w - S_{or}}{1 - S_{wi} - S_{or}}\right)^{n_o} \tag{2.5}$$

$$k_{rw} = {k_{rw}}^{0}(S_{wn})^{n_w} = {k_{rw}}^{0}\left(\frac{S_w - S_{wi}}{1 - S_{wi} - S_{or}}\right)^{n_w} \tag{2.6}$$

Where:

k_{ro}: Oil relative permeability

${k_{ro}}^{0}$: Endpoint oil relative permeability

k_{rw}: Water relative permeability

${k_{rw}}^{0}$: Endpoint water relative permeability

S_{on}: Normalized oil saturation

S_{wn}: Normalized water saturation

S_w: Water saturation

S_{or}: Residual oil saturation

S_{wi}: Irreducible water saturation

n_w: Corey exponent to water

n_o: Corey exponent to oil

The MBC model can give the qualitative acceptance of wettability by considering different values of n_o and n_w. Ideally, these curves should be found in core scale experiments performed under reservoir temperature and pressure. Still, due to the time-consuming and expensive process, this empirical-based relation can be used for simplicity.

2.4 Capillary Pressure

Capillary forces occur when two immiscible fluid phases are present in the pore space. Each of the immiscible fluids has different pressure, which is noticeable because of the curved interface between the two phases. This pressure difference is called capillary pressure and normally denoted as P_c (Dandekar, 2006). The capillary forces result from different reservoir rock and fluid properties, including surface and interfacial tension, pore size, geometry, and wetting angle (Ahmed, 2006). The definition of capillary pressure is as follows:

$$P_c = P_{nw} - P_w \tag{2.7}$$

Where P_c is the capillary pressure, P_{nw} is the pressure of the non-wetting phase, and P_w is the pressure of the wetting phase.

The three different capillary pressures can be written as:

$$P_{cow} = P_o - P_w \tag{2.8}$$
$$P_{cgo} = P_g - P_o \tag{2.9}$$
$$P_{cgw} = P_g - P_w \tag{2.10}$$

The interface for two immiscible fluids can have a curved interface described by two radii of curvatures: R_1 and R_2. The capillary pressure can then be calculated by:

$$P_c = \sigma\left(\frac{1}{R_1} + \frac{1}{R_2}\right) \tag{2.11}$$

Where σ is the interfacial tension and R_1 and R_2 are principle radii of curvature (Falode & Manuel, 2014).

In a porous rock, the pore channels can be treated as a bunch of capillary tubes. For a capillary tube where R_1=R_2=R, the interfacial curvature between two immiscible fluids can be treated as:

$$R = \frac{r}{cos\theta} \tag{2.12}$$

The capillary pressure for a cylindrical tube can then be written as (Zolotuchin, 2000):

$$P_c = \sigma\left(\frac{1}{R_1} + \frac{1}{R_2}\right) = \frac{2\sigma \cdot cos\theta}{r} \tag{2.13}$$

Capillary forces can either aid or oppose the displacement of one fluid phase by another. During water flooding, the pressure of the non-wetting phase should preferentially be higher than the wetting phase to displace oil from a porous medium. Otherwise, the capillary forces can together with frictional forces, prevent flow of oil (Dandekar, 2006).

2.5 Low Salinity Water Flooding

Bernard (1967) introduced a new EOR-method first using different sodium chloride brine and compared it with distilled water injection. The brines with NaCl content in the ranges of 1-15% did not clarify any effect on the incremental oil recovered. It was not before the NaCl concentration was around 1% that residual oil saturation was reduced. The LSWF technique did not get any major attention in the petroleum industry until Jadhunandan and Morrow (1995) and Tang and Morrow (1999) confirmed the enhancement of oil recovery with LSWF in the 1990s. Over the years, comprehensive coreflood experiments have revealed that LSWF can positively affect oil recovery in both secondary and tertiary modes (Austad et al., 2010).

LSWF has also been tested for multiple field trials to validate the potential of increased oil recovery (Abdulla et al., 2013; Al-Qattan et al., 2018; McGuire et al., 2005; Skrettingland et al., 2011; Webb et al., 2004). Webb et al. (2004) field application on LSWF revealed a significant reduction of residual oil (25-50%) when a log-inject-test was utilized. Various field trials have also been done using single well chemical tracer tests (SWCTT). One of these field observations was reported by McGuire et al. (2005), who claimed that a 6-12% increase in oil recovery was observed in a field in Alaska. British Petroleum company (BP) has also done extensive research on the Endicott field in Alaska's north slope. In the pilot area tested by BP, a decrease in residual oil saturation from 41% to 28% was observed (Seccombe et al., 2010).

Not every field trial for LSWF has revealed a significant change in oil recovery. The SWCTT field pilot in the Snorre Field indicated only low or no response from LSWF. Skrettingland et al. proposed that the lack of response from LSWF could be connected to the initial wetting state, being water wet. This means that the initial wetting is already close to optimal, and traditionally seawater will have the same effect as LSWF. Other examples of unsuccessful field application are Bastrykskoye Field in Russia and Sijan Field in Syria (Ahmetgareev et al., 2015; Katende & Sagala, 2019; Mahani et al., 2011).

Despite the increasing interest in LSWF, there is still not a consistent mechanistic explanation behind the enhanced oil recovery. The unreliable responses from the different field trials indicate that more than one mechanism is responsible for the low salinity (LS) effect. The different mechanisms proposed for LSWF will be reviewed in the following section.

2.5.1 Proposed Mechanisms

Numerous researchers have tried to find a consensus behind the additional oil produced by LSWF. The complex chemical interactions that occur between the oil-brine-rock during LSWF make the mechanism hard to comprehend. The most frequently mentioned mechanisms proposed in the literature are an increase in pH, fines migration, expansion of electrical double layer, multicomponent ionic exchange, and wettability alteration.

Multi-component Ionic Exchange (MIE)

For an originally oil-wet reservoir, polar compounds (resins and asphaltene) are bond to multivalent cations on the clay surface. These complexes can actively promote petroleum reservoirs to a more oil wet state (Lager et al., 2008; Rueslatten et al., 1994). When low salinity water with different electrolyte concentrations is injected, disturbance of the equilibrium of formation water occurs. The variations in the ionic concentration of LSW allow the divalent cations such as Mg^{2+} and Ca^{2+} to be substituted with monovalent cations. The multicomponent ion exchange initiates releasing of polar components from the clay surface, resulting in a shift in wettability towards more water wet state. The desorption or release of polar components by MIE should lead to a favorable increase in recovery (Lager et al., 2006; Pouryousefy et al.,

2016). Some of the mechanisms presented for MIE, explain how divalent cations can act as bridges between negatively charged oil and negatively charged clay surface. Cation bridging and other possible mechanisms for MIE, are presented in Figure 2.3 (Lager et al., 2008).

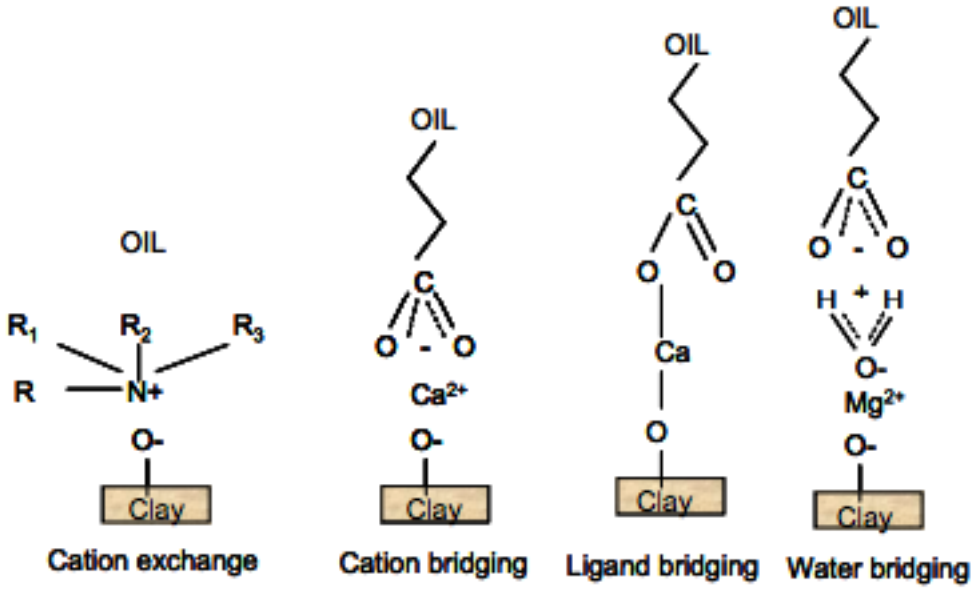

Figure 2.3: Possible mechanisms for MIE (Lager et al., 2008).

Migration of Fines

Migration of fines from a rock surface during LSWF process was suggested by Tang and Morrow (1999). The mechanism is based on the principle that when low salinity water is injected, fines with oil particles are detached from the solid surface (Figure 2.4). The release of fines could result in increased water wetness and incremental oil recovery. Furthermore, the detachment of fines can lead to pore throat blocking in originally high permeable zones. This could result in changed fluid flow paths and thereby increase the volumetric sweep efficiency. RezaeiDoust et al. (2009) proposed that the diversion of fluid flow was more important than the wettability alteration connected to fines releasement and considered the behavior of these particles to be similar to polymers.

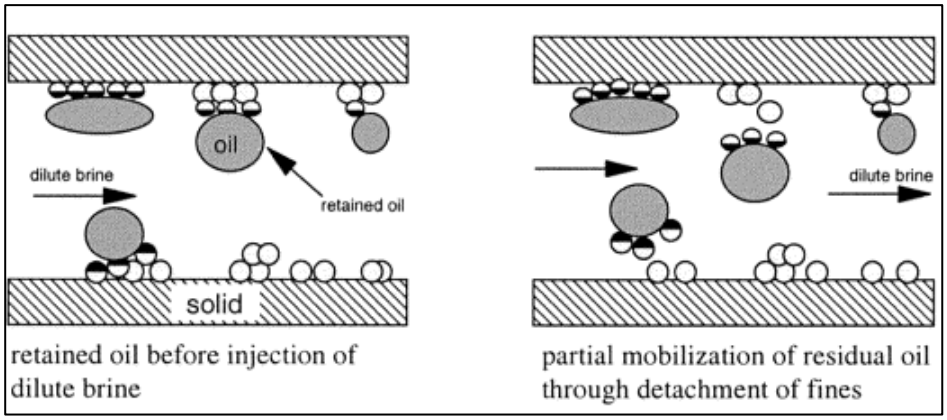

Figure 2.4: Schematic of detachment of fines during a low salinity process (Tang & Morrow, 1999).

pH Effect

McGuire et al. (2005) proposed that a pH increase, while low salinity water was injected, was the reason behind the improved oil recovery. The increase in pH led to in-situ formation of surfactant, which led to lower IFT as seen for the older method alkaline flooding. Lager et al. (2006) disagreed by revealing that in-situ surfactant could only be generated for crude oil with acid number (AN) > 0.2 mgKOH/g. Nevertheless, LS effects had been observed for a North Sea reservoir with acid number (AN) < 0.05 mgKOH/g.

Austad et al. (2010) proposed another chemical mechanism where pH effect was an essential factor for incremental recovery by LSWF. The amount of clay played a crucial role, as the imbalance between the silica or the aluminum layers could cause a negatively charged clay surface acting like a cation exchanger. Initially, pH at chemical equilibrium can be as low as 5-6 due to dissolved CO_2 and H_2S. For pH values in these ranges, the environment will start adsorption of both acidic and basic components from crude oil, but also cations such as Mg^{2+} and Ca^{2+} from the formation water. Injection of low salinity water will disturb the chemical equilibrium and desorption of Ca^{2+} cations occur. Consequently, the local pH will start to increase on the clay surface due to the substitution of Ca^{2+} by H^+. This results in a fast reaction between OH^- and adsorbed acid/base organic material. Both acidic and basic crude oil components will be detached from the clay surface, turning the rock into a more water wet state.

Double-layer Expansion

Double-layer expansion (DLE) was suggested by Ligthelm et al. (2009) to be responsible for the wettability alteration process in sandstone reservoirs during LSWF. Reduced screening potential of the cations was observed when LSW with reduced electrolyte content and a reduced number of multivalent cations was injected. This led to the expansion of the electrical double layers surrounding the oil and clay interface, resulting in increased electrical potential or zeta potential on the rock/brine and oil/brine interface. The increased magnitude of zeta potential resulted in increased electrostatic repulsion force between oil particles and clay surface. Once the repulsive force conquered the binding force, oil particles were desorbed from the clay surface and less of the rock surface was coated in oil. This in turn, resulted in a wettability alteration for the reservoir rock towards more water wet condition (Figure 2.5) (Ligthelm et al., 2009).

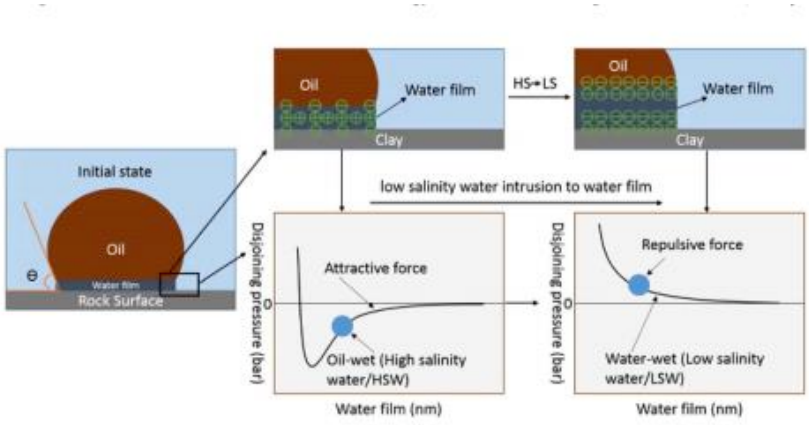

Figure 2.5: The result of double layer expansion when either low salinity water or high salinity water is injected (Zhang et al., 2020).

Wettability Alteration

Wettability alteration is considered the most accepted mechanism controlling the effect of LSWF (Austad et al., 2010; Lager et al., 2006; Ligthelm et al., 2009; Morrow et al., 1998). However, the exact physical explanation behind the wetting modification is not yet settled. Wettability alteration for LSWF in sandstone rocks was first reported by Tang and Morrow (1999) and Lager et al. (2007). They related the wettability modification to the composition of injected brine, presence of clay, oil composition, and composition of formation water. Several

experimental investigations on LSW brine a few years later, revealed that it can affect the endpoints and shape of relative permeability curves (Fjelde et al., 2012; Rivet, 2009; Webb et al., 2004). Consequently, the wettability alteration during LSWF could result in lower water relative permeability and higher oil relative permeability (Dang et al., 2016).

The most reliable physical explanation for the wettability change in an oil-brine-rock (OBR) system is mainly due to ion exchange between the injected water and formation water along with dissolution/precipitation reactions. Regarding this physical explanation, the wettability alteration can be modeled by a shift in relative permeability curves due to ion exchange and geochemical reactions (Dang et al., 2016).

2.5.2 Screening Criteria for LSWF

LSWF is considered a rising method to improve oil recovery from reservoirs today. LSWF is beneficial in many ways, including favorable incremental recovery, compatibility with other EOR methods, simple implementation onshore and offshore, and being environmentally friendly. Like any other EOR technique, it is crucial to conduct a comprehensive study of the reservoir before implementing LSWF. A summary of different screening criteria for LSWF is given in Table 2.2 (Dang et al., 2015b).

Laboratory and field studies have detected incremental oil recovery for LSWF in sandstone and carbonate reservoirs (Al-Attar et al., 2013; Cissokho et al., 2010; Hamouda & Gupta, 2017; Morrow & Buckley, 2011). Since the wettability alteration is considered the main mechanism behind LSWF, the factors affecting the process need to be considered before the implementation of LSWF in a new reservoir.

There is an agreement in literature that the optimal sandstone for LSWF must contain the right amount of clay. The presence of clay was first emphasized by Tang and Morrow (1999). However, they did not detail what type of clay that played the most important role. Lager et al. (2007) proposed that kaolinite played a crucial role in additional oil recovery for LSWF. Contrarily, Austad et al. (2010) displayed that kaolinite had the least effect on incremental oil recovery due to the low cation exchange capacity. Most of the experiments found in the

literature have been conducted with kaolinite clay, consequently it is hard to conclude what the optimum clay characteristics are for LSWF implementation (Chavan et al., 2019).

Table 2.2: Screening criteria for LSWF (Dang et al., 2015b).

Property	**Preferred**
Reservoir	• Sandstone • Carbonate
Crude Oil	• Contains polar components
Clay Minerals	• Sufficient amount of clay • Medium sand with high cation exchange capacity • High porosity and permeability
Reservoir Minerals	• Calcite • Dolomite
Formation Water	• Contains divalent cations such as Ca^{2+} and Mg^{2+}
Initial Wettability	• Oil wet or mixed wet
Injection Fluid	• Lower salinity than formation water • Must contain divalent ions • Must promote the adsorption of divalent ions.

Dang et al. (2015b) investigated 10 different geological realizations for the same clay distribution but with different clay content. Their observations were that higher clay content in the reservoir can increase the benefit of using LSW (Figure 2.6). These observations were also consistent with several core flooding experiments and pilot tests done by Jerauld et al. (2008). Since the presence of clay has a vital role in the wettability alteration process, extensive core analysis and well log interpretation must be done before implementation for the relevant field. Further investigations based on both types and amounts of clay could also provide a more precise screening criterion for LSWF.

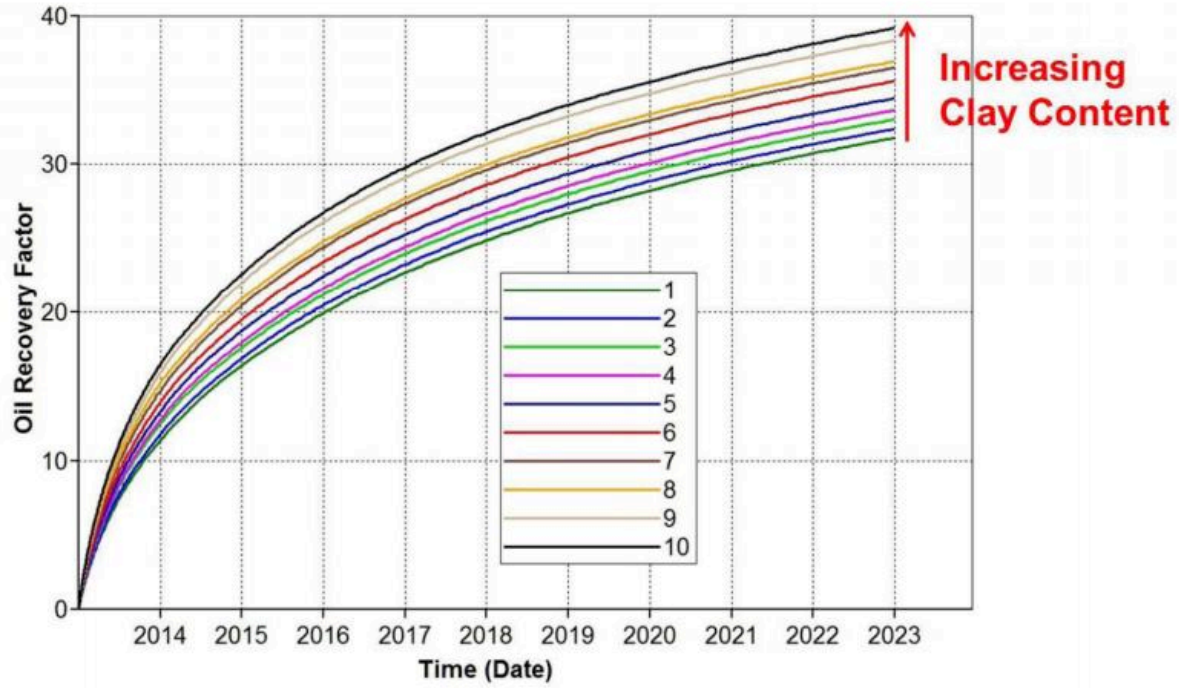

Figure 2.6: Oil recovery factor for increasing clay content (Dang et al., 2015b).

The initial wetting state of the reservoir is also mentioned as an important criterion. To observe advantageous incremental oil recovery for LSWF, the initial wetting state should be from oil wet to mixed wet. Reservoir candidates for LSWF should not be too strongly water wet, since the modification of the relative permeability curves is very small which can result in unsuccessful LSWF implementation. For reservoir environments which are already strongly water wet, seawater flooding or other EOR techniques could be more beneficial (Dang et al., 2015b).

Another criterion mentioned in literature is the composition and presence of formation water. No LS effect is seen for dry output cores saturated with 100% oil. In addition, divalent ions such as calcium (Ca^{2+}) and magnesium (Mg^{2+}) must be present for clastic rocks to observe wettability alteration. In cases where divalent cations are lacking, desorption of calcium can occur, which can promote adverse wettability alteration (Dang et al., 2015b; Strand et al., 2016).

There is limited evidence related to the correlation of oil properties such as viscosity or API gravity and LSWF benefits. However, the oil composition indirectly affects both the enhanced oil recovery and the physical properties of the oil. There is a mutual agreement that the crude

oil composition must contain polar components to observe any additional oil recovery with LSWF (Chavan et al., 2019; Fjelde et al., 2012; Fjelde et al., 2014). Laboratory testing on synthetic or depolarized oils has not given any additional oil with LSWF (Austad et al., 2010).

Based on the literature reviewed it is hard to interpret the exact guideline for LSWF screening criteria. Supplementary sensitivity analysis should be performed to study which of the criteria have the most impact on LSWF. It is also worth mentioning that different reservoirs have unique ionic environments that are challenging to establish. This is mainly due to the natural reactions and disruptions by human interventions that affect the formation water's ionic composition. A detailed screening process must be carried out to determine the LSWF potential for a reservoir candidate (Dang et al., 2015b).

2.5.3 Numerical Modeling of LSWF

Numerical modeling of LSWF has occasionally been mentioned in literature for the last two decades. Jerauld et al. (2008) presented the first numerical model of LSWF based on a modified Buckley and Leveret water flooding model. The salinity was modeled as a single-lumped component which was a function of relative permeability, capillary pressure, viscosity, and aqueous phase density. However, only a simple empirical dependence was used to model residual oil saturation. A comparable LSWF model was presented by Wu and Bai (2009) for porous and fractured sandstone reservoirs.

Sorbie and Collins (2010) proposed a simple LSWF pore-scale model connected to the multicomponent ion exchange (MIE) and expansion of electrical double layer mechanisms. These mechanisms led to desorption of organic compounds and thereby decrease in residual oil. However, the pore-scale model proposed was based on multiple predictions that implied that supplementary experiments were vital to confirm the result.

Omekeh et al. (2012) presented a mathematical model where multicomponent ion exchange and mineral dissolution/precipitation was included. They investigated how these mechanisms would affect the pH and the releasement of divalent cations. The numerical model considered a simple two-phase flow of water and oil. The water phase consisted of Na^+, Ca^{2+}, Mg^{2+} and

SO_4^{2-} ions involved in multicomponent ion exchange. In addition, the components were time-dependent, based on mineral dissolution/precipitation reactions of calcite, magnesite, and sulphate. The main low salinity mechanism was a fast ion exchange process on the clay surface, resulting in releasement of cations. The desorption of cations was implemented numerically as a change in relative permeability that led to an increase in oil mobility.

Dang et al. (2013) tested a new compositional model using the simulator GEM^{TM} that captured all of the geochemical reactions that occur during LSWF. LSWF was modeled based on the consensus that wettability alteration towards increased water wetness was the main mechanism behind the additional oil recovery. The physical explanation behind the wettability alteration was that the ion exchange process initiated the adsorption of divalent ions, which facilitated mineral dissolution and changed the formation water ionic composition. It was assumed that this geochemical process caused a change in the wetting condition towards a more water wet state. Dang et al. (2013) validated the new core-scale model with experimental data and compared it with another geochemistry software, PHREEQC. Dang et al. (2016) extended the geochemical core-scale model to field-scale for the Brugge field. This model is the origin of the LSWF model presented in this thesis. In the next chapter, the field-scale LSWF model is presented using the compositional EOS simulator GEM^{TM}.

3. Methodology

The first section in this chapter includes a short description of the reservoir simulator GEM™, the PVT- software WinProp and the analysis tool CMOST™ that are offered by CMG. After the software introduction, a brief description of Eclipse conversion to GEM™ is provided. The following sections include an extensive description of the LSWF simulation model and the screening criteria for the geological model evaluated for this thesis.

3.1 Reservoir Simulation Software by CMG

3.1.1 GEM™ - Compositional and Unconventional Simulator

GEM™ is an equation of state (EOS) compositional and unconventional simulator optimal for simulating EOR methods such as chemical flooding, miscible displacement, and thermal recovery. GEM™ is one of the three reservoir simulation applications offered by the software company Computer Modelling Group Ltd (CMG). Additional feature available in GEM™ is that it can be run in three different modes: explicit, fully implicit, and adaptive implicit. In addition, GEM™ can calculate the phase equilibrium compositions and the different densities of the oil and gas phase by either Peng-Robinson or Soave-Redlich-Kwong equation of state (GEM, 2019).

Since wettability alteration is considered the main mechanism behind LSWF, it is important to include it in the simulation model. GEM™ is optimal for capturing ion exchange reactions, intra-aqueous reactions, mineral dissolution/precipitation, and wettability alteration during LSWF. In GEM™, it is possible to choose different intra-aqueous reactions and mineral dissolution/precipitation based on the composition of the formation water and the rock properties considered. It is also possible to define several relative permeability tables for the different rock types where each table corresponds to an interpolant parameter (GEM, 2019; Sierra et al., 2020).

To build a simulation input file for GEM™, the software tools Builder or text editor cEDIT is used. Builder consists of 8 sections, including I/O control, reservoir properties, components,

rock-fluid, initial conditions, numerical, geomechanics, and well & recurrent. After running the input file in GEM^{TM}, three output files are created; output restart file (RST), output Simulation Results File (SRF), and an output file (Figure 3.1) (GEM, 2019).

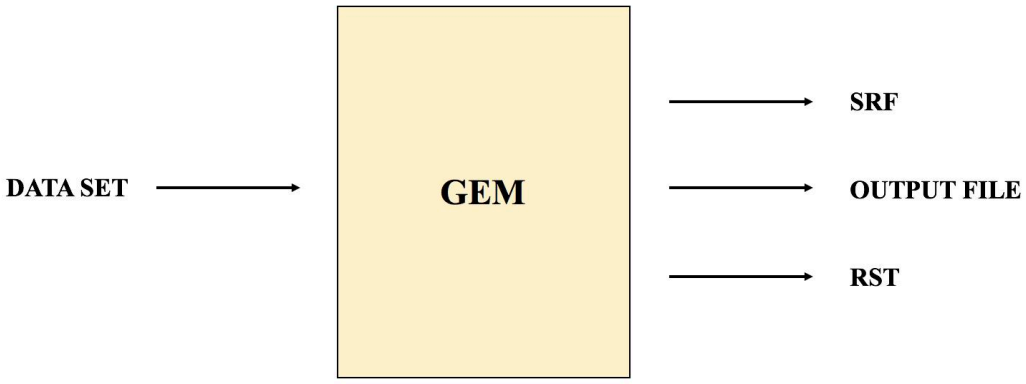

Figure 3.1: Illustration of the different output files created in GEM^{TM} (GEM, 2019).

3.1.2 WinProp – Fluid Property Characterization Tool

WinProp is a pVT-software that is included in CMG's reservoir simulator package. The pVT-software can be used for fluid characterization, fraction splitting, lumping of components, matching laboratory data through regression, phase diagram construction and much more. It can generate compositional fluid models that can be used in GEM^{TM}, or black oil tables that can be used in the IMEX reservoir simulator. WinProp has an extensive library of components that can be used if critical properties of the components are not available in the experimental data. Calculation of the viscosity model can be done by either the Jossi, Stiel and Thodus (JST) correlation or by the Pedersen correlation.

The aqueous model needed for polymer flooding, surfactant flooding, and LSWF can also be configured in the pVT-software. WinProp has the possibility of implementing the multicomponent ion exchange, intra-aqueous, and mineral dissolution/precipitation rate reactions that occur during LSWF. The relevant geochemical reactions can be found in Geo-chemistry databases (WinProp, 2019).

3.1.3 CMOST-AI - Intelligent Optimization and Analysis Tool

The software CMOST™ works with CMG simulators to perform tasks such as assisted history matching, optimization, sensitivity analysis, and uncertainty assessment. CMOST™ can strengthen business decisions for oil companies by using artificial intelligence optimization methods. The calculation engines that are available in CMOST™ are CMG Designed Exploration and Controlled Evolution (DECE), CMG Bayesian Engine, Particle Swarm Optimization (PSO), Differential Evolution (DE), and Latin Hypercupe. By using these available features in CMOST™, the engineers can gain unique insight into how the reservoir behaves (CMOST-AL, 2019).

The history matching functionality can be used to calibrate simulation models with production history data effectively. Optimization can be done to improve development strategies by changing different parameters such as well placement, injection rate, oil production constraints, etc. The objective function during optimization is often physical quantities such as cumulative oil produced, oil recovery factor, or monetary values such as NPV. Moreover, CMOST™ can do a comprehensive sensitivity analysis of the effect of the most influential parameters on the objective functions. Experiments created by the engine chosen are simulated for different data ranges of the parameters selected. Afterward, CMOST™ generates graphical plots that make it easier to extract useful information about the parameters Figure 3.2. The engines available can also calculate how the interactions between the parameters affect the objective functions (CMOST-AL, 2019).

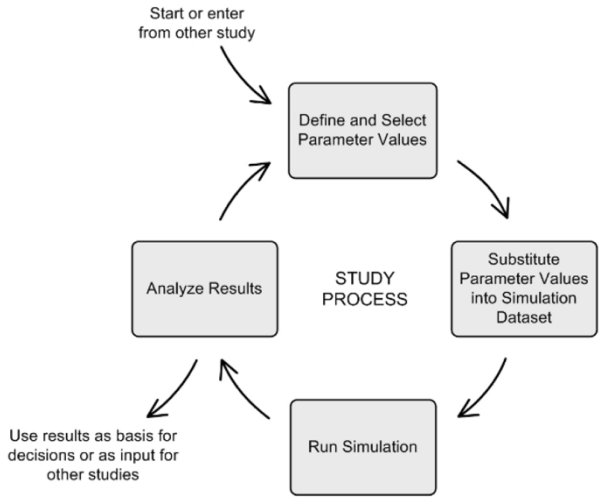

Figure 3.2: Illustration of the CMOST study process (CMOST-AL, 2019).

3.2 Eclipse Conversion

An Eclipse conversion was done to be able to use real geological data from Gullfaks K1/K2 segment. Since the original reservoir model was an Eclipse file (E100), the application DataImporter by CMG was used to convert the datafile to GEM™. DataImporter has automated Eclipse conversion that makes the conversion workflow easier. By DataImporter, an IMEX™ file is created, which is a three-phase black-oil simulator. To convert the data file to GEM™, the file must be opened in builder where conversion of simulator type is available.

The sections build-up in Eclipse and GEM™ are described in Table 3.1. Out of the sections included in the Eclipse file, the grid section is the most similar to GEM™ (Table 3.2). Nevertheless, significant adjustments need to be made to ensure that the grid section is appropriately converted (DataImporter, 2019).

Table 3.1: Overview of sections in Eclipse and GEM™ (DataImporter, 2019).

ECLIPSE 100 SECTIONS	GEM SECTIONS
RUNSPEC	
GRID	GRID
EDIT (OPTIONAL)	
PROPS	MODEL+ROCKFLUID
REGIONS (OPTIONAL)	
SOLUTION	INITIAL
SUMMARY	
	NUMERICAL
SCHEDULE	RUN

Table 3.2: The different keywords in the grid section for Eclipse and GEM (DataImporter, 2019).

ECLIPSE 100 KEYWORDS	GEM KEYWORDS
COORD	COORD
ZCORN	ZCORN
DX, DY, DZ	DI, DJ, DK
PORO	POR
PERMX/Y/Z	PERMI/J/K
NTG	NETGROSS
ACTNUM	NULL
MULTX/Y/Z	TRANSI/J/K
NNC	SCONNECT

The geological properties such as porosity, permeability, and transmissibility multipliers had to be adjusted to capture the desired result. In addition, DataImporter did not correctly convert the rock-fluid model, initial condition, and well & recurrent data sections. It should be noted that the black oil fluid model needs to be replaced with compositional fluid data. The sections that are not converted by DataImporter are configured manually by the data conveyed in section 3.3.

3.3 Low Salinity Water Flooding Simulation Model

The geological model used in this study is a slightly modified version of the original model of the Gullfaks K1/K2 segment as briefly explained above. Compared to the original model, the number of production wells is changed from 5 to 3 for the base case to simplify the simulation model. In addition, the topography is illustrating a mirror image of the original model due to the converted coordinate arrays. The fluid model consists of oil composition data from a Statfjord core, and water analysis from Fjelde et al. (2012) and geochemical reactions. This model is constructed to investigate a numerical field-case for LSWF, by using some real geological data from Gullfaks.

3.3.1 Reservoir Description

A three-dimensional field-scale LSWF model was developed in GEM^{TM} by CMG. The reservoir model is based on a corner point grid with 45, 75, 17 grids in I, J, and K-direction, respectively. There are 6 active wells, where 3 injectors and 3 producers are placed as indicated in Figure 3.3. The injector wells are controlled by a maximum BHP of 350 bar and a maximum water injection rate of 1500 Sm^3/d. The production wells are controlled by a minimum BHP of 300 bar and oil production rate of 2000 Sm^3/d.

The formation water occupies the bottom layers, and oil occupies the upper layers (Figure 3.4). In addition, the reservoir permeability is higher in the upper layers compared to the layers closer to the bottom (Figure 3.5). The transmissibility multiplier defines that the vertical permeability in k-direction is 10 times less than the horizontal permeability for most of the layers, TRANSK= 0.1. Other basic fluids and rock properties included in the reservoir description are defined in Table 3.3.

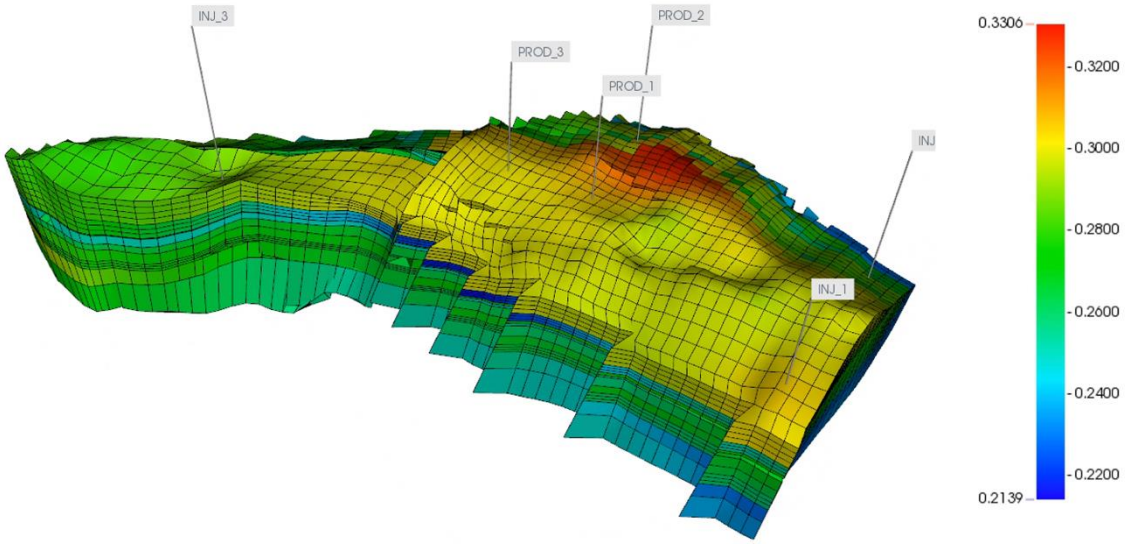

Figure 3.3: Porosity distribution for the field-scale LSWF model.

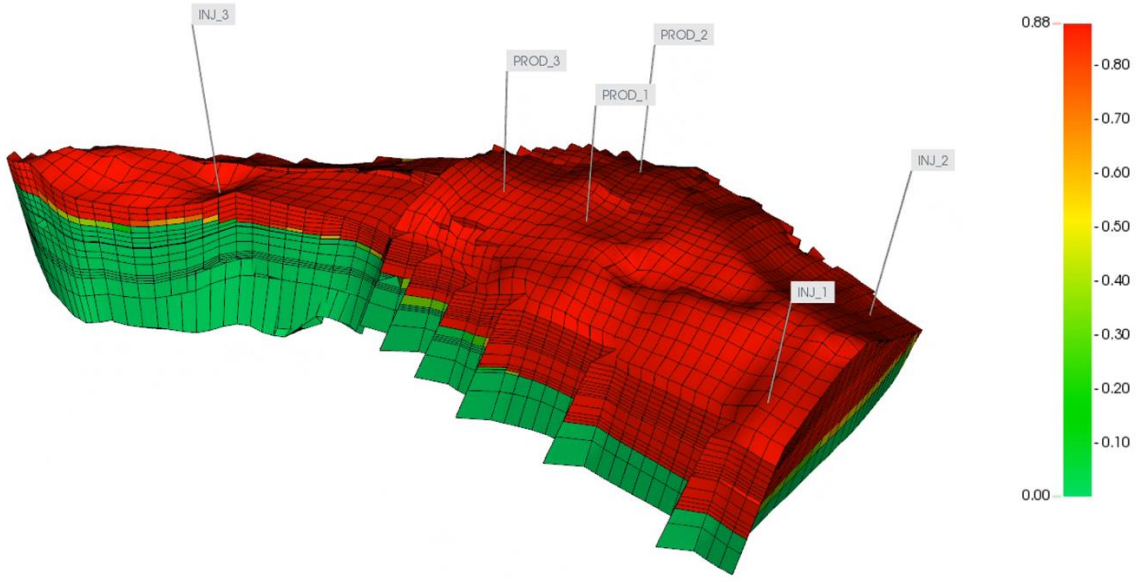

Figure 3.4: Oil saturation distribution for the field-scale LSWF model.

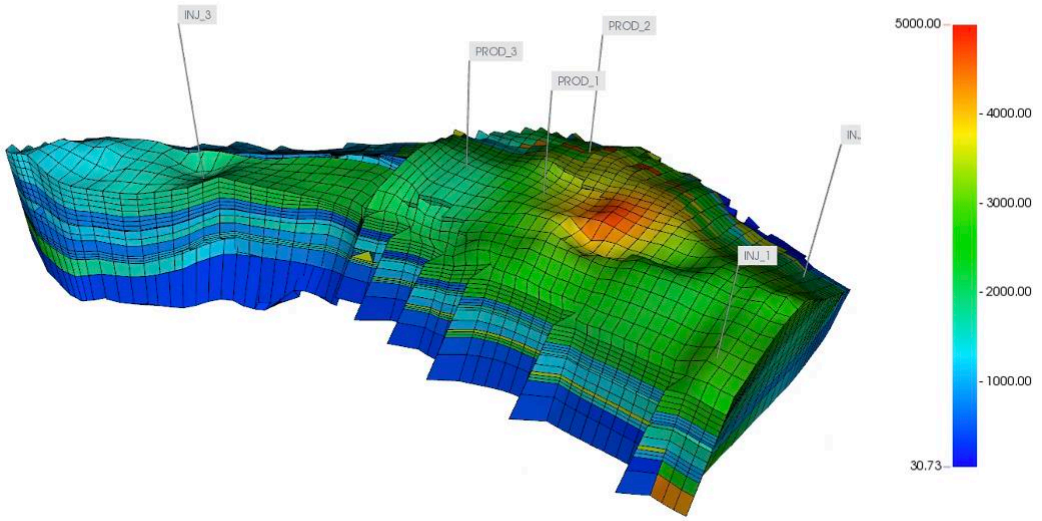

Figure 3.5: Permeability distribution in I-direction for the field-scale LSWF model.

Table 3.3 Modified rock and fluid properties used for the K1/K2 segment simulation model in GEM™.

Property	Value
Corner point grid	45x75x17
Porosity	0.25 – 0.33
Permeability (D)	0.2 – 5
Rock type	Sandstone
Mineralogy composition	Calcite and Magnesite
Initial water saturation	0.123
Initial oil saturation	0.87
Reservoir pressure (bar)	320
Reservoir temperature (°C)	71.1

3.3.2 Fluid and Rock Model

The difference between a compositional reservoir simulator such as GEM^{TM} and Eclipse 100 reservoir simulator is how they handle fluid composition. The fluid model in the original Gullfaks Eclipse file is a black oil pVT-model, meaning that the hydrocarbon only consists of two components, oil and gas, dependent on pressure and the total composition. Moreover, the black oil pVT-model is utilized as input in forms of tables.

The compositional simulator GEM^{TM} allows for including more components, and the changes to the composition of the fluid phases are based on the Peng-Robinson equation of state or the Soave-Redlich-Kwong equation of state. Compositional simulators are generally more computationally demanding than black oil simulators. Therefore, selection of reduced number of components and parameters can be generated in WinProp or other pVT- software.

The crude oil composition used in WinProp to generate a compositional fluid model for Gullfaks K1/K2 segment is illustrated in Table 3.4. The oil composition needed to contain a small amount of CO_2, because injection of LSW without CO_2 can give inaccurate results. The oil composition data is based on gas chromatography done on a Statfjord core. To reduce CPU time for the simulation model, the number of components describing the oil phase were lumped to 8 (Table 3.5). The lumped components were used as input for the crude oil model in the GEM^{TM} simulator.

Table 3.4: Oil composition data from a Statfjord core found in the Gullfaks- database.

Component	Mol [%]
N2	1.058
CO2	0.177
C1	46.109
C2	5.935
C3	4.415
i-C4	0.943
n-C4	2.419
i-C5	1.035
n-C5	1.410
C6	2.218
C7	3.952
C8	4.579
C9	3.207
C10+	22.543
Sum	**100.000**

Table 3.5: Lumped components of the crude oil model.

Lumped Components	Mol [%]
CO2	0.177
N2 - C1	47.167
C2	5.935
C3	4.415
C4 - C6	8.025
C7 - C12	17.778
C13 - C17	6.689
C18+	9.814
Sum	**100.00**

The modeling of LSWF using GEM™ assumes that a water analysis is done on the formation water in addition to representative sandstone analysis. The rock and water analysis determines the aqueous and mineral reactions that need to be included in the model. For the K1/K2 segment, no water analysis is available and therefore water analysis from Fjelde et al. (2012) is used with some modifications. Since the dissolution/precipitation of calcite and magnesite is very important and will affect the results during LSWF, both mineral reactions are included in the model. An overview of the aqueous and mineral reactions included in the model is presented in Table 3.6.

Table 3.6: Mineral reactions and aqueous reactions included in the simulation model.

Aqueous Reactions
$CO_2\,(aq) + H_2O \leftrightarrow H^+ + HCO_3^-$
$H^+ + OH^- \leftrightarrow H_2O$
Mineral Reactions
$Calcite + H^+ \leftrightarrow Ca^{2+} + HCO_3^-$
$Magnesite + H^+ \leftrightarrow Mg^{2+} + HCO_3^-$

3.3.3 Screening Criteria for Gullfaks K1/K2 segment

To validate if the Gullfaks K1/K2 segment is a good candidate for LSWF, the screening criteria in section 2.5.2 are reviewed. Based on the crude oil criteria, the oil composition contain polar components. Polar components are acid and base materials in crude oil and act like surface active materials retained onto the reservoir rock during LSWF (Mokhtari & Ayatollahi, 2019). Based on the pVT-data used in this study the oil composition consists of typical naphthenic acids considered as simple polar components.

The formation water has a salinity level of 45 000 ppm, which is considerably high compared to LSWF, which is usually in the ranges from 500-5000 ppm. This indicates that injection brine will have considerably lower salinity than formation water, meaning that the criteria are fulfilled. Furthermore, lack of analysis of the formation water makes the determination of divalent ions present challenging to examine.

The initial wetting of the reservoir is an important factor that affects the amount of incremental oil produced during an LSWF process. As mention in section 2.5.2 a strongly water wet reservoir may not be a good candidate for LSWF implementation. The segment K1/K2 is considered water wet, but LSWF can still alter the wettability towards a strongly water wet reservoir. The expected incremental oil for the Gullfaks segment is therefore less than for an oil wet to a mixed wet reservoir. In this study for the LSWF model, initial oil wet-like relative permeability curves were chosen as base case to get a preferable sensitivity analysis. Later in the thesis, sensitivity analysis on representative relative permeability curves for a sandstone reservoir is investigated.

Another criterion that is mentioned in section 2.5.2 is the presence of clay. Clay type is one of the most discussed topics, and it is a mutual understanding that clay highly affects the wettability alteration process. The amount of clay present in the segment can be identified from gamma ray logging measurements that respond to potassium and thorium content variation in the formation. Gamma ray log-plots for the given wells in the Gullfaks K1/K2 segment was created by Mkilindi (2019). Based on the different full-log plots Mkilindi (2019) evaluated, the presence of clay is high in the formation.

Despite that some of the screening criteria are fulfilled for LSWF, K1/K2 is lacking representative data for geochemical modeling of LSWF. A water analysis on cores needs to be completed to guarantee that the formation water consists of divalent ions. If the divalent ions such as calcium and magnesium do not exist in the reservoir, the LSWF will have no effect. In addition, representative relative permeability data is essential to model the wettability alteration that occurs during LSWF. In this study, only the geological data is used from the K1/K2 model to build a field-scale LSWF model.

3.3.4 Geochemical Model

In this section, the geochemical reaction models captured in GEM^{TM} for LSWF are presented. These include homogeneous reactions (intra-aqueous reactions) and heterogeneous reactions consisting of multiple ion exchange and mineral precipitation/dissolution. During LSWF the geochemical reactions is considered the main contributors to a change in wettability toward

increased water wetness. Since the main mechanism considered for this LSWF model is the wettability alteration mechanism, these geochemical reactions are essential to include (Adegbite et al., 2017; Dang et al., 2013).

Intra-aqueous and Mineral Reactions

The aqueous reactions included in the LSWF model are reversible and instantaneous. Based on Bethke (2007) assumptions, equilibrium constants are used in modeling of chemical reactions. The chemical equilibrium constant for the species and ions in the aqueous phase is calculated as follow:

$$K_{eq} = \frac{\alpha(H^+)\alpha(HCO_3^-)}{\alpha\big(CO_2(aq)\big)\alpha(H_2O)} \tag{3.1}$$

Where $\alpha(.)$ is the activity of species in the aqueous phase. The relationship between the activity of species, α_i, and the molality, m_i is given in (3.2):

$$\alpha_i = \gamma_i m_i \tag{3.2}$$

Where γ_i is the activity coefficient of the species. The value of $\alpha(CO_2(aq))$ is equal to its molality, meaning that the activity coefficient, γ_i is equal to 1. For non-ideal solutions, the activity coefficient must be calculated through models such as the Davies equation or B-dot model. In GEM^{TM}, the activity coefficients are calculated using the B-dot model (Bethke, 2007; Dang et al., 2015a).

Furthermore, reactions between the aqueous species and the reactive minerals are taken place during LSWF. For reactive minerals that are not in state of equilibrium with the ions in aqueous phase, precipitation or dissolution will occur. These reactions are slower than the intra-aqueous reactions. The rate of mineral dissolution/precipitation is calculated as (GEM, 2019):

$$r_\beta = \hat{A}_\beta k_\beta \left(1 - \frac{Q_\beta}{K_{eq,\beta}}\right), \beta = 1, \ldots., R_{mn} \tag{3.3}$$

Where different variables/constants of mineral reaction β is:

r_β = Reaction rate [mol/(m^3/s)]

$\hat{A}_\beta$ = Reactive surface area [m^2/m^3]

k_β = Reaction rate constant [mol/m^{2}s]

$K_{eq,\beta}$ = Chemical equilibrium constant

Q_β = Activity product

Rmn = Number of mineral reactions

The chemical equilibrium constant, $K_{eq,\beta}$, can be found in literature (Kharaka et al., 1988). The $Q_\beta/K_{eq,\beta}$ is termed as the saturation index of the reaction. The saturation index determines that precipitation occurs if $Q_\beta/K_{eq,\beta} < 1$ and dissolution occurs if $Q_\beta/K_{eq,\beta} > 1$. The reaction rate constant, k_β, can be calculated as follow for different temperature T (GEM, 2019):

$$k_\beta = k_{0\beta} \exp\left[-\frac{E_{a\beta}}{R}\left(\frac{1}{T}-\frac{1}{T_0}\right)\right] \tag{3.4}$$

Where:

$E_{a\beta}$ = Activation energy (J/mol)

$k_{0\beta}$ = Reaction rate constant at reference temperature [mol/m^{2}s]

T_0 = Reference temperature (K)

T = Temperature (K)

R = Universal gas constant (8.314 J/(mol K)

Ion Exchange Reactions

Initially, there is a thermodynamic equilibrium between the ions in the formation water and ions adsorbed to the clay surface. Disruptions of chemical equilibrium by LSW will cause ion exchange reactions to arise (GEM, 2019). Dang et al. (2016) presented a much better history match of Fjelde et al. (2012) LSWF experiment when ion exchange reactions, cation exchange capacity of clays, volume fraction of rock, the concentration of the cation, and the selectivity coefficients were introduced. The two most common ion exchange reactions where X denotes the clay mineral in the reservoir rock (calcite and magnesite) are given as:

$$Na^+ + \frac{1}{2}(Ca - X_2) \leftrightarrow \frac{1}{2}Ca^{2+} + (Na - X) \tag{3.5}$$

$$Na^+ + \frac{1}{2}(Mg - X_2) \leftrightarrow \frac{1}{2}Mg^{2+} + (Na - X) \tag{3.6}$$

In this thesis, Ca^{2+}/Mg^{2+} are taken up by the exchanger and Na^+ is released from the clay surface when low salinity water is injected, similar to what Dang et al. (2016) proposed. For high salinity water flooding the reverse reactions occur. Similar to chemical equilibrium reactions, ion exchange reactions are identified with equilibrium constants defined as (GEM, 2019):

$$K_{Na/Ca} = \frac{[\alpha(Ca^{2+})]^{0.5}\ \alpha\ (Na - X)}{\alpha(Na^+)[\alpha(Ca\ -\ X_2)]^{0.5}} \tag{3.7}$$

$$K_{Na/Mg} = \frac{[\alpha(Mg^{2+})]^{0.5}\ \alpha(Na - X)}{\alpha(Na^+)\ [\alpha(Mg - X_2)]^{0.5}} \tag{3.8}$$

where α is the activity. The activity coefficients such as $[Ca - X_2]$, $[Na - X]$ and $[Mg - X_2]$ can be difficult to evaluate, therefore selectivity coefficient is often used instead of equilibrium constant. By rewriting equations (3.7) and (3.8), the selectivity coefficients can be calculated as:

$$K'_{Na/Ca} = \frac{\zeta(Na - X)[m(Ca^{2+})]^{0.5}}{[\zeta(Ca - X_2)]^{0.5} m(Na^+)} \cdot \frac{[\gamma(Ca^{2+})]^{0.5}}{\gamma(Na^+)} \tag{3.9}$$

$$K'_{Na/Mg} = \frac{\zeta(Na - X)[m(Mg^{2+})]^{0.5}}{[\zeta(Mg - X_2)]^{0.5} m(Na^+)} \cdot \frac{[\gamma(Mg^{2+})]^{0.5}}{\gamma(Na^+)} \tag{3.10}$$

Where $\zeta[Ca - X_2]$, $\zeta[Na - X]$ and $\zeta[Mg - X_2]$ correspond to the ion exchange equivalent fraction of Ca^{2+}, Na^+ and Mg^{2+} on the exchanger, respectively, and m is the molality and γ is activity coefficient. The ion exchange equivalent fractions represent the exchangeable amount

of Ca^{2+}, Na^{+} and Mg^{2+} on the clay surface. In GEM^{TM}, the property CEC (Cation exchange capacity) is also connected to the exchanger. The CEC parameter indicates the amount of ions that can be adsorbed onto the clay surface. GEM^{TM} expresses moles for all components as moles per grid block bulk volume. Consequently, the total moles of the species $[Na-X]$, $[Ca-X_2]$ and $[Mg-X_2]$ are represented by VN_{Na-X}, VN_{Ca-X_2} and VN_{Mg-X_2}. Where V is the total grid block bulk volume and N is total number of moles. The following equation must be fulfilled for a given value of CEC in the grid block:

$$VN_{Na-X} + 2VN_{Ca-X_2} + 2VN_{Mg-X_2} = V\varphi(CEC) \tag{3.11}$$

Or

$$N_{Na-X} + 2N_{Ca-X_2} + 2N_{Mg-X_2} = \varphi(CEC) \tag{3.12}$$

where the ion exchange equivalent fractions for the given species can be calculated by:

$$\zeta[Na-X] = \frac{N_{Na-X}}{\varphi(CEC)} \tag{3.13}$$

$$\zeta[Ca-X_2] = \frac{N_{Ca-X_2}}{\varphi(CEC)} \tag{3.14}$$

$$\zeta[Mg-X_2] = \frac{N_{Mg-X_2}}{\varphi(CEC)} \tag{3.15}$$

3.3.5 Relative Permeability Curves

There is a mutual understanding that the wettability alteration towards increased water wetness is the main mechanism behind the incremental oil recovery during LSWF. In GEM^{TM}, this effect is modeled by a wettability shift as seen in Figure 3.6. Two sets of relative permeability tables are defined under the ROCK-FLUID section under the keyword KRINTRP 1-2. The first one corresponds to the high salinity curves (oil wet), and the second one corresponds to the low salinity curves (water wet). The relative permeability curves are usually based on core flooding

experiments done on representative cores from the field. Since the K1/K2 segment lacks representative data, modified relative permeability data is used to present a simulation case optimal for further sensitivity analysis. Therefore, the endpoints and curvature for the relative permeability curves are modified to demonstrate that LSWF reduces the S_{or} in a porous rock (Almeida da Costa et al., 2021).

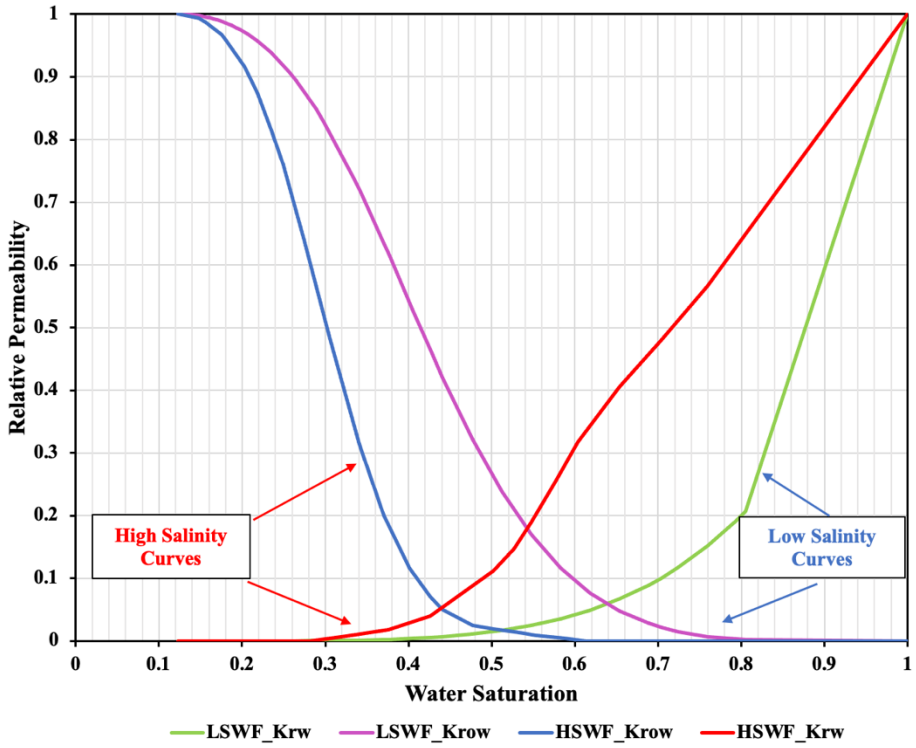

Figure 3.6: Relative permeability shift in LSWF modeling.

For wettability alteration modeling for sandstones, different choice of interpolant can be used. The interpolant is defined under the keyword INTCOMP and the different interpolant choices in GEM in order of preference are (GEM, 2019):

- Ion exchange equivalent fraction of an ion on the rock surface ($\zeta[Na-X], \zeta[Ca-X]$)
- Aqueous molalities of any aqueous species (Ca^{2+} or Na^{+})
- Porosity fraction change due to mineral deposition

Since the multicomponent ion exchange is considered the main mechanism behind the wettability alteration during LSWF, the ion exchange equivalent fraction of a divalent ion was used as interpolant. The ion exchange equivalent fraction of $[Ca-X2]$ was chosen as

interpolant since it has a strong effect on the oil and water relative permeability. In addition, it was generally used as interpolant in other numerical studies on LSWF (Dang et al., 2016; Dang et al., 2013; Jahanbani & Torsæter, 2018). ζ[Ca-X2] represents the amount of Ca^{2+} adsorbed to the clay surface during a multicomponent ion exchange process.

The keyword INTCOMP_VAL defines the interpolation parameter of each interpolating set. When the ion exchange equivalent fraction of [Ca-X2] is equal to or higher than 0.7, the low salinity curves are used. If it is less than or equal to 0.3, the high salinity curves are used. For values in between 0.3 and 0.7, an interpolation between the two curves will occur, which will be explained later. The interpolation parameters are defined based on how the ion exchange equivalent fraction of [Ca- X2] changes during injection of either LSWF or HSWF.

The general concept of relative permeability interpolation is explained in the GEM^{TM} manual (GEM, 2019). An example of interpolation between water relative permeability curves are illustrated in Figure 3.7. The curves, A and B, have different shapes and endpoints meaning that the critical water saturation and residual oil saturation are different for the two cases. For this example, it is assumed that the interpolant variable is a component mole phase *x*. When using a component phase mole fraction as an interpolant the keyword DTRAPW is used as interpolant parameter. Initially, the interpolation factor, ω_ω^i need to be introduced:

$$\omega_\omega^i = \left(\frac{x^i - x_\omega^A}{x_\omega^B - x_\omega^A}\right)^{n_\omega} \tag{3.16}$$

where x^i is the grid block mole fraction, x_ω^A and x_ω^B are mole fractions associated with curve A and B and n_ω is the curvature exponent. After introducing the interpolation factor, the saturation endpoint can then be computed as follows:

$$S_{wcrit}^i = \left(1 - \omega_\omega^i\right) S_{wcrit}^A + \omega_\omega^i S_{wcrit}^B \tag{3.17}$$

$$S_{oirw}^i = \left(1 - \omega_\omega^i\right) S_{oirw}^A + \omega_\omega^i S_{oirw}^B \tag{3.18}$$

Following, the saturations S_w^A and S_w^B will need a scaling of the block saturation S_w,

$$S_w^A = S_{wcrit}^A + \left(S_w - S_{wcrit}^i\right)\left(\frac{1 - S_{oirw}^A - S_{wcrit}^A}{1 - S_{oirw}^i - S_{wcrit}^i}\right) \tag{3.19}$$

$$S_w^B = S_{wcrit}^B + \left(S_w - S_{wcrit}^i\right)\left(\frac{1 - S_{oirw}^B - S_{wcrit}^B}{1 - S_{oirw}^i - S_{wcrit}^i}\right) \tag{3.20}$$

The corresponding relative permeability K_{rw}^A and K_{rw}^B are then found by a straight table look-up. The water relative permeability for a component phase mole fraction between the two curves can then be estimated from:

$$K_{rw} = \left(1 - \omega_\omega^i\right)k_{rw}^A + \omega_\omega^i k_{rw}^B \tag{3.21}$$

In similar manner, the oil relative permeability of a grid block can be calculated:

$$K_{ro} = \left(1 - \omega_o^i\right)k_{ro}^A + \omega_o^i k_{ro}^B \tag{3.22}$$

Where the oil relative permeability interpolation factor ω_o^i is a function of the current interpolation variable of the block, x^i, x_o^A and x_o^B which are oil phase interpolation parameters at the curves A and B defined by DTRAPN, and the curvature exponent as:

$$\omega_o^i = \left(\frac{x^i - x_o^A}{x_o^B - x_o^A}\right)^{n_o} \tag{3.23}$$

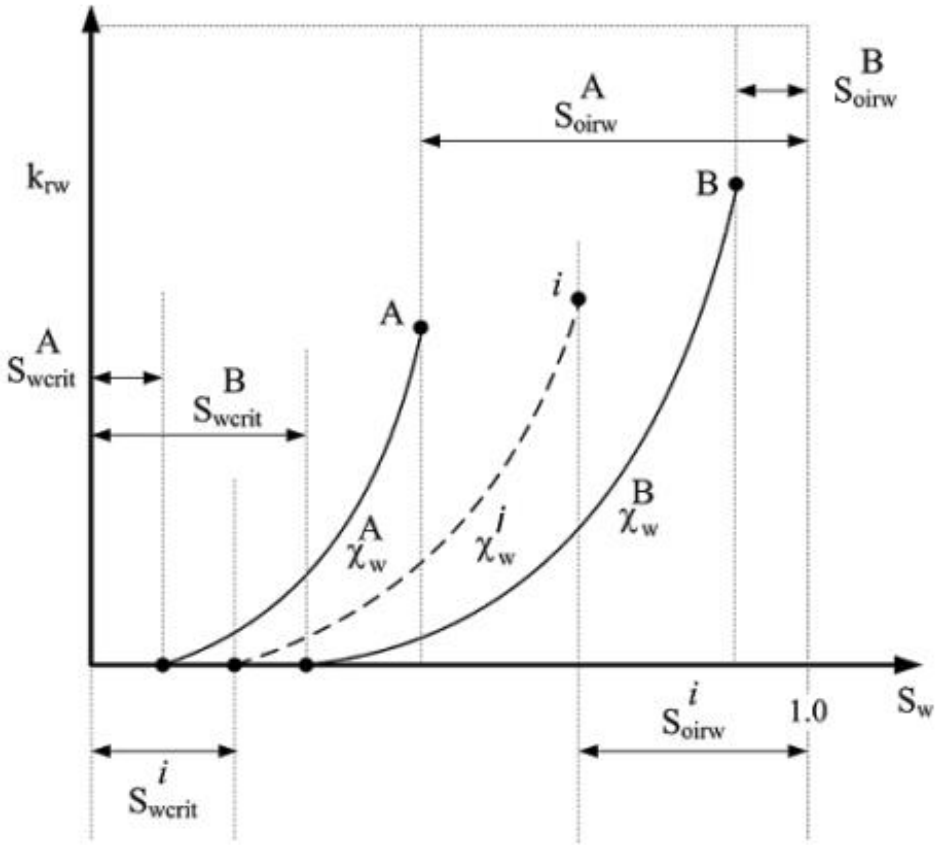

Figure 3.7: Interpolation between two water relative permeability curves, A and B (GEM, 2019).

4. Results and Discussion

To evaluate the performance of LSWF in this study, a high salinity water flooding (HSWF) model is created for comparison purposes. The model is first optimized for water injection control for two different objective functions. The optimized water injection control is then implemented for the LSWF model, and incremental oil recovery is assessed. Finally, a comprehensive sensitivity analysis is done on grid refinement, timing of injection, brine concentrations and two relative permeability models.

4.1 Optimization in CMOST

To analyze the potential of LSWF, high salinity water flooding (HSWF) in secondary mode is selected as base case for this simulation. To establish the optimal base case for HSWF, CMOST was used to do a well control optimization. In Table 4.1, the parameters used for the optimization are presented. Two different objective functions were used to find the optimal base case. First, an optimization on cumulative oil production was done, followed by net present value (NPV) optimization to include the economic viability.

The initial production scheme used for this optimization is based on the water flooding setup presented in Roman (2013) with some modifications. The maximum oil production rate of 2000 Sm^3/day and minimum bottom hole pressure of 300 bar was imposed for the production wells. The injection wells were set to maximum water injection rate of 1200 Sm^3/day and maximum bottom hole pressure of 350 bar. Additionally, the production wells were shut-in at water cut limit of 90% or at minimum oil production rate of 50 Sm^3/day.

Table 4.1: Optimization parameters.

Parameter	Default	Type	Data Range Values
Water Rate Injector 1-3 (Sm^3/day)	1200	Continuous Real	900 – 1500

The first optimization used cumulative oil production as objective function. The CMG DECE (Designed Exploration and Controlled Evolution) optimizer was used to create experiments

with different optimization parameters to find the optimal solution. In the exploration stage, the DECE optimizer searches the space randomly to store as much information as possible about the solution space. The exploration stage is followed by the controlled evolution stage, where statistical analyses are done on the simulation results. In the statistical analysis, every candidate value of the parameters is examined to eliminate those that do not improve the solution quality (CMOST-AL, 2019).

A tendency to a trend for the optimal solution can be observed from experiment 15 in Figure 4.1. Since each run was computationally heavy, the optimization method only performed 50 jobs to obtain the optimal cumulative oil production. Experiment number 47 gave the optimal solution, given the values presented in Table 4.2.

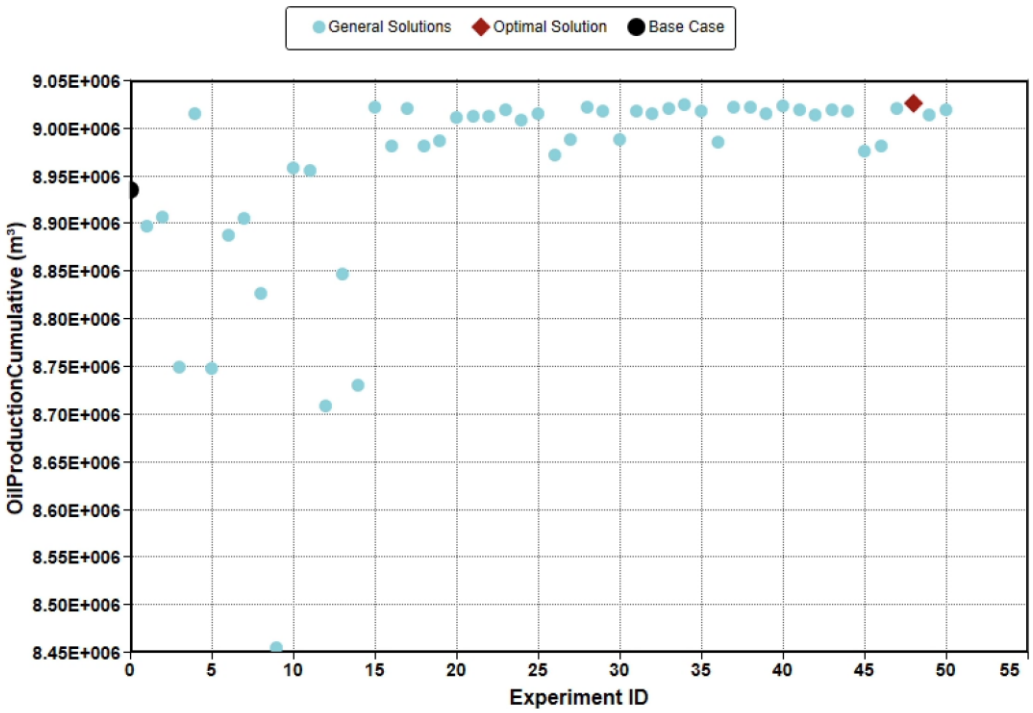

Figure 4.1: Oil production cumulative for the experiments simulated in CMOST.

Table 4.2: Parameters for optimal solution using cumulative oil production as objective function.

Parameters	Value
Water Rate Injector 1 (Sm^3/day)	1008 Sm^3/day
Water Rate Injector 2 (Sm^3/day)	1353 Sm^3/day
Water Rate Injector 3 (Sm^3/day)	1341 Sm^3/day

The objective function for the second optimization was NPV and the economical variables included are presented in Table 4.3. The cash inflow depends on the oil price, oil rate and the yearly discount rate. Furthermore, the cash outflow depends on the operational expenses (OPEX), which in this study includes oil production cost, water injection cost and water production treatment cost. Some of the economic variables are taken from Sierra et al. (2020).

Table 4.3: Economic parameters for NPV optimization.

Parameters	Value	Unit
Oil price	377.4	USD/m^3
Oil production cost	62.90	USD/m^3
Water injection cost	3.14	USD/m^3
Production water treatment	6.29	USD/m^3
Yearly discount rate	10	%

The engine CMG DECE created and ran 50 experiments to find the optimal NPV. The optimal case was found to be experiment 37, where NPV corresponds to 1947 MMUSD (Figure 4.2). Table 4.4 shows the optimal injection rate for each injection well.

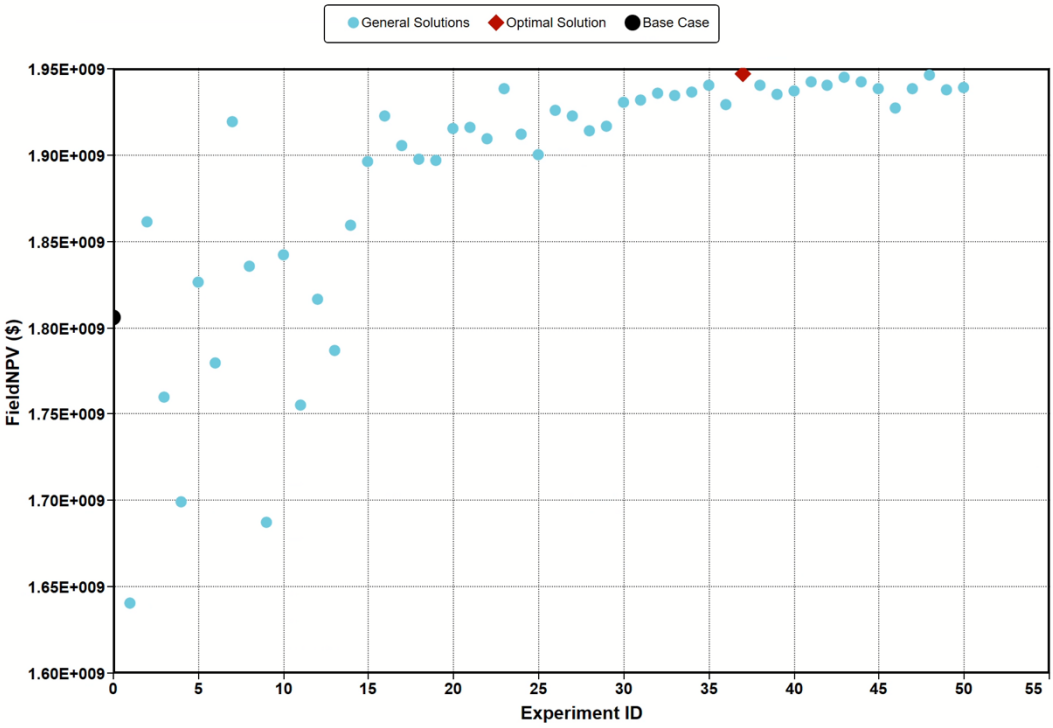

Figure 4.2: Field NPV for the experiments simulated in CMOST.

Table 4.4: Parameters for optimal solution using NPV as objective function.

Parameter	Value
Water Rate Injector 1 (Sm^3/day)	1500 Sm^3/day

In this thesis, the optimal case for NPV will be used as HSWF base case. A more comprehensive description of the selected base case is going to be presented in the next section. Furthermore, a comparison with an LSWF model with the same well control as prepared in this section is reviewed.

4.2 Base Case (HSWF)

The base case introduced in this section is based on the optimized HSWF case. The chemical composition of the high salinity water (HSW) is presented in Table 4.5. The HSW composition is adapted from Fjelde et al. (2012) with some modifications. These are the same ion concentrations used for HSWF in Sierra et al. (2020) field-scale modeling study of Namorado field using GEM^{TM}.

Table 4.5: HSW composition adapted from Fjelde et al. (2012) with some modification.

Ion	HSW (mol/l)
Na^+	1.32622
Ca^{2+}	0.14794
Mg^{2+}	0.01746
Cl^-	1.67773
H^+	4.24E-06
HCO3-	0.00202
OH-	4.03E-09

The HSW was injected from production start in 2013 until the production wells were shut in after approximately 10 years. Figure 4.3 illustrates that the recovery of original oil in place (OOIP) reaches 50.13 % after 10 years of injecting synthetic seawater (HSW). The corresponding total oil production is $8.919 \cdot 10^6$ m^3.

The production rate for each well is illustrated in Figure 4.4. The oil rates decrease rapidly before they stabilize at different rates. Prod_1 remains at a stable rate of approximately 1000 Sm^3/day before it starts decreasing drastically after 7 years. Prod_2 stabilizes at a lower rate of around 750 Sm^3/day before it starts decreasing after 6 years. Prod_3 is stabilized at the highest rate of around 1300 Sm^3/day before it decreases and finally stops producing after around 9 years.

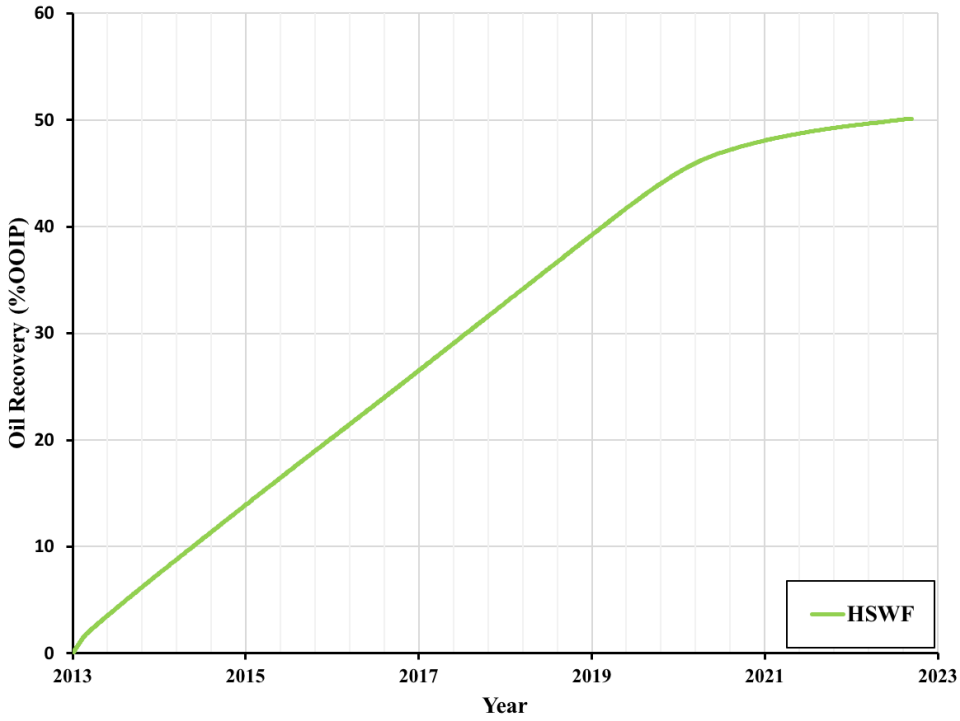

Figure 4.3: The base case oil recovery introduced by optimization on NPV.

As expected, the water cut of the three producers shows the opposite trend of the oil production rates and has the maximum value at the end of production. The behavior denotes that the producers will have a water breakthrough around 2019. Subsequently, the percentage of water produced will increase significantly until the water cut constraint of 90% is reached between 2022 and 2023 (Figure 4.5). Figure 4.6 shows the water injection rates of the three injectors. The water rate is constant at 1500 Sm^3/day for all the injector wells before they are shut down a few months before 2023.

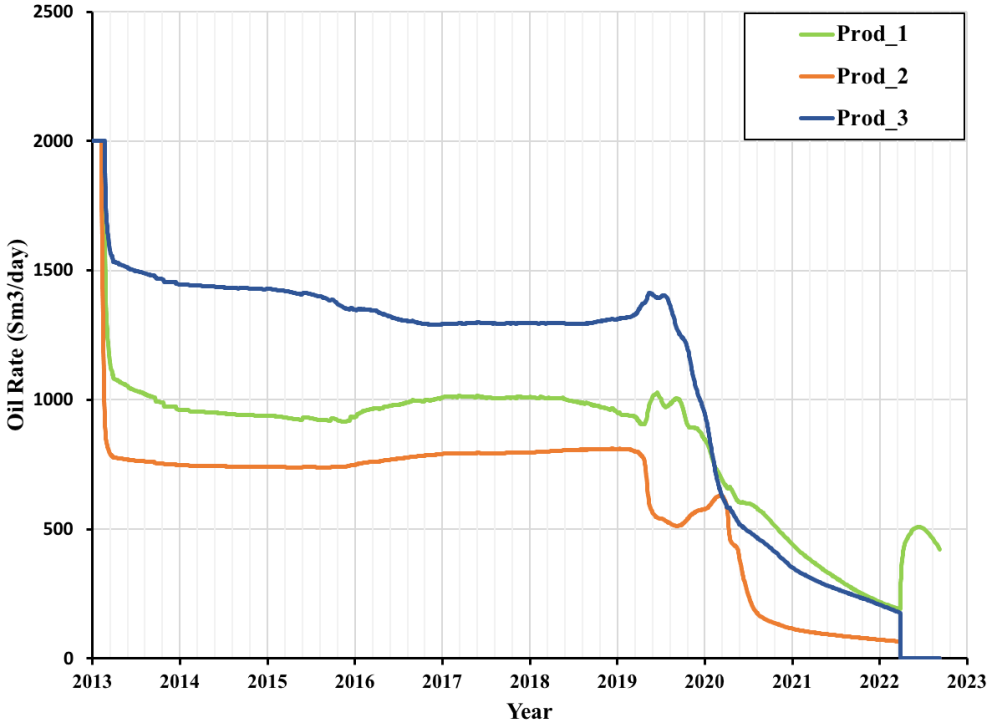

Figure 4.4: The oil production rate of the three producers.

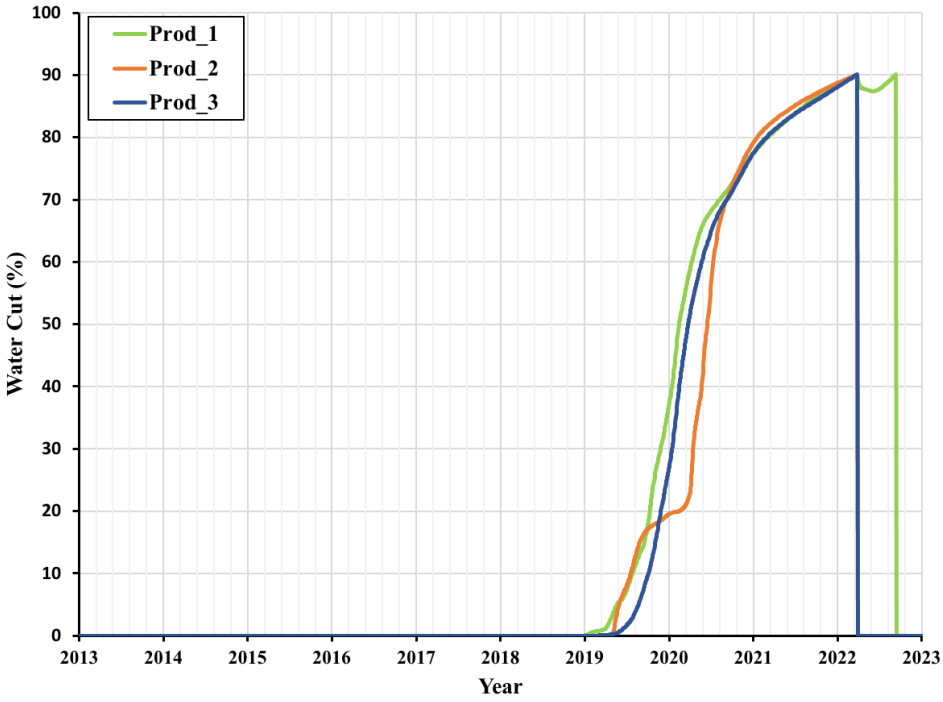

Figure 4.5: Water cut of the three producers.

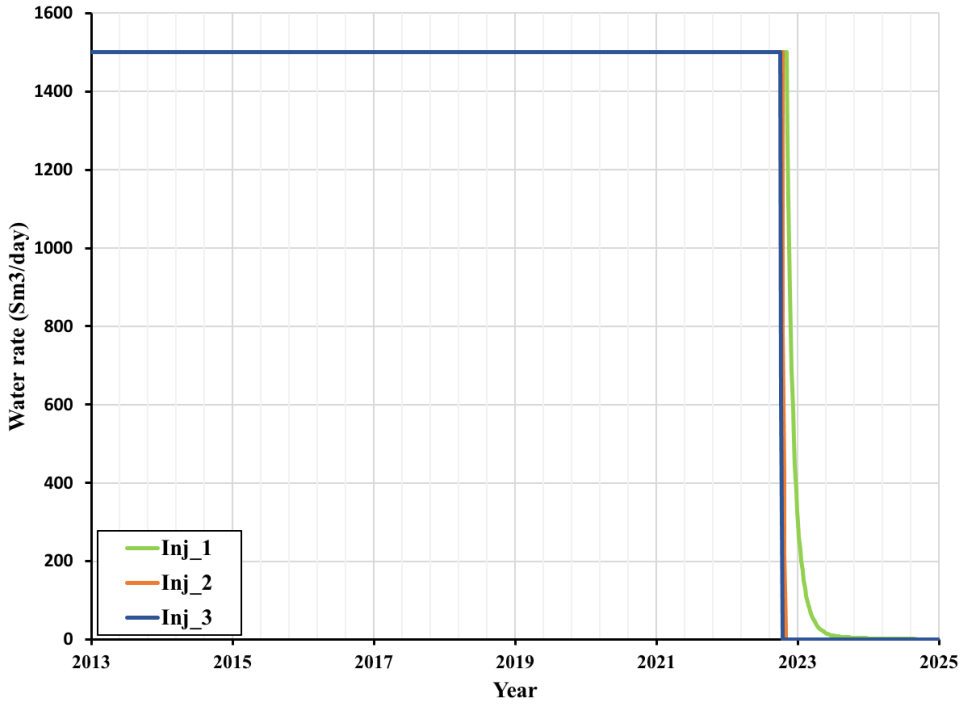

Figure 4.6: Water injection rate of the three injectors.

4.3 Comparison of LSWF and HSWF

To investigate the effect of low salinity water injection in a sandstone reservoir, LSWF in is compared with HSWF, both in secondary mode. The ion composition of the LSW injected and the geochemical reaction parameters are reviewed in Table 4.6 and Table 4.7. The LSWF base case was diluted 10 times compared to HSWF base case. As observed in Figure 4.7, an incremental oil recovery of 9% is observed for LSWF compared to HSWF. The increase is due to the favorable wettability alteration that occurs during LSWF. It is important to mention that the relative permeability curves used in this simulation are representing an initial oil wet-like sandstone reservoir, in order to observe a significant change in oil recovery to have a better sensitivity analysis later for discussion.

The oil production rate scheme indicates that with LSWF, the production will continue for 2 more years compared to HSWF before the constraints are violated (Figure 4.8). The solid line (LSWF) displays that the production will end a few months before 2025. The increased production time can be explained by delayed water breakthrough for LSWF, as observed in

Figure 4.9 (the water cut constraint is violated later in the field lifetime as a result of wettability alteration). There is no difference in oil recovery for HSWF and LSWF before water breakthrough though.

Table 4.6: Ion composition of HSW and LSW

Ion	HSW (mol/l)	LSW (mol/l)
Na^+	1.32622	0.1326
Ca^{2+}	0.14794	0.0148
Mg^{2+}	0.01746	0.0018
Cl^-	1.67773	0.1677
H^+	4.24E-06	4.24E-06
HCO3-	0.00202	0.00202
OH-	4.03E-09	4.03E-09

Table 4.7: Geochemical reaction parameters for LSWF model.

Geochemical reaction parameters	Value
CEC (eq/m^3)	50
Interpolation parameter LSW	0.7
Interpolation parameter HSW	0.3
Volume fraction calcite	0.02
Volume fraction magnesite	0.02

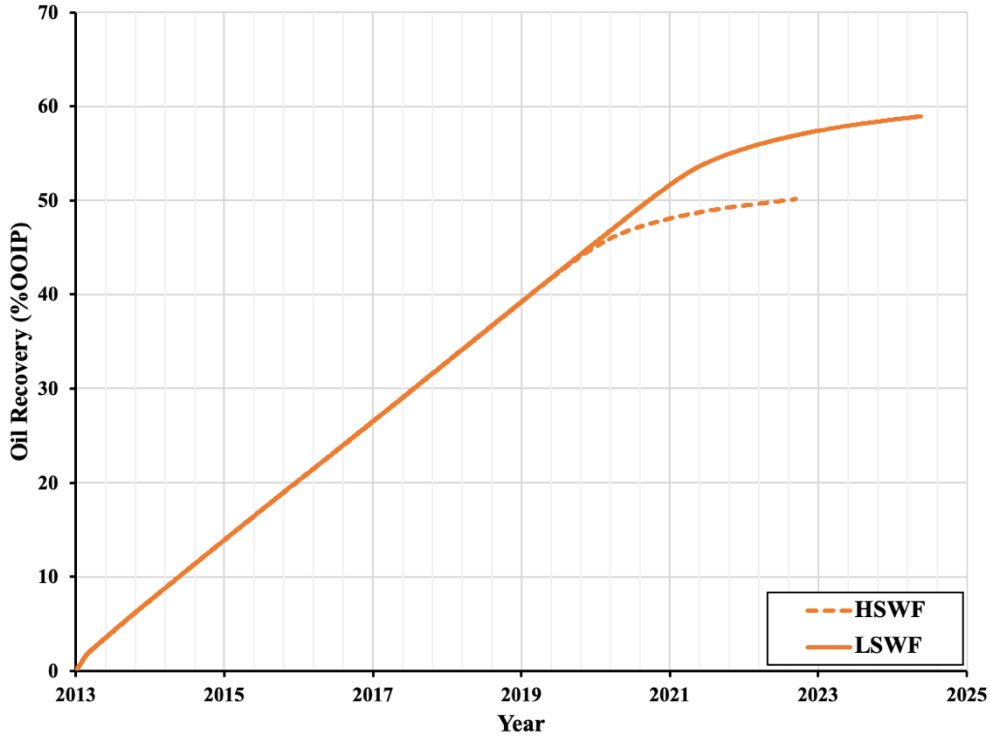

Figure 4.7: Oil recovery of HSWF versus LSWF.

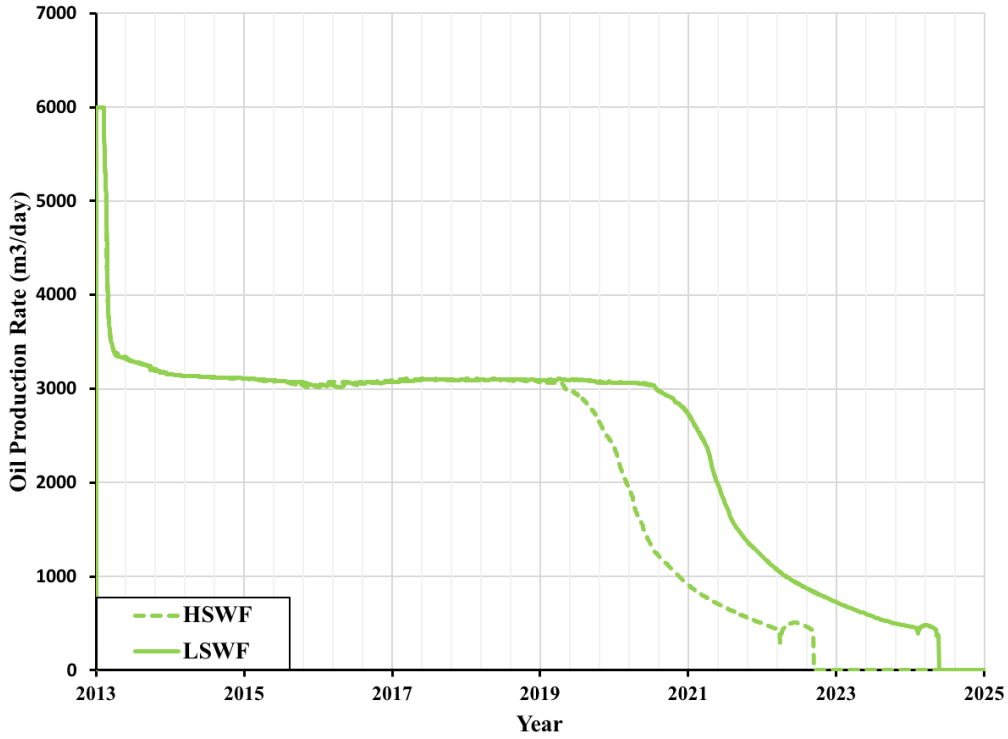

Figure 4.8: Oil production rate of HSWF versus LSWF.

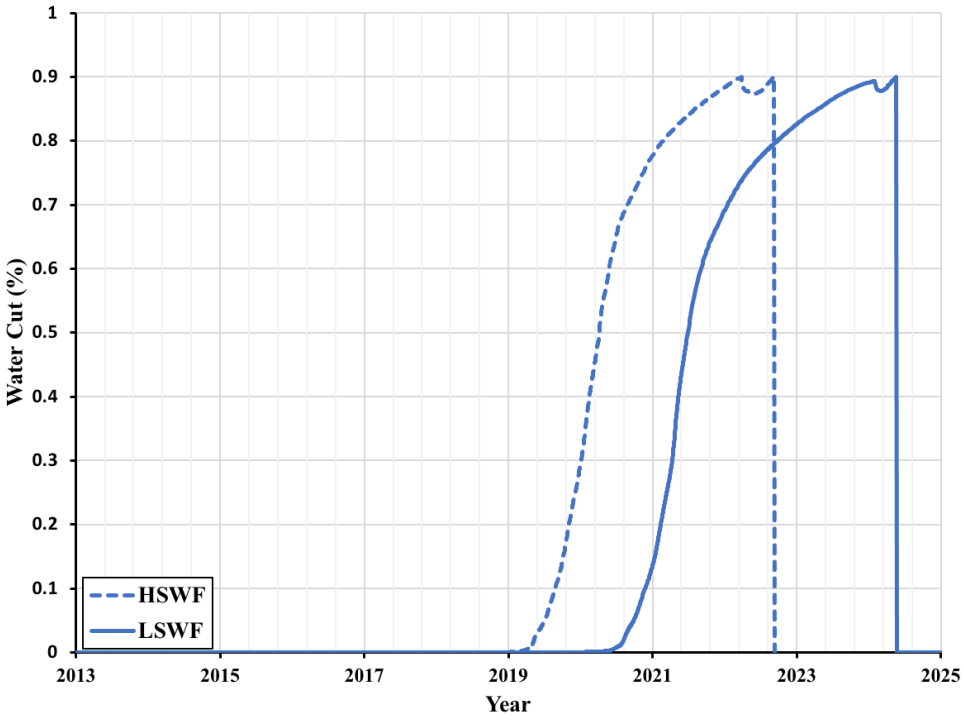

Figure 4.9: Water cut of HSWF versus LSWF.

The effect of wettability alteration is modeled through a shift in relative permeability towards a more water wet state. The shift is done based on the value of the ion exchange equivalent fraction of [Ca-X2]. It is considered that ζ[Ca-X2] can indicate how much Ca^{2+} is adsorbed/desorbed onto the clay surface.

The low salinity curves are used for ζ[Ca-X2] values equal to or higher than 0.7. For values of ζ[Ca-X2] in between 0.7 and 0.3, interpolation between the low salinity and high salinity curves will occur. In addition, for values less than 0.3, the high salinity curves will be used. Figure 4.10 illustrates the ζ[Ca-X2] distribution for the last year of production during LSWF and HSWF. The ion exchange equivalent fraction distribution after LSWF is as high as 0.61 around the injectors and reduces to values close to 0.55 around the producers. Therefore, an interpolation will occur since the values are in between the interpolation limits. The yellowish area around the producers is closer to the low salinity interpolation value. Hence, a higher percentage of the ζ[Ca-X2] corresponds to the low salinity curve. This is the main contributor to the increased oil recovery seen for LSWF.

During HSWF, the value of ζ[Ca-X2] around the injectors is given as 0.26. ζ[Ca-X2] towards the producers increases to values around 0.35-0.45. The ζ[Ca-X2] values are significantly lower for HSWF compared to LSWF. It means that the majority of ζ[Ca-X2] are closer to the high salinity interpolation value. Consequently, there will not be a shift towards a more water wet state and this will result in a lower oil recovery compared to LSWF.

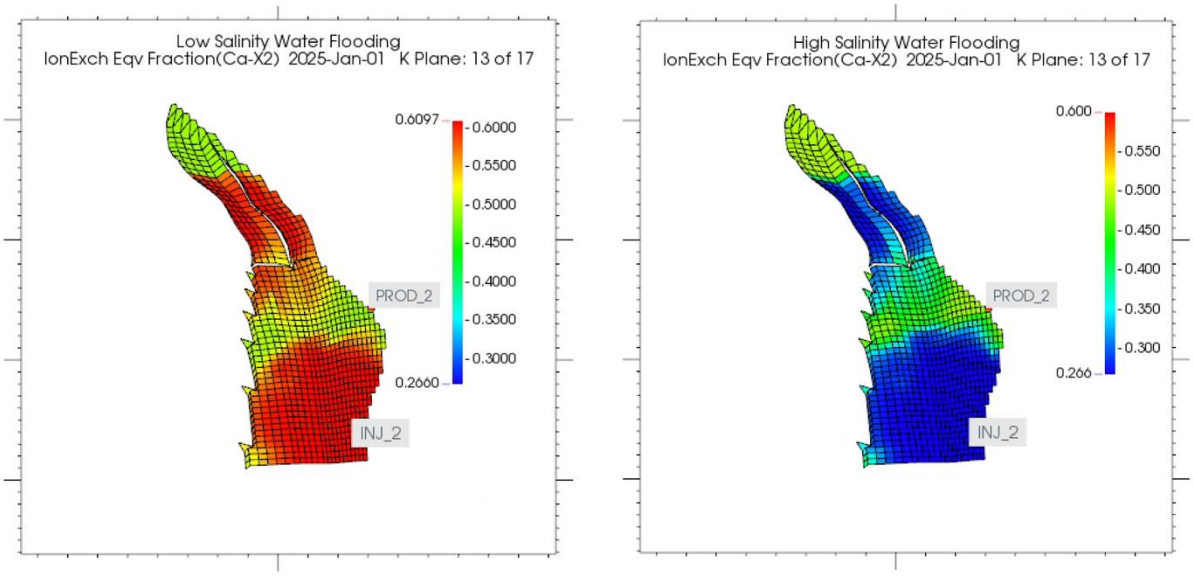

Figure 4.10: Distribution of ion exchange equivalent fraction of [Ca-X2] for LSWF and HSWF for the last year of production.

Figure 4.11 clarifies the behavior of ζ[Ca-X2] at Prod_2 over the 12 production years during LSWF. The ζ[Ca-X2] remains constant at 0.49 for about 8 years before the LSW reaches the producer and the value of the ζ[Ca-X2] increases towards 0.55. The increase seen for ζ[Ca-X2] is due to the ion exchange reaction that occurs between Ca^{2+} and Na^{+} (Equation 3.5). The tendency or the affinity of the different ions to adsorb can explain the ion exchange reaction (Ca^{2+} has higher affinity to adsorb in competition with Na^{+}). The molality of Ca^{2+} shows the opposite trend where the molality stays constant at 0.147 mol/l before it starts to decrease when the LSW replaces the formation water. The molality of Ca^{2+} around the producer on the last day of production indicates that LSW has fully entered the area. The opposite trends of the molality of Ca^{2+} and ζ[Ca-X2] indicate that with a significant drop in salinity of the injected water, an adsorption of Ca^{2+} will occur when the LSW has displaced the FW. This adsorption leads to the shift in relative permeability curves, which is the main reason why an increase in oil recovery is observed. These results support the hypothesis presented by Dang et al. (2016).

Similarly, Figure 4.12 describes the behavior of ζ[Ca-X2] at Inj_2 over the 12 production years during LSWF. Since the LSW is injected from the start of production, there is a rise in ζ[Ca-X2] from 0.49 to 0.61 already in 2013. During the rest of the production time, the ζ[Ca-X2] remains constant. The molality of Ca^{2+} shows the opposite trend where it first has the molality of the formation water (Ca^{2+} of 0.147 mol/l), before it drastically decreases towards the molality of the LSW water (Ca^{2+} of 0.0147 mol/l). Since there is adsorption of Ca^{2+} almost from the start nearby the injector unlike for Prod_2, the shift in relative permeability is expected to be more significant around the injector. This agrees with Figure 4.10 where ζ[Ca-X2] increase during LSWF around the injectors is more significant than around the producers.

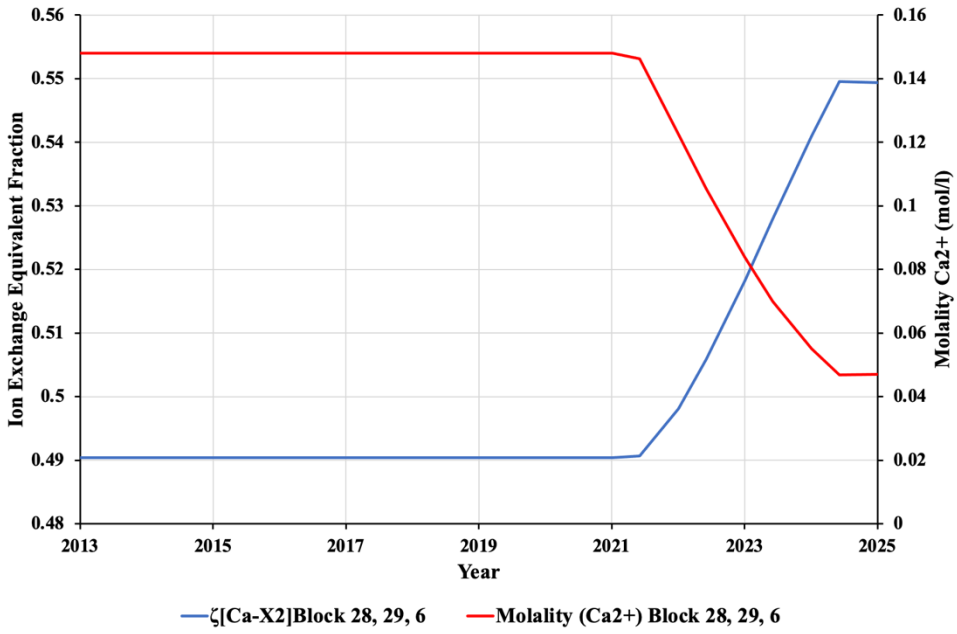

Figure 4.11: Effluent molality of Ca^{2+} and ion exchange equivalent fraction of Ca-X2 at Prod_2.

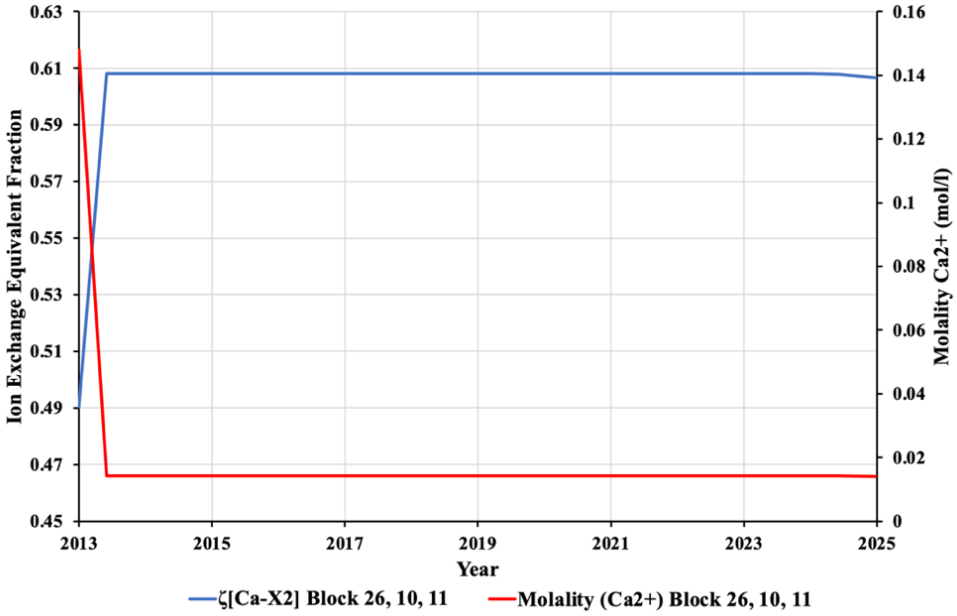

Figure 4.12: Molality of Ca^{2+} and ion exchange equivalent fraction of Ca-X2 at Inj_2.

Figure 4.13 illustrates the ion exchange equivalent fraction of [Na-X] at the Inj_2 and Prod_2. Since adsorption of Ca^{2+} is observed in this study, the ion exchange equivalent fraction of [Na-X] is expected to decrease with an increase in ion exchange equivalent fraction of [Ca-X2]. The scheme clarifies that ζ[Na-X] decreases when LSW is injected due to the ion exchange process between Ca^{2+} and Na^{+}.

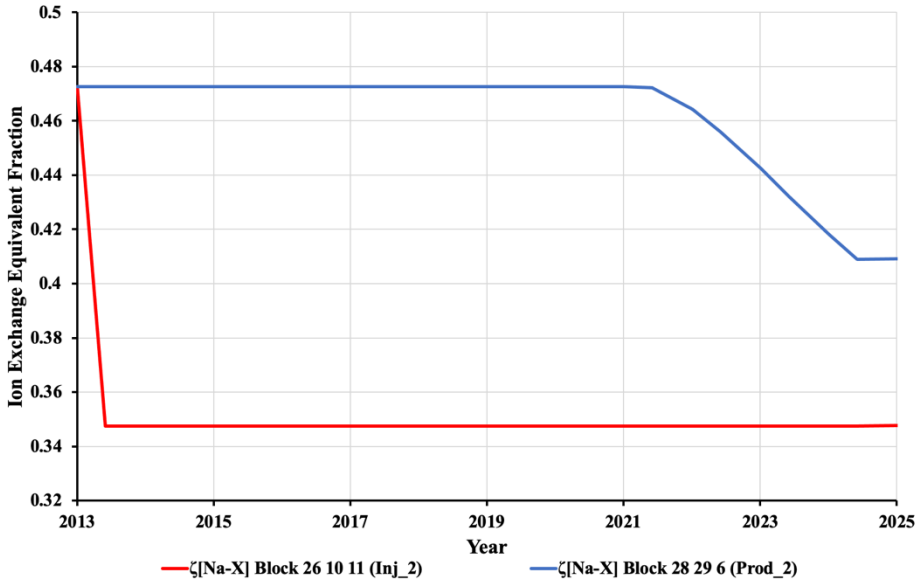

Figure 4.13: Ion exchange equivalent fraction of [Na-X] at Inj_2 and Prod_2.

However, it cannot be argued that the geochemical reactions are the only physical explanation behind the wettability alteration process (Dang et al., 2016). Based on Figure 4.14, there is a pH increase around the injectors when LSW invades the reservoir. The change in pH can indicate that different mechanisms are contributing to the wettability alteration process during LSWF. The pH increase can interact simultaneously with other mechanisms proposed such as MIE, which can strengthen the LS effect. However, Lager et al. (2008) and Rezaeidoust et al. (2009) did not detect any direct relationship between increased oil recovery and pH when they investigated LSWF.

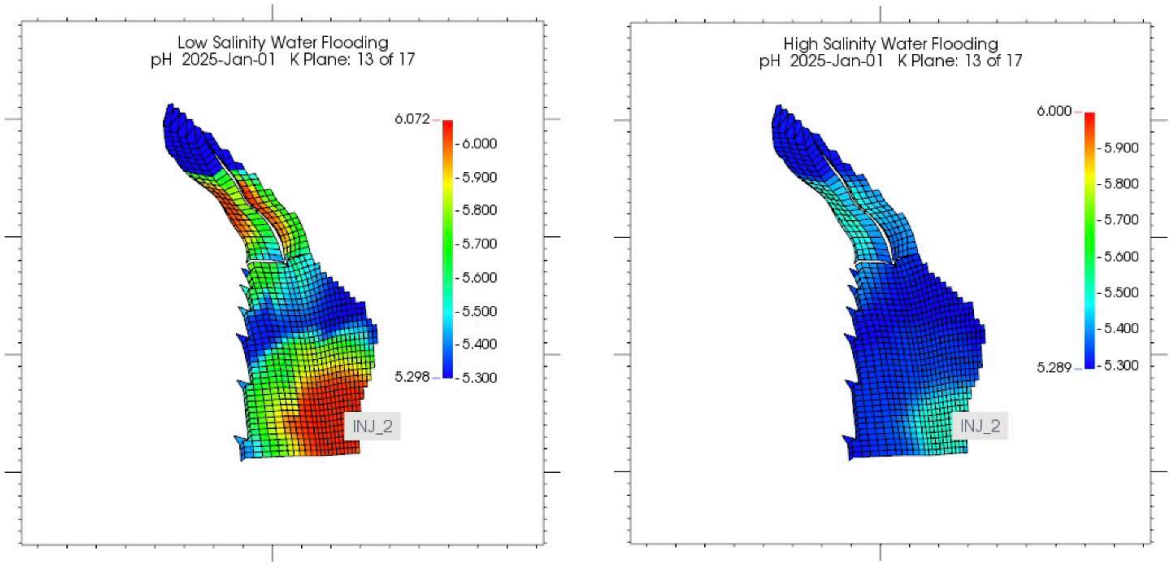

Figure 4.14: pH variation during LSWF and HSWF.

4.4 Sensitivity Analysis

Sensitivity analysis on different parameters that affect the result is essential in reservoir modeling. The main sensitivity studies done in this thesis are performed on grid refinement, the timing of injection, brine concentrations, and sensitivity parameters' influence on two different relative permeability sets during LSWF. The software CMOST™ by CMG is used for sensitivity analysis on brine concentrations and two relative permeability models to identify which parameters have the greatest effect on oil recovery. In general, the objective of the sensitivity analysis is to develop a better understanding of how the different parameters affects the modeling of LSWF in GEM™.

4.4.1 Grid Refinement

Three low salinity models are run to highlight the grid refinement impact on LSWF modeling. The models evaluated consist of the original grid (the grid system used in previous sections), finer grid and a coarser grid system (Table 4.8). The fundamental grid in the LSWF model is a corner-point grid type, meaning that the placement of grid corners is flexible to define non-standard shapes and distributions of grid blocks (GEM, 2019). The original grid system consists of 45, 75, 17 corner-point grid blocks in I, J, K-directions. In order to refine the reservoir, the keyword *REFINE is implemented in the Input/Output control section for the given block addresses that are going to be refined.

The coarse grid model is created by merging layers in K-direction. The properties for the new layers are generated through arithmetic averaging of porosity, cation exchange capacity, net to gross ratio, permeability, and transmissibility multiplier. However, the permeability and transmissibility multiplier in K-direction are calculated through harmonic averaging.

Table 4.8: The different grid systems evaluated for sensitivity.

Grid system	Total number of grid blocks
Fine grid	100 272
Original grid	57 375
Coarse grid	23 625

Figure 4.15 and Figure 4.16 show the results of the simulations performed for the different grid systems. It can be observed that the coarse grid model has a 4% lower oil recovery factor and a shorter plateau period compared to the original grid model. In addition, the production wells are shut in approximately two years earlier than in the original grid. The fine grid model shows a trend similar to the original grid model with only 0.5% increase in oil recovery.

In a numerical model with a coarser grid system, relative permeability effects and numerical dispersion can reduce oil recovery. Furthermore, the sweep efficiency can be reduced compared to a finer grid model (Aggrey et al., 2014; Chandrashegaran, 2015). For geochemical modeling, a fine grid model will give a more precise results of the geochemical reactions that occur during LSWF. However, considering the extra computational time the fine grid model is demanding, the original grid model is fine enough for further sensitivity analysis in this work.

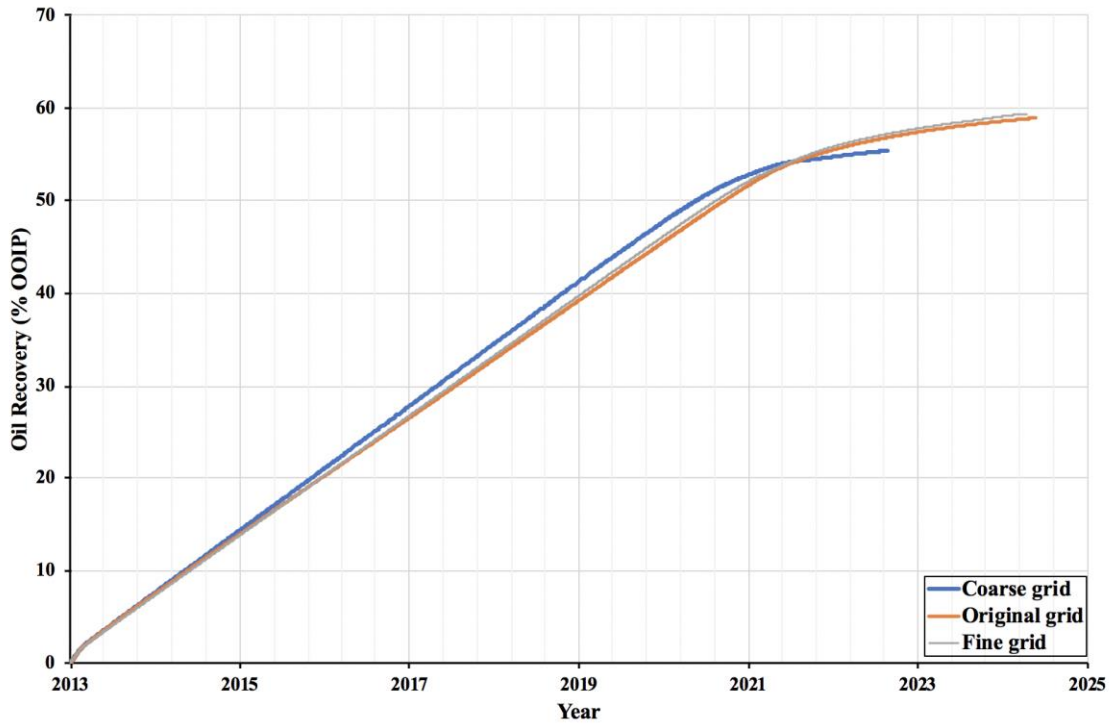

Figure 4.15: Oil recovery for the three different grid systems.

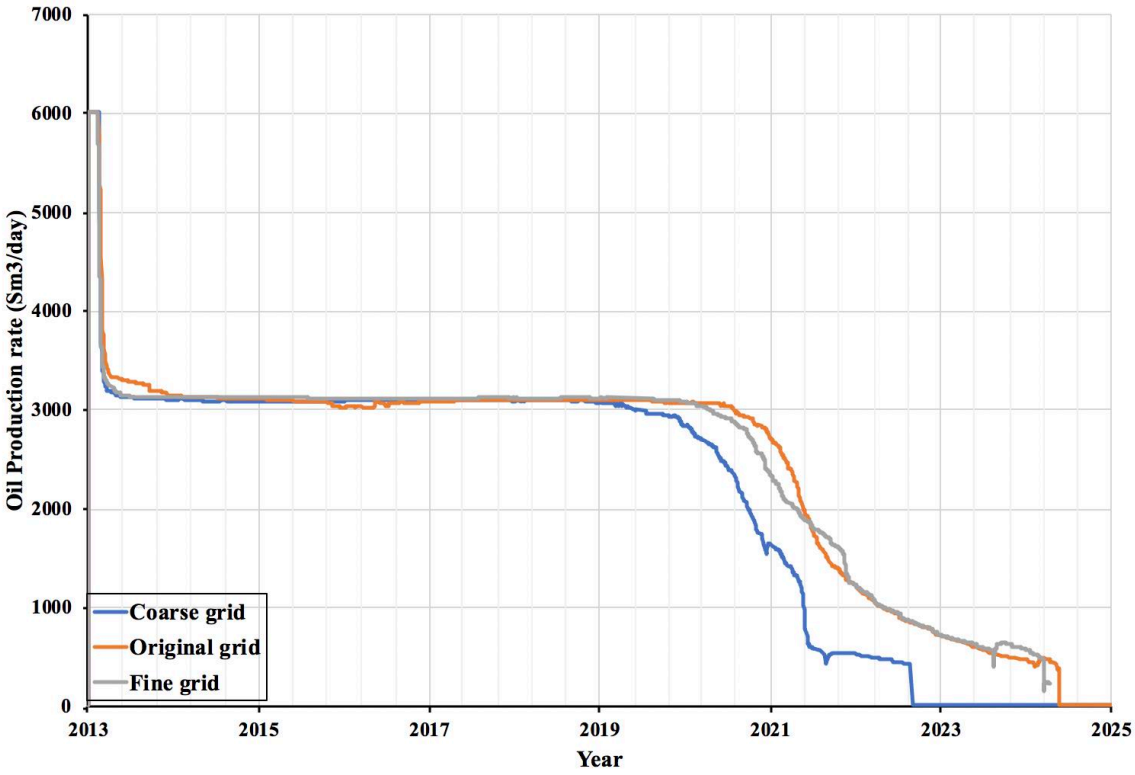

Figure 4.16: Oil production rate for the three different grid systems.

4.4.2 Timing of injection

The timing of injection is a key factor that affects the oil recovery performance of LSWF. The majority of oil reservoirs today are already flooded with conventional HSWF and thus implementation in tertiary mode must be considered. The effect of secondary LSWF compared to tertiary LSWF has been investigated both at core scale and field scale by different authors (Adegbite et al., 2017; Agbalaka et al., 2008; Almeida da Costa et al., 2021; Dang et al., 2015a; Zhang et al., 2007). Zhang et al. (2007) concluded that most of the LSWF experiments detected incremental oil recovery for both recovery stages, but sometimes for only one or the other. In some studies, such as Rivet et al. (2009) and Skrettingland et al. (2011), only incremental oil recovery for secondary mode was observed. Nasralla et al. (2011) indicated that LSW injection in tertiary mode could reduce incremental oil recovery due to fines migration that might block some of the pore throats. In this section, simulations have been performed for four different timing of injection cases.

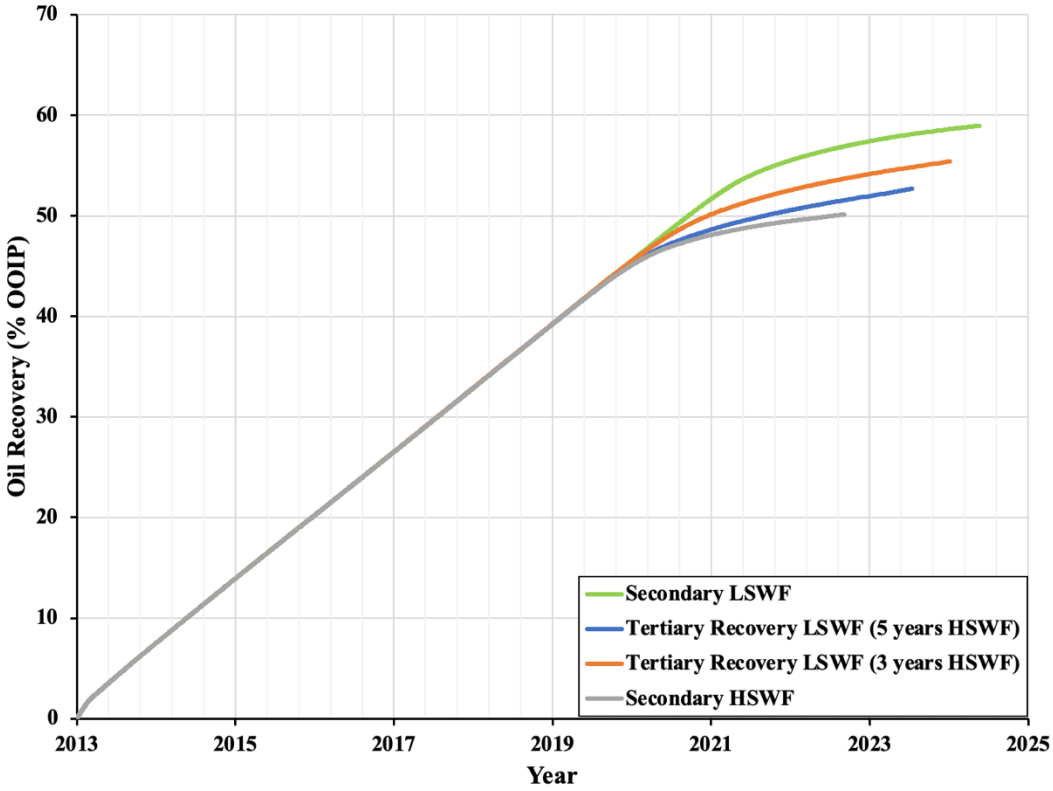

Figure 4.17: Timing of injection effect on oil recovery performance.

Figure 4.17 illustrates the oil recovery for secondary HSWF, secondary LSWF, and two different tertiary mode LSWF cases. The blue line (tertiary mode LSWF) indicates that the reservoir is first flooded with HSW for 5 years before LSW is injected for the remaining production time. Furthermore, the orange line shows that the reservoir was first flooded with HSW for 3 years before LSW was injected. These two tertiary LSWF cases resulted in a final oil recovery factor of 52.7 % and 55.5 %, respectively. Even though the tertiary mode recovery schemes with LSWF resulted in higher recovery than conventionally secondary mode HSWF, the secondary mode LSWF is the most effective injection method with a recovery factor of 59%. These results imply that earlier injection of LSW allows the water to disperse and thereby more time is available to react with reservoir rock and the fluids present (Egbe, 2019). In other words, earlier onset of LSWF will result in higher oil recovery, which agrees with literature (Adegbite et al., 2017; Almeida da Costa et al., 2021; Dang et al., 2015a). In addition, necessary equipment for LSWF can be installed at an early phase to avoid additional costs that are often related to tertiary recovery setup on older platforms (Dang et al., 2015b).

4.4.3 Brine Concentrations

In the following section, the effect of reducing the injected brine concentration on oil recovery is investigated. It has been confirmed by researchers that the concentration of the injected water affects the LSWF oil recovery (Al-Saedi et al., 2019; Sadeed et al., 2018). It is expected that the oil recovery will increase at lower salinity ranges. The modified ion concentrations are shown in Table 4.9 where the lower limit demonstrates the LSW composition presented by Fjelde et al. (2012). The effect on oil recovery by lowering the concentration of ions was investigated in CMOST.

Table 4.9: Ion concentrations tested for sensitivity analysis.

Ions	Base Case (mol/l)	Data Range Settings	
		Lower limit (mol/l)	Upper limit (mol/l)
Na^+	0.132622	0.0132622	0.132622
Ca^{2+}	0.014794	0.0014794	0.014794
Mg^{2+}	0.0018	0.00018	0.0018
Cl^-	0.167773	0.016773	0.167773

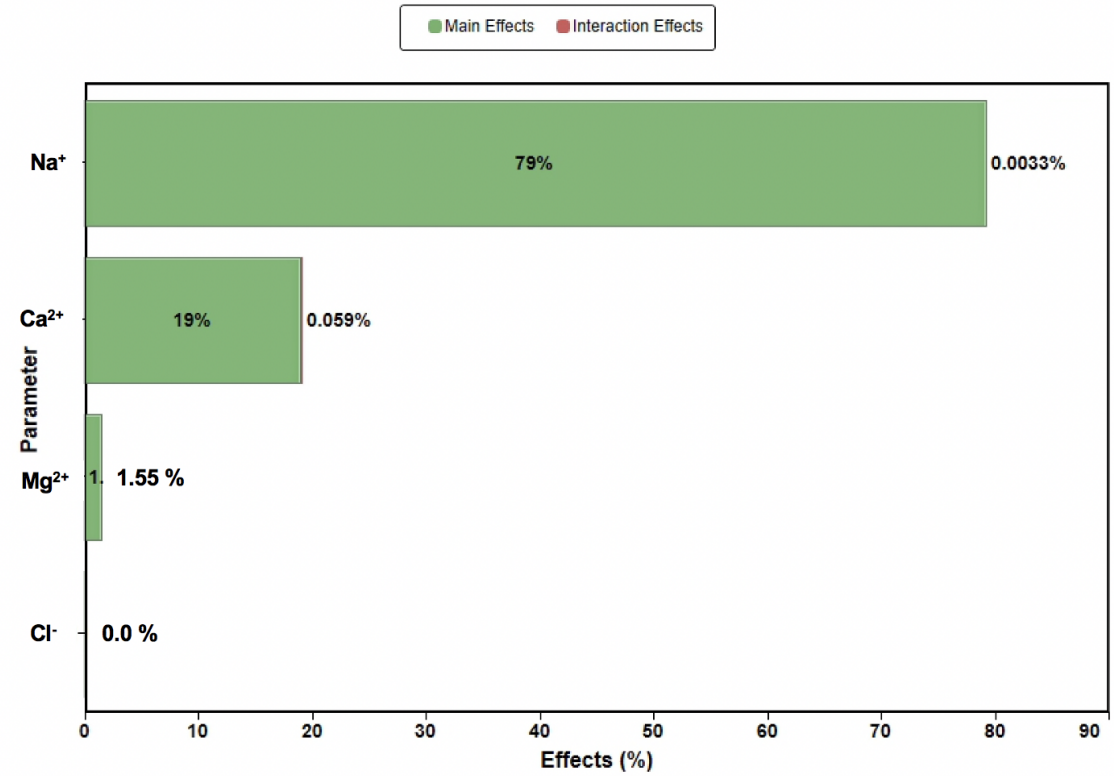

Figure 4.18: Ion concentrations effects on oil recovery.

Figure 4.18 illustrates that the most influential parameter on oil recovery is the concentration of Na^+. Almeida da costa et al. (2021) did a similarly sobol analysis for their simulation case study where they also used ζ[Ca-X2] as the interpolant. In their sensitivity analysis, Na^+ concentration had also the greatest effect on oil recovery.

Figure 4.19-Figure 4.22 illustrates the difference in ion exchange equivalent fractions of Na^+ and Ca^{2+} on the clay surface when water with base case concentration and reduced concentration is injected. The modified concentration demonstrates the concentration at the lower limit presented in Table 4.9. When salinity of the injected water decreases, the decrease in ion exchange equivalent fraction of [Na-X] and the increase in ion exchange equivalent fraction of [Ca-X2] are more significant compared with the base case which supports the hypothesis presented by Dang et al. (Dang et al., 2016). Again, the changes are more visible around the injector. The reduction of ζ[Na-X] is only minor at the producer, but at the injector the decrease is more evident from 0.47 to 0.15. The decrease of ζ[Na-X] and increase of ζ[Ca-X2] indicate that ion exchange occurs, and reduction of Na^+ in the injected water promotes Ca^{2+} adsorption on the clay surface. This ion exchange leads to favorable wettability alteration and consequently additional oil recovery by lowering the salinity of the injected water. However, after a certain concentration, further reduction will not lead to additional oil recovery. This can be due to the lack of free ions on the rock surface that can compensate for the Na^+ reduction in the injected brine (Esene et al., 2018).

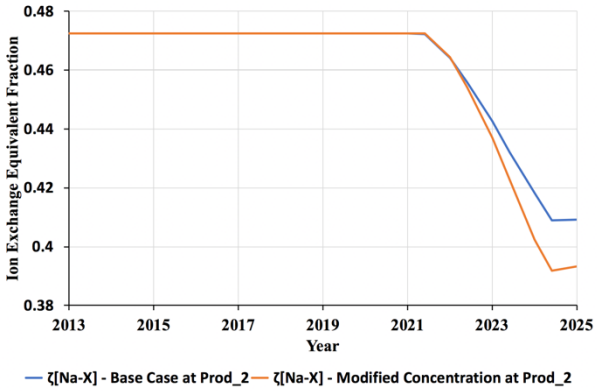

Figure 4.19: ζ[Na-X] at Prod_2 for base case and modified concentration.

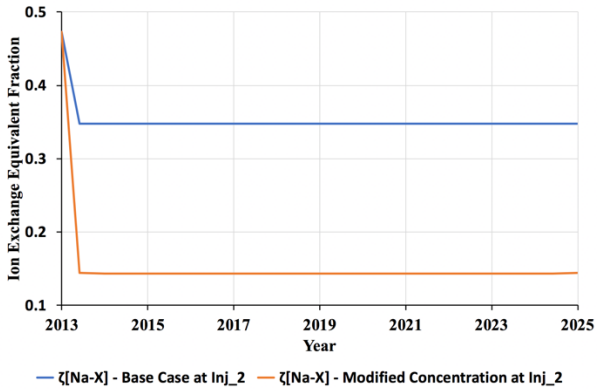

Figure 4.20: ζ[Na-X] at Inj_2 for base case and modified concentration.

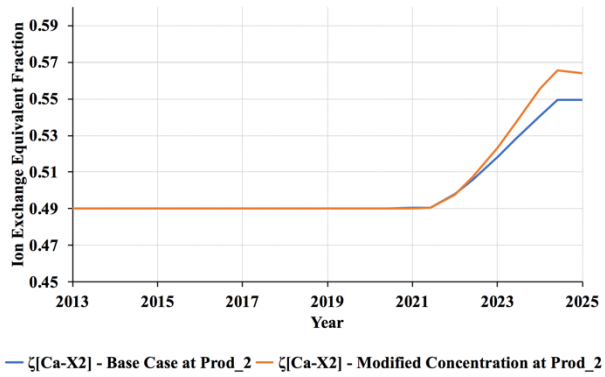

Figure 4.21: ζ[Ca-X2] at Prod_2 for base case and modified concentration.

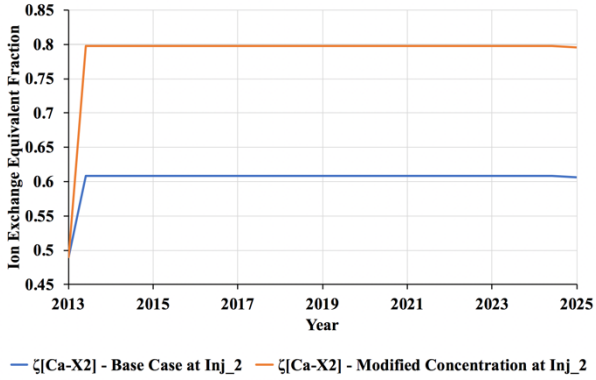

Figure 4.22: ζ[Ca-X2] at Inj_2 for base case and modified concentration.

The second most influential parameter on oil recovery in Figure 4.18 is the concentration of Ca^{2+}. When the salinity of injected water is reduced, more Ca^{2+} ions will be adsorbed onto the clay surface resulting in increased ζ[Ca-X2] (Figure 4.21 and Figure 4.22). Due to the interpolant values chosen, bigger proportion of the reservoir will correspond to the LSW relative permeability curves, making the reservoir even more water wet than the base case. In the case of modified (lower) concentrations of the injected water, only 1.5% incremental oil is observed (Figure 4.23). The slight change in recovery factor can be explained by the minor changes in ion exchange equivalent fractions nearby the producers. The interpolant values chosen for the relative permeability curves may be chosen differently to obtain more oil recovery.

The pH around the injectors will increase when lowering the salinity of the injected brine. Compared to the base case, an increase of 1 in pH is seen for the modified (lower) concentration (Figure 4.24). As discussed in section 4.3, the local increase can indicate that different mechanisms contribute and interact simultaneously, which is favorable for the LS effect.

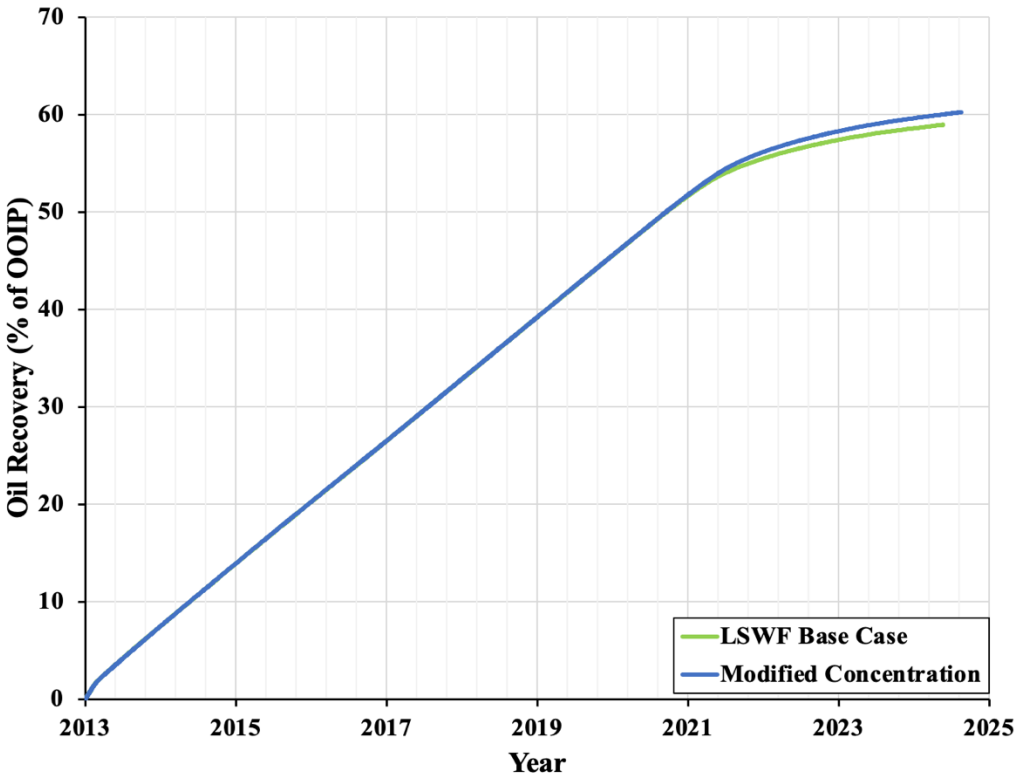

Figure 4.23: Incremental oil recovery for modified concentration of the injected brine.

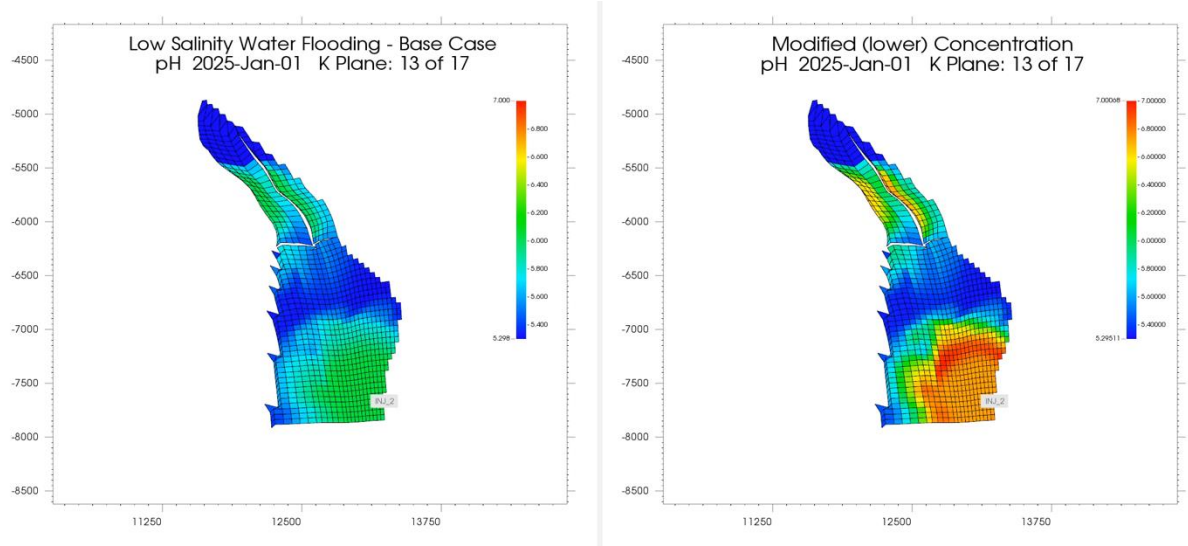

Figure 4.24: pH variations in the reservoir for the last year of production for different brine concentrations.

4.4.4 Relative Permeability Models

In this section, sensitivity parameters related to wettability alteration are going to be evaluated for two different relative permeability models. These two models are evaluated as case 1 and case 2, where case 1 is the same relative permeability system (initially oil wet-like system) as presented earlier in this thesis (Figure 4.25). For case 1, the wettability shift from HS to LS curves was significant to present a simulation case optimal for sensitivity analysis. The second relative permeability system (case 2), represents a more realistic case for a initially water wet-like sandstone reservoir (Pedersen, 2018). As observed in Figure 4.25 and Figure 4.26, there is less change in relative permeability when wettability alteration occurs for case 2 compared to case 1.

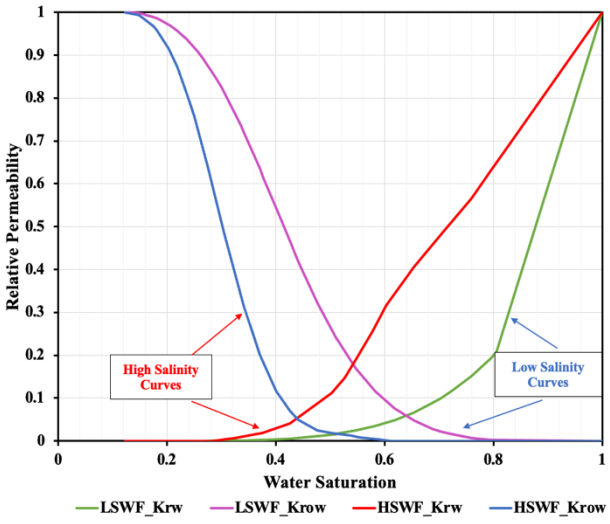

Figure 4.25: Relative permeability curves for case 1.

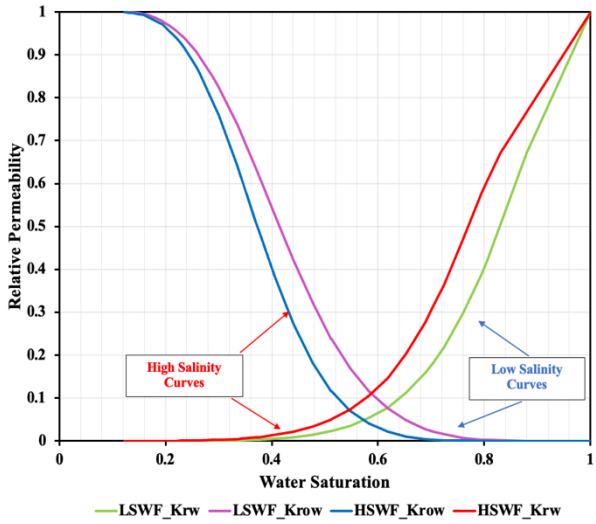

Figure 4.26: Relative permeability curves for case 2.

In Figure 4.27, incremental oil recovery for case 1 and case 2 are illustrated. As observed, there is considerable difference in incremental oil recovery for the two cases. Case 1 shows incremental recovery factor of nearly 9%. In comparison, the incremental recovery factor for case 2 is 4.5%. Case 2 has an overall higher recovery factor than case 1, which can be explained by the differences in S_{or} for the relative permeability curves used. Case 1 had a final S_{or} of 0.20 after LSWF, compared to case 2 with a S_{or} of 0.12.

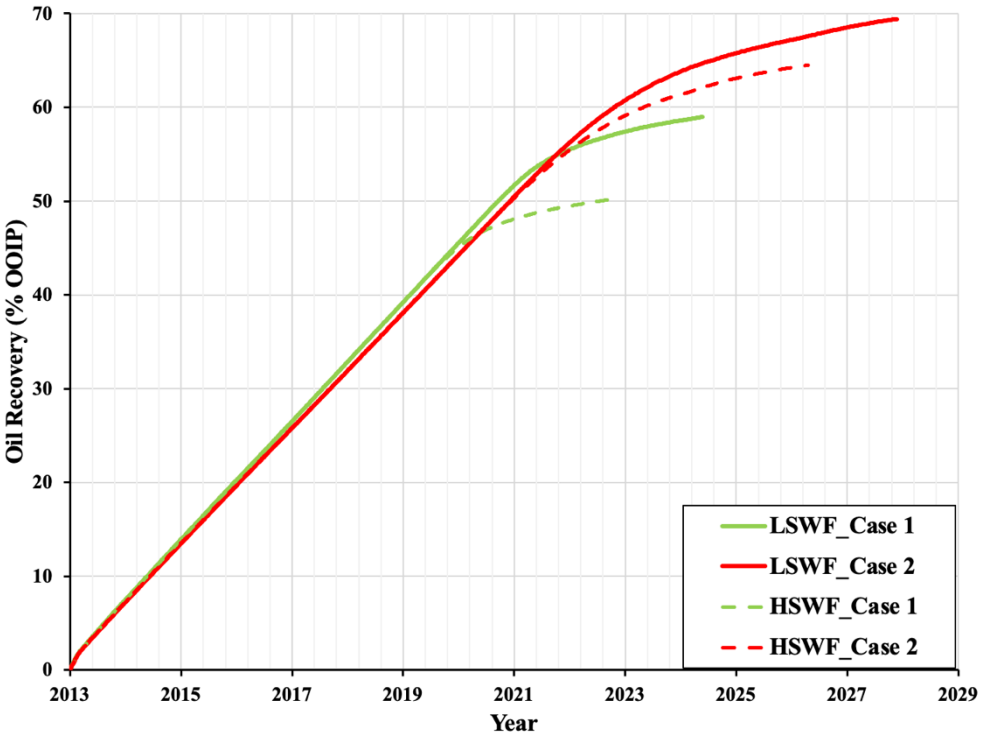

Figure 4.27: Oil recovery for LSWF and HSWF for the two relative permeability models.

The parameters affecting oil recovery are evaluated for case 1 and case 2 in CMOST™. The parameters chosen for sensitivity study are S_{or} for the LSW curve, interpolation values for LS curves and HS curves, volume fraction of magnesite and calcite, and the cation exchange capacity (CEC). All the parameters included for the sensitivity analysis influence the wettability alteration process that is modeled as the main mechanism for LSWF. The parameters are corresponding to the keywords TSORW, INTCOMP_VAL, CEC-IEX, VOLUME_FRACTION-MINERAL in GEM™.

Sensitivity Analysis for Case 1

To do a sensitivity analysis in CMOST, the data range settings for the given sensitivity parameters must be defined. For case 1, the data range settings are shown in Table 4.10. The engine Response Surface Methodology (RSM) created 46 experiments with combinations of the sensitivity parameters to explore the effect on oil recovery. The oil recovery factors for the corresponding runs are illustrated in Figure 4.28.

Table 4.10: The parameters used for sensitivity analysis for case 1

Sensitivity Parameters	Base Case	Data Range Settings	
		Lower limit	Upper limit
CEC (eq/m^3)	50	30	100
Interpolation parameter LSW	0.7	0.5	0.8
Interpolation parameter HSW	0.3	0.1	0.4
Volume fraction calcite	0.02	0.015	0.3
Volume fraction magnesite	0.02	0.015	0.3
S_{or} (LSW)	0.2	0.1	0.23

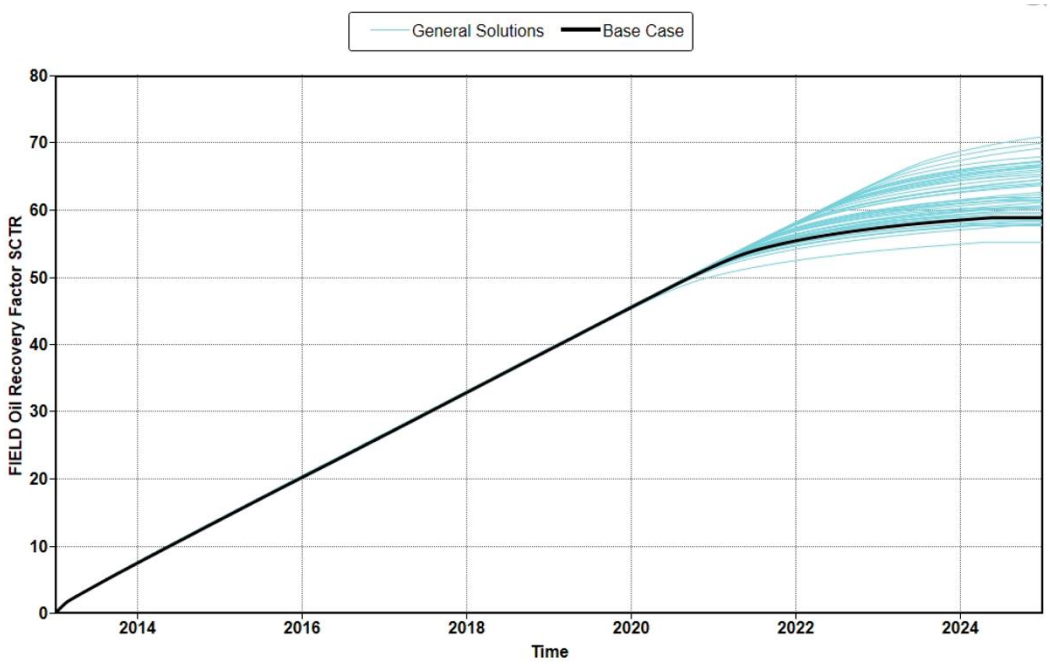

Figure 4.28: Oil recovery factors for the 46 experiments simulated for case 1.

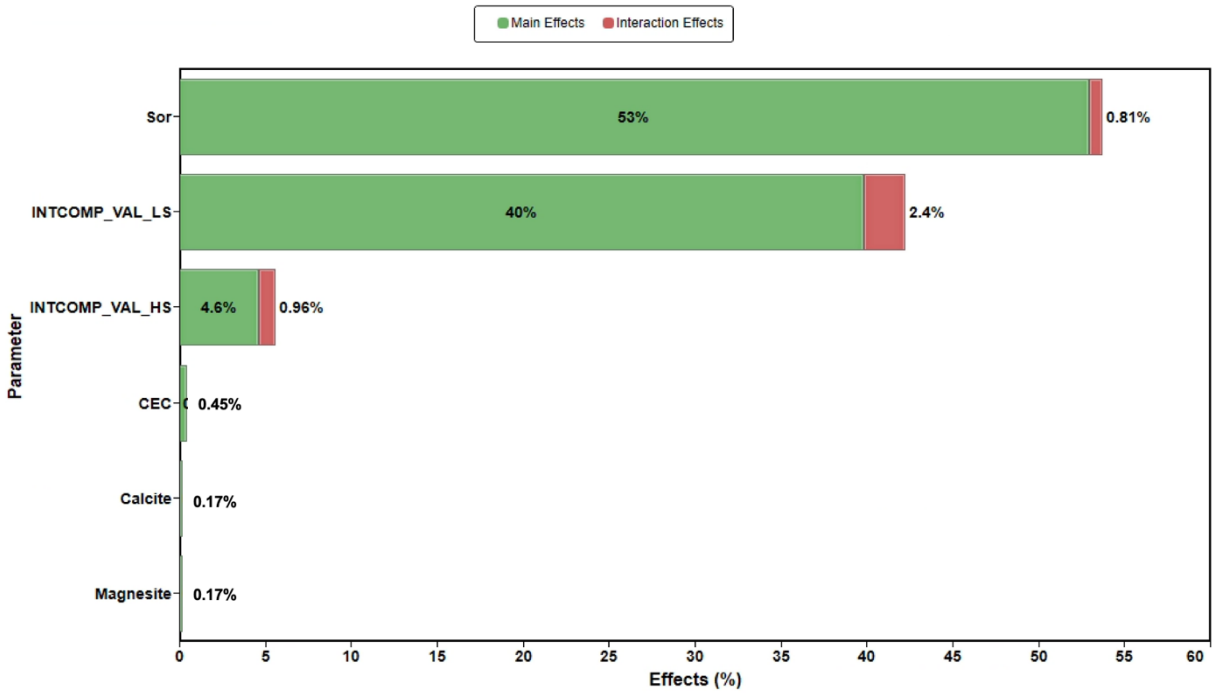

Figure 4.29: The sensitivity parameters' effect on oil recovery for case 1.

Figure 4.29 illustrates the main and interaction effects of the sensitivity parameters chosen for analysis. Based on this plot, changing the S_{or} for the LSW relative permeability curve has the greatest impact on oil recovery. The cross plot of the relationship between oil recovery factor and S_{or} (LSW) is illustrated in Figure 4.30. The oil recovery factor varies from 55% to 71%, for the given ranges of S_{or} (LSW) values. The trend indicates for smaller values of S_{or} (LSW), which is strongly related to the wettability alteration process, higher oil recovery is seen. The saturation crossover of K_{ro} and K_{rw} will be shifted towards more water wet system when S_{or} (LSW) is smaller. Consequently, more oil is released at the clay surface and thereby higher recovery rates is seen.

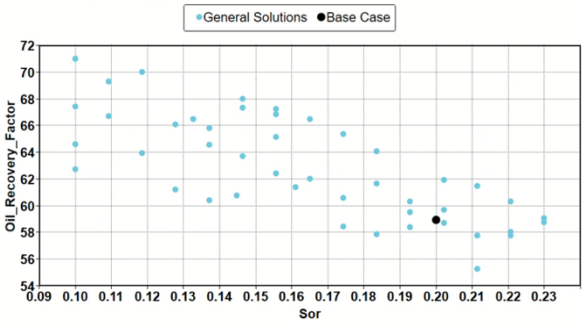

Figure 4.30: Cross plot of the relationship between S_{or} (LSW) and oil recovery factor.

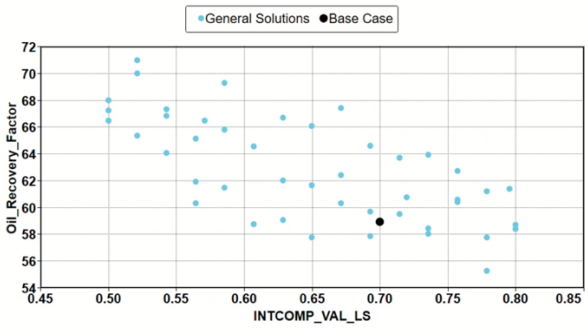

Figure 4.31: Cross plot of the relationship between interpolant value of LS curves and oil recovery factor.

The second most influential parameter is interpolant value of LS relative permeability curves. The interpolant value used for base case is not optimal for achieving maximum oil recovery. As illustrated in Figure 4.10, the ion exchange equivalent fraction of [Ca-X2] reaches the maximum value of 0.61 after flooding with LSW. By lowering the interpolant value of the LS curves, a higher percentage of the ion exchange equivalent fraction values in the reservoir will correspond to the LS curves. It means that the wettability shift towards increased water wetness will be more significant, resulting in higher oil recovery factors (Figure 4.31).

Less effect is seen on oil recovery when changing the CEC parameter and mineral content of calcite/magnesite. Cation exchange capacity for a given rock describes the amount of ions that can be adsorbed on the rock surface. Figure 4.32 illustrates the adsorption of Ca^{2+} for the different CEC values. As observed, the CEC parameter does not have a significant effect on the ion exchange equivalent fraction of [Ca-X2]. Only a minor increase is seen for reduced CEC values which matches the experimental result presented by Pouryousefy et al. (2016). Furthermore, calcite dissolution can contribute as a Ca^{2+} source for ion exchange process which can affect the wettability alteration, but in this study the effect was minor (Jahanbani & Torsæter, 2018).

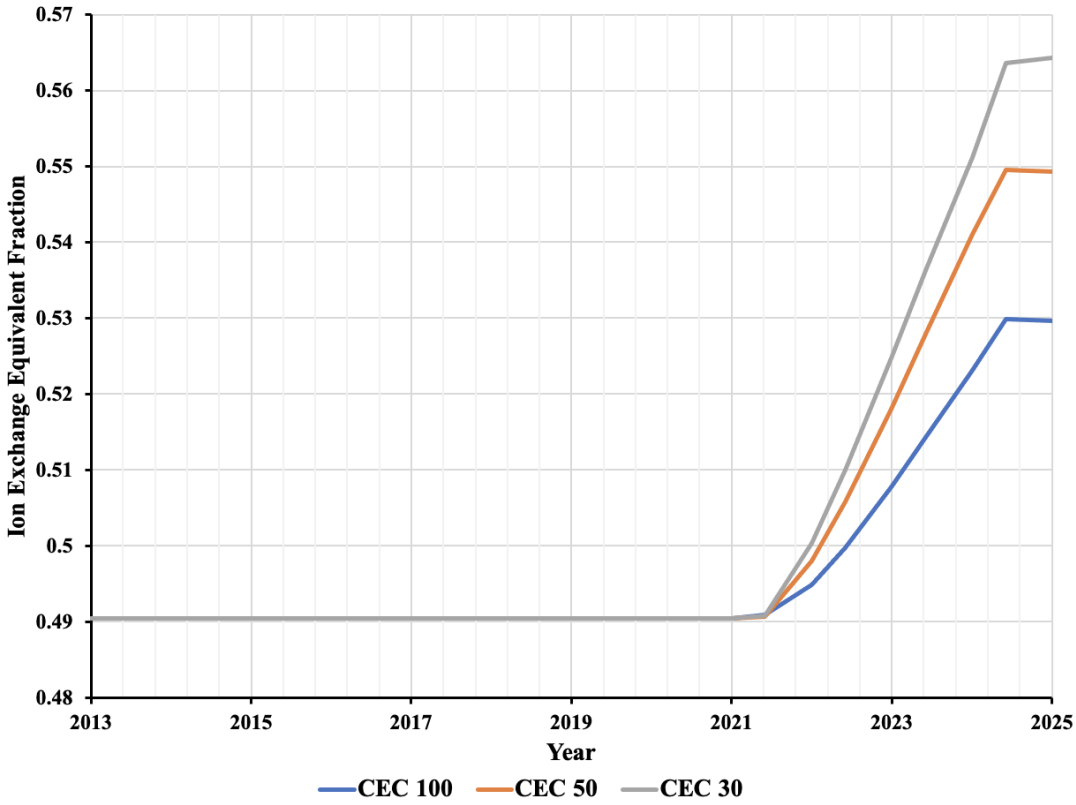

Figure 4.32: Effect of CEC on ion exchange equivalent fraction of [Ca-X2] at Prod_2.

The most influential parameters, TSORW and INTCOMP_VAL, are modified and simulated for incremental oil recovery compared to LSWF base case. Figure 4.33 illustrates the incremental oil recovery factor achieved by changing S_{or} (LSW) from 0.20 (base case) to 0.10. The increase in oil recovery factor corresponds to the value of 5.7 % compared to the base case. Figure 4.34 shows the incremental oil recovery when the interpolation value of LS curves is changed from 0.7 (base case) to 0.5. The corresponding increase in oil recovery is 4.2 %. The difference in incremental oil recovery seen for the two figures seems reasonable based on the impact the influential parameters had on the objective function (Figure 4.29). By changing both the S_{or} (LSW) and the interpolation value to 0.10 and 0.5, respectively, an incremental oil recovery of 12.7% is seen (Figure 4.35).

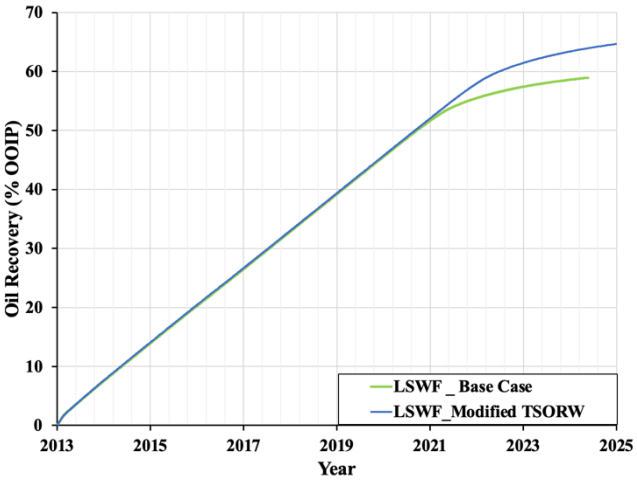

Figure 4.33: Incremental oil recovery for modified S_{or} (LSW).

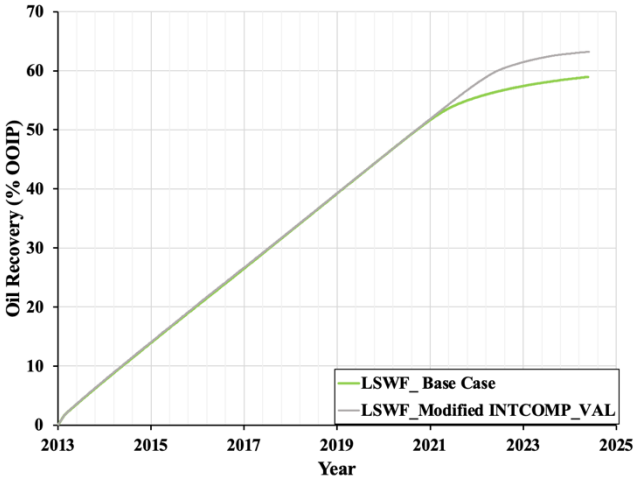

Figure 4.34: Incremental oil recovery for modified interpolant value for LS curves.

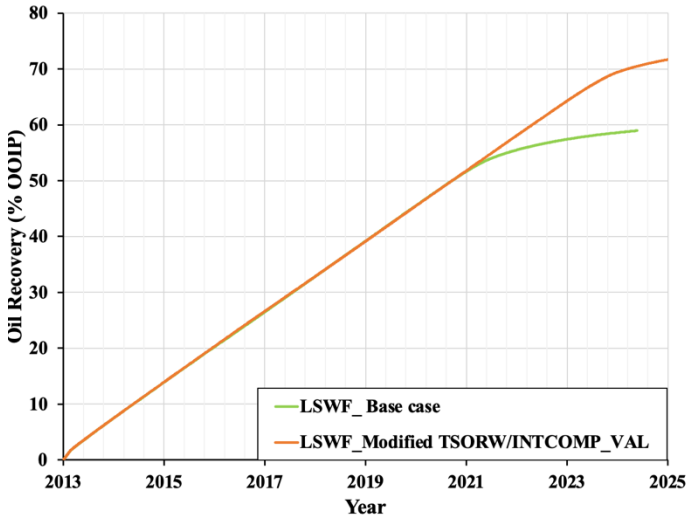

Figure 4.35: Incremental oil recovery for modified S_{or} (LSW) and interpolant value for LS curves.

Sensitivity analysis for Case 2

Sensitivity analysis in CMOST is done on the second relative permeability system presented in Figure 4.26 (Case 2). This system provides more realistic results for sandstone reservoirs on the Norwegian continental shelf. The engine RSM was used to make 46 experiments for the given ranges of the sensitivity parameters to explore the effect on oil recovery (Table 4.11). The default parameters for the case 2 are similar to case 1, except for residual oil saturation. The oil recovery factors for the corresponding runs are presented Figure 4.36.

Table 4.11: The parameters used for sensitivity analysis for case 2.

Sensitivity Parameters	Base Case	Data Range Settings	
		Lower limit	Upper limit
CEC (eq/m^3)	50	30	100
Interpolation parameter LSW	0.7	0.5	0.8
Interpolation parameter HSW	0.3	0.1	0.4
Volume fraction calcite	0.02	0.015	0.3
Volume fraction magnesite	0.02	0.015	0.3
S_{or} (LSW)	0.12	0.08	0.16

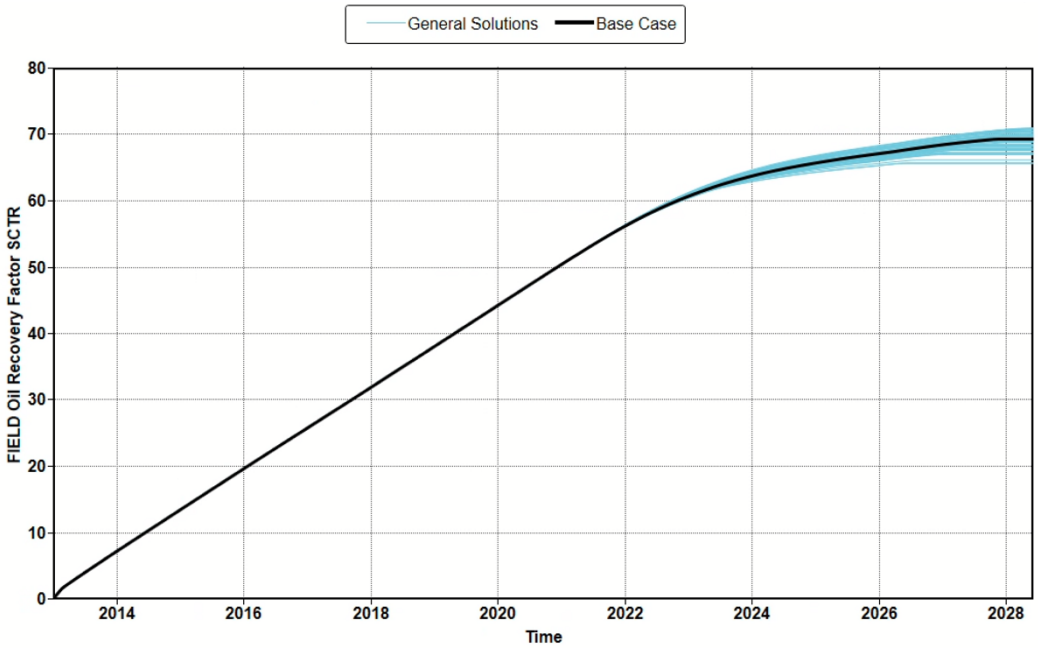

Figure 4.36: Oil recovery factor for the 46 experiments simulated for case 2.

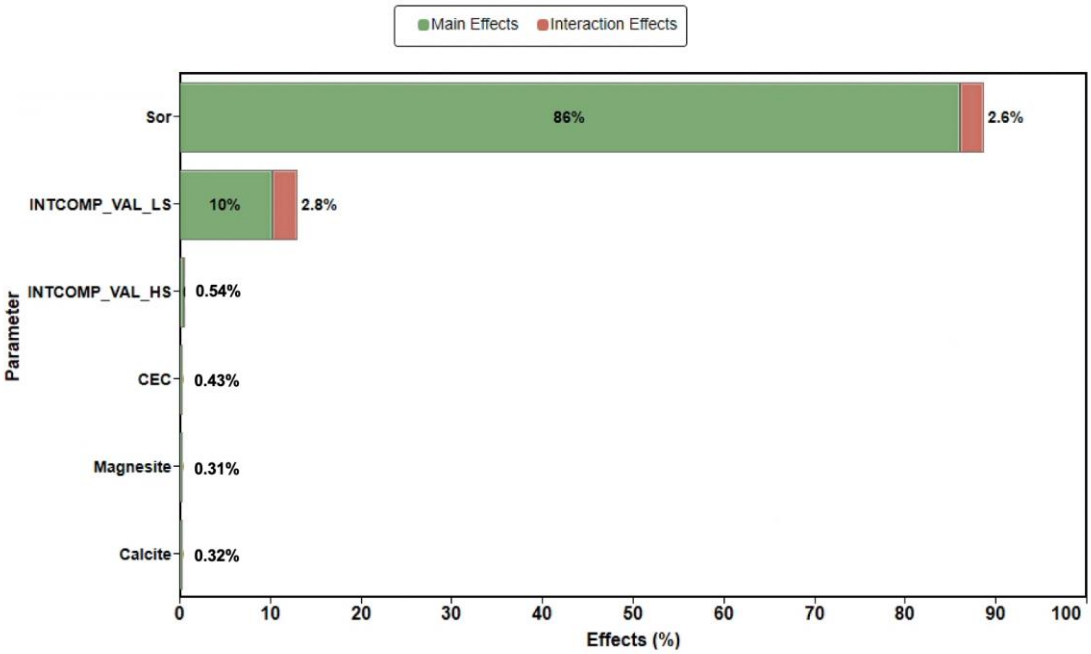

Figure 4.37: The sensitivity parameters' effects on oil recovery for case 2.

The most influential parameter for case 2 is the S_{or} (LSW) (Figure 4.37). As shown in 4.38 the oil recovery factor increases when S_{or} (LSW) decreases. Changes in oil recovery factor from 65.5% to 71.2% are seen when S_{or} (LSW) ranges from 0.16 to 0.08. Similar to case 1, the crossover of the LS oil and water relative permeability curves will be shifted a bit to the right when S_{or} (LSW) is reduced. However, since S_{or} (LSW) is already significantly low, only a small effect is seen on incremental oil recovered when changing the value to 0.08.

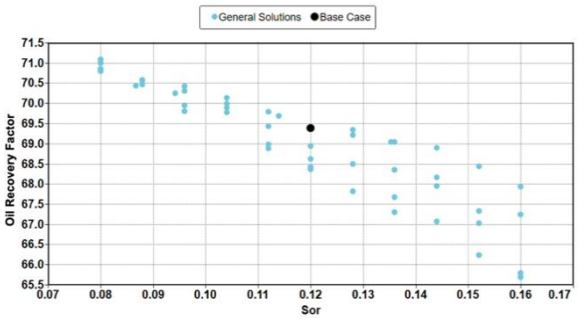

Figure 4.38: Cross plot of the relationship between S_{or} (LSW) and oil recovery factor.

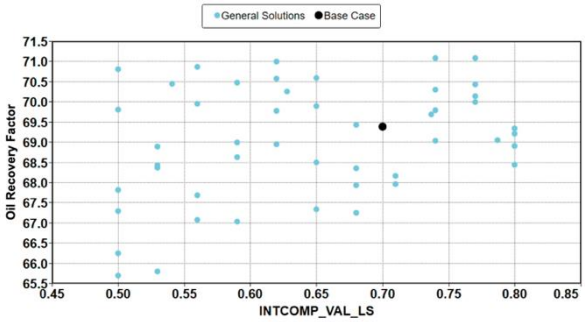

Figure 4.39: Cross plot of the relationship between interpolant value of LS curves and oil

The second most influential parameter is the interpolant value for the LS relative permeability curves. Compared to the case 1, the effect on oil recovery is smaller due to less change in relative permeabilities when wettability alteration occurs during LSWF. Hence, there is no significant trend when investigating the cross plot for interpolant value of LS curves in Figure 4.39

In Figure 4.40, reduction of S_{or} (LSW) from 0.12 (base case) to 0.08 and reduction of interpolant value (LS curves) from 0.7 (base case) to 0.5 are demonstrated. An increase in oil recovery factor of 1.5% is seen after modification of the sensitivity parameters. When these parameters are modified, more of the ζ[Ca-X2] will correspond to the reduced S_{or} (LSW) value. This means that the wettability alteration from HS to LS curves will be more significant. Consequently, more oil is mobilized, and the water cut limit is reached a few months later than for base case.

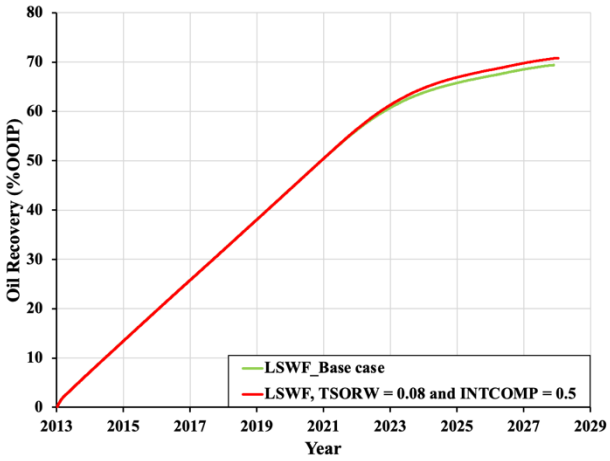

Figure 4.40: Oil recovery factor with reduced S_{or} (LSW) and interpolant value of the LS curves.

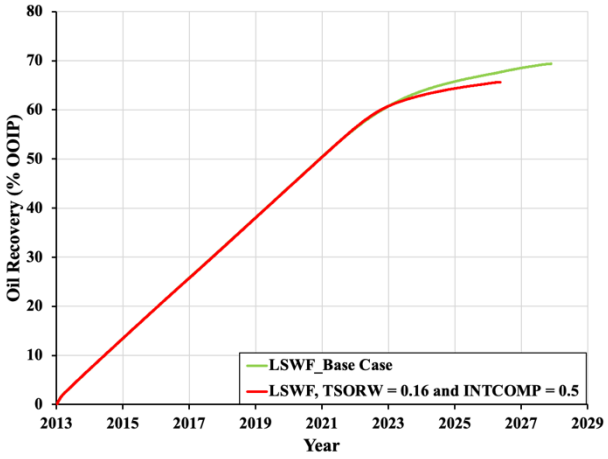

Figure 4.41: Oil recovery factor with increased S_{or} (LSW) and reduced interpolant value of the LS

Figure 4.41 illustrates the recovery factor when S_{or} (LSW) is increased from 0.12 (base case) to 0.16 and interpolant value for (LS curves) is reduced from 0.7 (base case) to 0.5. The results illustrate a negative effect on oil recovery. When the interpolant value is reduced, more of the ζ[Ca-X2] will correspond to the LS relative permeability curves in this case with increased S_{or}. It can also be observed that the production wells stop producing a few months before base case. This is due to the earlier violation of the water cut constraint when S_{or} (LSW) is higher. In addition, the S_{or} (LSW) is very close to the S_{or} value of the HSW curve (0.17). Consequently, only a minor wettability alteration will occur when LSW is injected.

5. Conclusion

In this thesis a LSWF synthetic field-scale model in GEM^{TM} is created based on Eclipse conversions and some synthetic data. In addition, WinProp by CMG has been introduced to develop a new compositional fluid model including oil composition data and geochemical reactions. Sensitivity on the synthetic LSWF field-scale model has been investigated for grid refinement, timing of injection, brine concentrations and the sensitivity parameters influence on two different relative permeability models for LSWF. The following conclusions can be drawn based on the assumptions for the LSWF model:

- By including multicomponent ion exchange, intra-aqueous reactions and mineral dissolution/precipitation and wettability alteration in the synthetic full-field model, incremental oil recovery of 9% was obtained by secondary mode LSWF.

- The main mechanism for the increased LSWF oil recovery was modeled through a shift (interpolation) in relative permeability. The interpolant was the ion exchange equivalent fraction of [Ca-X2]. The ζ[Ca-X2] increased and ζ[Na-X] decreased, which confirmed the hypothesis of Ca^{2+} adsorption presented by Dang et al. (2016). This increase in ζ[Ca-X2] was the main reason why incremental oil recovery was observed.

- The pH variations observed for LSWF and HSWF indicated an increase in pH during LSWF. The pH increase can indicate that different mechanisms are contributing to the wettability alteration process during LSWF, which can strengthen the LS effect.

- Three LSWF models with a varying number of grid blocks were evaluated for grid refinement sensitivity analysis. The coarse model had 4% lower oil recovery factor and a shorter plateau period compared to the original model. The finer grid showed a more similar trend as the original model, with only 0.5% increase in oil recovery factor. Since the finer grid is significantly more computationally demanding, it can be concluded that the original grid is fine enough to capture the geochemical reactions during LSWF.

- The sensitivity analysis of timing of injection confirmed that earlier onset of LSWF will result in higher recovery rates. The highest oil recovery factor of LSWF in tertiary mode was 55.5%. The secondary mode LSWF was most effective with oil recovery of 59%. By including LSWF in secondary mode in the development plan for a field, additional costs related to later phase EOR setup can be avoided.

- The effect of lowering the concentrations of ions in the injected water was investigated in CMOST^{TM}. Based on the sobol analysis, the reduction of Na^+ concentration had the most significant impact on oil recovery. This is because Na^+ enhances Ca^{2+} adsorption at the clay surface. The modified (lower) concentration compared to base case resulted in 1.5% increase in incremental oil recovery. The interpolant values for the relative permeability curves may be chosen differently, to observe a more significant change in oil recovery.

- The sensitivity on the two relative permeability models indicates that a more significant change in K_{ro} from HS curves to LS curves results in a greater change in incremental oil recovery. It can be concluded that the corresponding interpolant values and S_{or} of the relative permeability curves are what mainly determines the incremental recovery. Given these results, it is essential to have representative relative permeability data for the given field. Regarding the magnesite/calcite minerals, they had a small effect in this sensitivity analysis. However, calcite is an important Ca^{2+} source for the ion exchange process that should be included for more correct modeling of LSWF.

- Any further generalization or conclusion is hard to determine based on this synthetic field-scale model. The model is based on some assumptions and does not include the exact fluid model, relative permeability model or spatial distribution of rock types for the Gullfaks K1/K2 segment. However, it can provide necessary insight on how wettability alteration modeling of field-scale LSWF is configured in GEM^{TM}.

6. Future Work

The modeling study for this thesis illustrates how GEM^{TM} can include the geochemical reactions that affect wettability alteration mechanism for LSWF. This model is using real geological data for a field-scale reservoir, but it is lacking representative data for the spatial distribution of rock types, relative permeability model and fluid model. On that note, it could be very interesting to implement a model that represents true field data for LSWF. Other recommendations for further work are:

- A more comprehensive screening of the Gullfaks K1/K2 segment for LSWF, including analysis of the formation water, initial wetting state, and distribution of clays.

- Tracer implementation to access communication between the different layers. The Gullfaks K1/K2 segment consists of several faults affecting the fluid flow in the reservoir.

- A more comprehensive optimization for LSWF. Also, including history matching for historical field behavior where well logs, fluid samples, and relative permeability data are available, followed by a probabilistic forecast and robust optimization, which can include well placement, well length, and well control.

- Implementation of LSWF in combination with other EOR-techniques such as polymers and surfactant flooding. By using LSWF in combination with polymers, less polymers are needed to reach the same viscosity targets.

- Sensitivity analysis on more of the geochemical reactions' parameters affecting the wettability alteration process, including the selectivity coefficients ($K'_{Na/Ca}$ and, $K'_{Na/Mg}$), the reactive surface area (m^2/m^3), activation energy (J/mol), and the reactions rates for calcite and magnesite (mol/m^2s). It could be interesting to investigate a field-scale LSWF model for larger reactive surface area and higher activation energy.

7. Bibliography

Abdallah, W., Buckley, J. S., Carnegie, A., Edwards, J., Herold, B., Fordham, E., . . . Ziauddin, M. (2007). Fundamentals of wettability. *Oilfield Review, 19*, 44-61.

Abdulla, F., Hashem, H. S., Abdulraheem, B., Al-Naqi, M., Al-Qattan, A., John, H., . . . Thawer, R. (2013). *First EOR Trial using Low Salinity Water Injection in the Greater Burgan Field, Kuwait*. Paper presented at the SPE Middle East Oil and Gas Show and Conference, Manama, Bahrain. https://doi.org/10.2118/164341-MS

Adegbite, J., Al-Shalabi P.E, E., & Ghosh, B. (2017). *Modeling the Effect of Engineered Water Injection on Oil Recovery From Carbonate Cores*. Paper presented at the SPE International Conference on Oilfield Chemistry, Montgomery, Texas.

Agbalaka, C. C., Dandekar, A. Y., Patil, S. L., Khataniar, S., & Hemsath, J. R. (2008). Coreflooding Studies to Evaluate the Impact of Salinity and Wettability on Oil Recovery Efficiency. *Transport in Porous Media, 76*(1), 77. doi:10.1007/s11242-008-9235-7

Aggrey, W. N., Afari, S., & Sarkodie, K. (2014). The New EOR Frontiers - Reduced Salinity Waterflooding. *Asian Journal of Applied Sciences, 2 (6)*.

Ahmed, T. (2006). *Working Guide to Reservoir Rock Properties and Fluid Flow*: Gulf Professional Publishing, Elsvier Inc.

Ahmed, T. (2010). Chapter 14 - Principles of Waterflooding. In T. Ahmed (Ed.), *Reservoir Engineering Handbook (Fourth Edition)* (pp. 909-1095). Boston: Gulf Professional Publishing.

Ahmetgareev, V., Zeinijahromi, A., Badalyan, A., Khisamov, R., & Bedrikovetsky, P. (2015). Analysis of Low Salinity Waterflooding in Bastrykskoye Field. *Petroleum Science and Technology, 33*(5), 561-570. doi:10.1080/10916466.2014.997390

Al-Attar, H. H., Mahmoud, M. Y., Zekri, A. Y., Almehaideb, R., & Ghannam, M. (2013). Low-salinity flooding in a selected carbonate reservoir: experimental approach. *Journal of Petroleum Exploration and Production Technology, 3*(2), 139-149. doi:10.1007/s13202-013-0052-3

Al-Qattan, A., Sanaseeri, A., Al-Saleh, Z., Singh, B. B. B., Al-Kaaoud, H., Delshad, M., . . . Kumer, K. (2018). *Low Salinity Waterflood and Low Salinity Polymer Injection in the Wara Reservoir of the Greater Burgan Field*. Paper presented at the SPE EOR

Conference at Oil and Gas West Asia, Muscat, Oman. https://doi.org/10.2118/190481-MS

Al-Saedi, H. N., Flori, R. E., & Brady, P. V. (2019). Effect of divalent cations in formation water on wettability alteration during low salinity water flooding in sandstone reservoirs: Oil recovery analyses, surface reactivity tests, contact angle, and spontaneous imbibition experiments. *Journal of Molecular Liquids, 275*, 163-172. doi:https://doi.org/10.1016/j.molliq.2018.11.093

Al-Shalabi P.E, E. (2014). *Modeling the Effect of Injecting Low Salinity Water on Oil Recovery from Carbonate Reservoirs.* (Doctor Degree).

Almeida da Costa, A., Mateo, J., Patel, R., Trivedi, J. J., Soares, J. B. P., Rocha, P. S., . . . Embiruçu, M. (2021). Can low salinity water injection be an efficient option for the Recôncavo Basin? An experimental and simulation case study. *Journal of Petroleum Science and Engineering, 202*, 108557. doi:https://doi.org/10.1016/j.petrol.2021.108557

Amott, E. (1959). Observations Relating to the Wettability of Porous Rock. *Transactions of the AIME, 216*(01), 156-162. doi:10.2118/1167-G

Austad, T., Rezaeidoust, A., & Puntervold, T. (2010). *Chemical Mechanism of Low Salinity Water Flooding in Sandstone Reservoirs*. Paper presented at the SPE Improved Oil Recovery Symposium, Tulsa, Oklahoma, USA. https://doi.org/10.2118/129767-MS

Bernard, G. G. (1967). *Effect of Floodwater Salinity on Recovery Of Oil from Cores Containing Clays*. Paper presented at the SPE California Regional Meeting, Los Angeles, California. https://doi.org/10.2118/1725-MS

Bethke, C. M. (2007). *Geochemical and Biogeochemical Reaction Modeling* (2 ed.). Cambridge: Cambridge University Press.

Brooks, R. H., & Corey, A. (1966). Properties of Porous Media Affecting Fluid Flow. *Journal of the Irrigation and Drainage Division, 92*, 61-88.

Burdine, N. T. (1953). Relative Permeability Calculations From Pore Size Distribution Data. *Journal of Petroleum Technology, 5*(03), 71-78. doi:10.2118/225-G

Chandrashegaran, P. (2015). *Low Salinity Water Injection for EOR*. Paper presented at the SPE Nigeria Annual International Conferance and Exhibition, Lagos, Nigeria. https://doi.org/10.2118/178414-MS

Chavan, M., Dandekar, A., Patil, S., & Khataniar, S. (2019). Low-salinity-based enhanced oil recovery literature review and associated screening criteria. *Petroleum Science, 16*(6), 1344-1360. doi:10.1007/s12182-019-0325-7

Cissokho, M., Bertin, H., Boussour, S., Cordier, P., & Hamon, G. (2010). Low Salinity Oil Recovery On Clayey Sandstone: Experimental Study. *Petrophysics, 51*(05), 9. Retrieved from https://doi.org/

CMOST-AL. (2019). Intelligent Optimization & Analysis Tool, Computer Modelling Group LTD.

Craig, F. F. (1971). *The reservoir engineering aspects of waterflooding* (Vol. vol. 3). New York: Henry L. Doherty Memorial Fund of AIME.

Dake, L. P. (1978). *Fundamentals of Reservoir Engineering*. Elsevier Science.

Dandekar, A. Y. (2006). *Petroleum Reservoir Rock and Fluid Properties*: Taylor & Francis Group, LLC.

Dang, Nghiem, L., Nguyen, N., Chen, Z., & Nguyen, Q. (2015a). *Modeling and Optimization of Low Salinity Waterflood*. Paper presented at the SPE Reservoir Simulation Symposium, Houston, Texas, USA. https://doi.org/10.2118/173194-MS

Dang, Nghiem, L., Nguyen, N., Chen, Z., & Nguyen, Q. (2016). Mechanistic modeling of low salinity water flooding. *Journal of Petroleum Science and Engineering, 146*, 191-209. doi:https://doi.org/10.1016/j.petrol.2016.04.024

Dang, Nghiem, L. X., Chen, Z. J., & Nguyen, Q. P. (2013). *Modeling Low Salinity Waterflooding: Ion Exchange, Geochemistry and Wettability Alteration*. Paper presented at the SPE annual technical conference and exhibition, New Orleans, Louisiana, USA. https://doi.org/10.2118/166447-MS

Dang, Nguyen, N. T. B., & Chen, Z. (2015b). *Practical Concerns and Principle Guidelines for Screening, Implementation, Design, and Optimization of Low Salinity Waterflooding*. https://doi.org/10.2118/174008-MS

DataImporter. (2019). DataImporter, Guide.

Derkani, M., Fletcher, A., Abdallah, W., Sauerer, B., Anderson, J., & Zhang, Z. (2018). Low Salinity Waterflooding in Carbonate Reservoirs: Review of Interfacial Mechanisms. *Colloids and Interfaces, 2*, 20. doi:10.3390/colloids2020020

Donaldson, E. C., & Alam, W. (2008). CHAPTER 1 - Wettability. In E. C. Donaldson & W. Alam (Eds.), *Wettability* (pp. 1-55): Gulf Publishing Company.

Egbe, D. I. O. (2019). *Geochemical Modeling of Low Salinity Waterflooding and Surfactant Flooding in Heterogeneous Low-Permeability Carbonate Cores.* (Master). NTNU,

Esene, C., Onalo, D., Zendehboudi, S., James, L., Aborig, A., & Butt, S. (2018). Modeling investigation of low salinity water injection in sandstones and carbonates: Effect of Na+ and SO42−. *Fuel, 232*, 362-373. doi:https://doi.org/10.1016/j.fuel.2018.05.161

Esmaeili, S., & Maaref, S. (2011). Investigating the effect of transient flow behavior from HSW to LSW on oil recovery in low-salinity water flooding simulation. *Journal of Petroleum Exploration and Production Technology, 9*(2), 1495-1515. doi:10.1007/s13202-018-0561-1

Falode, O., & Manuel, E. (2014). Wettability Effects on Capillary Pressure, Relative Permeability, and Irredcucible Saturation Using Porous Plate. *Journal of Petroleum Engineering, 2014*, 465418. doi:10.1155/2014/465418

Fjelde, I., Asen, S. M., & Omekeh, A. (2012). *Low Salinity Water Flooding Experiments and Interpretation by Simulations*. https://doi.org/10.2118/154142-MS

Fjelde, I., Omekeh, A. V., & Sokama-Neuyam, Y. A. (2014). *Low Salinity Water Flooding: Effect Of Crude Oil Composition*. https://doi.org/10.2118/169090-MS

Ganat, T. A.-A. O. (2020). *Fundamentals of Reservoir Rock Properties*(1st ed. 2020. ed.).

GEM. (2019). Compositional & Unconventional Simulator, Computer Modelling Group LTD.

Hamouda, A. A., & Gupta, S. (2017). Enhancing Oil Recovery from Chalk Reservoirs by a Low-Salinity Water Flooding Mechanism and Fluid/Rock Interactions. *Energies, 10*(4). doi:10.3390/en10040576

Jadhunandan, P. P., & Morrow, N. R. (1995). Effect of Wettability on Waterflood Recovery for Crude-Oil/Brine/Rock Systems. *SPE Reservoir Engineering, 10*(01), 40-46. doi:10.2118/22597-PA

Jahanbani, A., & Torsæter, O. (2018). *Numerical Simulation Of Low Salinity Water Flooding: Wettability Alteration Considerations*. Paper presented at the In Proceedings of the 16th European Conference on the Mathematics of Oil Recovery, ECMOR XVI 2018, Barcelona, Spain.

Kallestad, A. B. (2020). Geochemical Modeling of Low Salinity Water Flooding and Investigation of Wettability Alteration Mechanism. *Specialization Project*.

Katende, A., & Sagala, F. (2019). A critical review of low salinity water flooding: Mechanism, laboratory and field application. *Journal of Molecular Liquids, 278*, 627-649. doi:https://doi.org/10.1016/j.molliq.2019.01.037

Kharaka, Y. K., Gunter, W. D., Aggarwal, P. K., Perkins, E. H., & DeBraal, J. D. (1988). *SOLMINEQ.88; a computer program for geochemical modeling of water-rock interactions* (88-4227). Retrieved from http://pubs.er.usgs.gov/publication/wri884227

Lager, A., Webb, K. J., & Black, C. J. J. (2007). *Impact of Brine Chemistry on Oil Recovery*. 14th European Symposium on IOR, Cairo, Egypt.

Lager, A., Webb, K. J., Black, C. J. J., Singleton, M., & Sorbie, K. S. (2006). Low Salinity Oil Recovery - An Experimental Investigation1. *Petrophysics, 49*(01), 8.

Lager, A., Webb, K. J., Collins, I. R., & Richmond, D. M. (2008). *LoSal Enhanced Oil Recovery: Evidence of Enhanced Oil Recovery at the Reservoir Scale*. https://doi.org/10.2118/113976-MS

Li, K., & Horne, R. N. (2006). Comparison of methods to calculate relative permeability from capillary pressure in consolidated water-wet porous media. *Water Resources Research, 42*(6). doi:https://doi.org/10.1029/2005WR004482

Ligthelm, D. J., Gronsveld, J., Hofman, J., Brussee, N., Marcelis, F., & van der Linde, H. (2009). *Novel Waterflooding Strategy By Manipulation Of Injection Brine Composition*. Paper presented at the EUROPEC/EAGE Conference and Exhibition, Amsterdam, The Netherlands. https://doi.org/10.2118/119835-MS

Mahani, H., Sorop, T. G., Ligthelm, D., Brooks, A. D., Vledder, P., Mozahem, F., & Ali, Y. (2011). *Analysis of Field Responses to Low-Salinity Waterflooding in Secondary and Tertiary Mode in Syria*. https://doi.org/10.2118/142960-MS

Mahmud, H. B., Arumugam, S., & Mahmud, W. (2019). Potential of Low-Salinity Waterflooding Technology to Improve Oil Recovery. *Enhanced Oil Recovery Processes - New Technologies*.

McGuire, P. L., Chatham, J. R., Paskvan, F. K., Sommer, D. M., & Carini, F. H. (2005). *Low Salinity Oil Recovery: An Exciting New EOR Opportunity for Alaska's North Slope*. Paper presented at the SPE Western Regional Meeting, Irvine, California. https://doi.org/10.2118/93903-MS

Miller, R. J. (1996). 7 - Petroleum Economics. In W. C. Lyons (Ed.), *Standard Handbook of Petroleum and Natural Gas Engineering* (pp. 985-1033). Houston: Gulf Professional Publishing.

Mokhtari, R., & Ayatollahi, S. (2019). Dissociation of polar oil components in low salinity water and its impact on crude oil–brine interfacial interactions and physical properties. *Petroleum Science, 16*(2), 328-343. doi:10.1007/s12182-018-0275-5

Morrow, N., & Buckley, J. (2011). Improved Oil Recovery by Low-Salinity Waterflooding. *Journal of Petroleum Technology, 63*(05), 106-112. doi:10.2118/129421-JPT

Morrow, N. R., Tang, G.-q., Valat, M., & Xie, X. (1998). Prospects of improved oil recovery related to wettability and brine composition. *Journal of Petroleum Science and Engineering, 20*(3), 267-276. doi:https://doi.org/10.1016/S0920-4105(98)00030-8

Muggeridge, A., Cockin, A., Webb, K., Frampton, H., Collins, I., Moulds, T., & Salino, P. (2013). Recovery rates, enhanced oil recovery and technological limits. *Philosophical transactions. Series A, Mathematical, physical, and engineering sciences, 372*(2006), 20120320-20120320. doi:10.1098/rsta.2012.0320

Nasralla, R. A., Alotaibi, M. B., & Nasr-El-Din, H. A. (2011). *Efficiency of Oil Recovery by Low Salinity Water Flooding in Sandstone Reservoirs*. https://doi.org/10.2118/144602-MS

Nwidee, L., Theophilus, S., Barifcani, A., Sarmadivaleh, M., & Iglauer, S. (2016). EOR Processes, Opportunities and Technological Advancements. In.

Omekeh, A. V., Friis, H. A., Fjelde, I., & Evje, S. (2012). *Modeling of Ion-Exchange and Solubility in Low Salinity Water Flooding*. Paper presented at the SPE Improved Oil Recovery Symposium, Tulsa, Oklahoma, USA. https://doi.org/10.2118/154144-MS

Pedersen, V. L. (2018). *Field Scale Simulation Study of Hybrid EOR.* (Master). Universitas Bergensis, Centre for Integrated Petroleum Reseach.

Pouryousefy, E., Xie, Q., & Saeedi, A. (2016). Effect of multi-component ions exchange on low salinity EOR: Coupled geochemical simulation study. *Petroleum, 2*(3), 215-224. doi:https://doi.org/10.1016/j.petlm.2016.05.004

Purcell, W. R. (1949). Capillary pressures - Their measurement using mercury and the calculation of permeability. *Trans. Aime, 186*.

Rausch, R. W., & Beaver, K. W. (1964). Case History of Successfully Water Flooding a Fractured Sandstone. *Journal of Petroleum Technology, 16*(11), 1233-1237. doi:10.2118/825-PA

Rivet, S. M. (2009). *Coreflooding Oil Displacements with Low Salinity Brine.* University of Texas at Houston, United States,

Roman, S. (2013). *Modeling of Miscible WAG Injection Using Real Geological Field Data.* (Master). Norwegian University of Science and Technology,

Rueslatten, H. G., Hjelmeland, O., & Selle, O. M. (1994). *Wettability of reservoir rocks and the influence of organo-metallic compounds. North Sea Oil and Gas Reservoirs.*

Sadeed, A., Tariq, Z., Janjua, A. N., Asad, A., & Hossain, M. E. (2018). *Smart Water Flooding: An Economic Evaluation and Optimization*. https://doi.org/10.2118/192330-MS

Satter, A., & Iqbal, G. M. (2016a). 3 - Reservoir rock properties. In A. Satter & G. M. Iqbal (Eds.), *Reservoir Engineering* (pp. 29-79). Boston: Gulf Professional Publishing.

Satter, A., & Iqbal, G. M. (2016b). 17 - Enhanced oil recovery processes: thermal, chemical, and miscible floods. In A. Satter & G. M. Iqbal (Eds.), *Reservoir Engineering* (pp. 313-337). Boston: Gulf Professional Publishing.

Seccombe, J., Lager, A., Jerauld, G., Jhaveri, B., Buikema, T., Bassler, S., . . . Paskvan, F. (2010). *Demonstration of Low-Salinity EOR at Interwell Scale, Endicott Field, Alaska*. https://doi.org/10.2118/129692-MS

Sierra, D. M., Rojas, A. A., & Araque, V. S. (2020). *Low Salinity Water Injection Optimization in the Namorado Field Using Compositional Simulation and Artificial Intelligence*. https://doi.org/10.2118/198995-MS

Skrettingland, K., Holt, T., Tweheyo, M. T. T., & Skjevrak, I. (2011). Snorre Low-Salinity-Water Injection—Coreflooding Experiments and Single-Well Field Pilot. *SPE Reservoir Evaluation & Engineering, 14*(02), 182-192. doi:10.2118/129877-PA

Sorbie, K. S., & Collins, I. R. (2010). *A Proposed Pore-Scale Mechanism for How Low Salinity Waterflooding Works*. https://doi.org/10.2118/129833-MS

Strand, S., Puntervold, T., & Austad, T. (2016). Water based EOR from clastic oil reservoirs by wettability alteration: A review of chemical aspects. *Journal of Petroleum Science and Engineering, 146*, 1079-1091. doi:https://doi.org/10.1016/j.petrol.2016.08.012

Tang, G.-Q., & Morrow, N. R. (1999). Influence of brine composition and fines migration on crude oil/brine/rock interactions and oil recovery. *Journal of Petroleum Science and Engineering, 24*(2), 99-111. doi:https://doi.org/10.1016/S0920-4105(99)00034-0

U.S Energy Information Administration. (2020). *International Energy Outlook.* Retrieved from https://www.eia.gov/outlooks/ieo/

Webb, K. J., Black, C. J. J., & Al-Ajeel, H. (2004). *Low Salinity Oil Recovery - Log-Inject-Log*. https://doi.org/10.2118/89379-MS

Willhite, D. W. G. a. G. P. (1998). *Enhanced Oil recovery* (Vol. 6). Society of Petroleum Engineers.

WinProp. (2019). Fluid Property Characterization Tool, Computer Modelling Group LTD.

Wu, Y.-S., & Bai, B. (2009). *Efficient Simulation for Low Salinity Waterflooding in Porous and Fractured Reservoirs*. https://doi.org/10.2118/118830-MS

Zhang, T., Li, Y., Li, C., & Sun, S. (2020). Effect of salinity on oil production: review on low salinity waterflooding mechanisms and exploratory study on pipeline scaling. *Oil & Gas Science and Technology - Revue d'IFPEN, 75*(1294-4475), 50. doi:https://doi.org/10.2516/ogst/2020045

Zhang, Y., Xie, X., & Morrow, N. R. (2007). *Waterflood Performance By Injection Of Brine With Different Salinity For Reservoir Cores*. https://doi.org/10.2118/109849-MS

Zitha, P., Felder, R., Zornes, D., Brown, K., & Mohanty, K. (2011). *Increasing Hydrocarbon Recovery Factors*.

Zolotuchin, A. B. (2000). *Introduction to petroleum reservoir engineering*. Kristiansand: Høyskoleforl.

Anna Bjørke Kallestad

Field-Scale Modeling of Low Salinity Water Flooding - Wettability Alteration

NTNU
Norwegian University of
Science and Technology